CITA ICAT
Canadian Institute for Theoretical Astrophysics
L'institut Canadien d'astrophysique théorique

13 July 2018

New Insights on Galaxy Formation from Comparing Simulations and Observations

Joel Primack, UCSC

with collaborators including Aldo Rodriguez-Puebla, Christoph Lee, Peter Behroozi, Miguel Aragon Calvo, Avishai Dekel, Sandy Faber, Doug Hellinger, Kathryn Johnston, Anatoly Klypin, Viraj Pandya, Rachel Somerville, & undergraduate researchers Radu Dragomir, Elliot Eckholm, & Tze Ping Goh

Dark Matter Ships on a Dark Energy Ocean

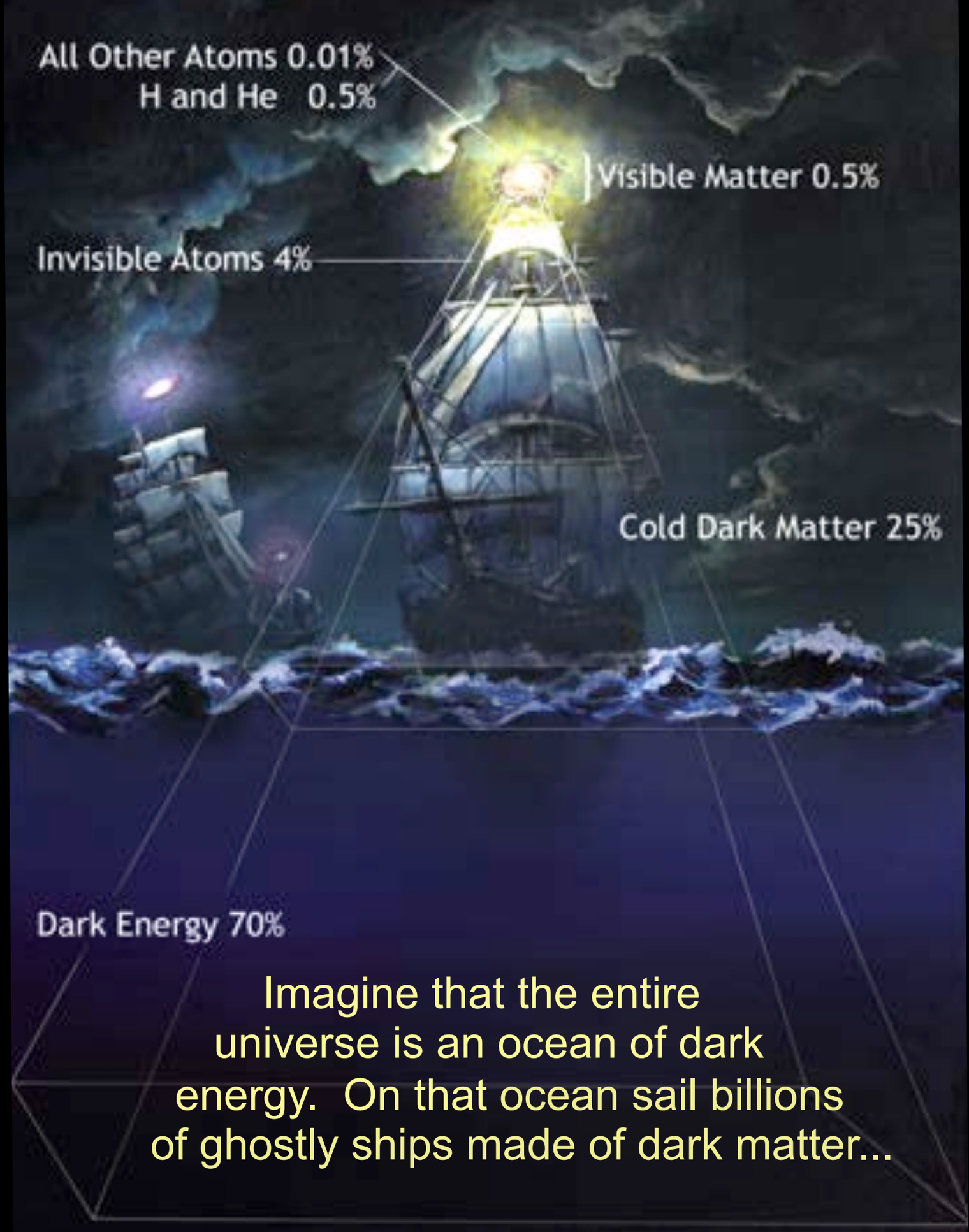

Matter and Energy Content of the Universe

ΛCDM

Double Dark Theory

CDM Structure Formation: Linear Theory

Cosmic Inflation: matter fluctuations enter the horizon with about the same amplitude

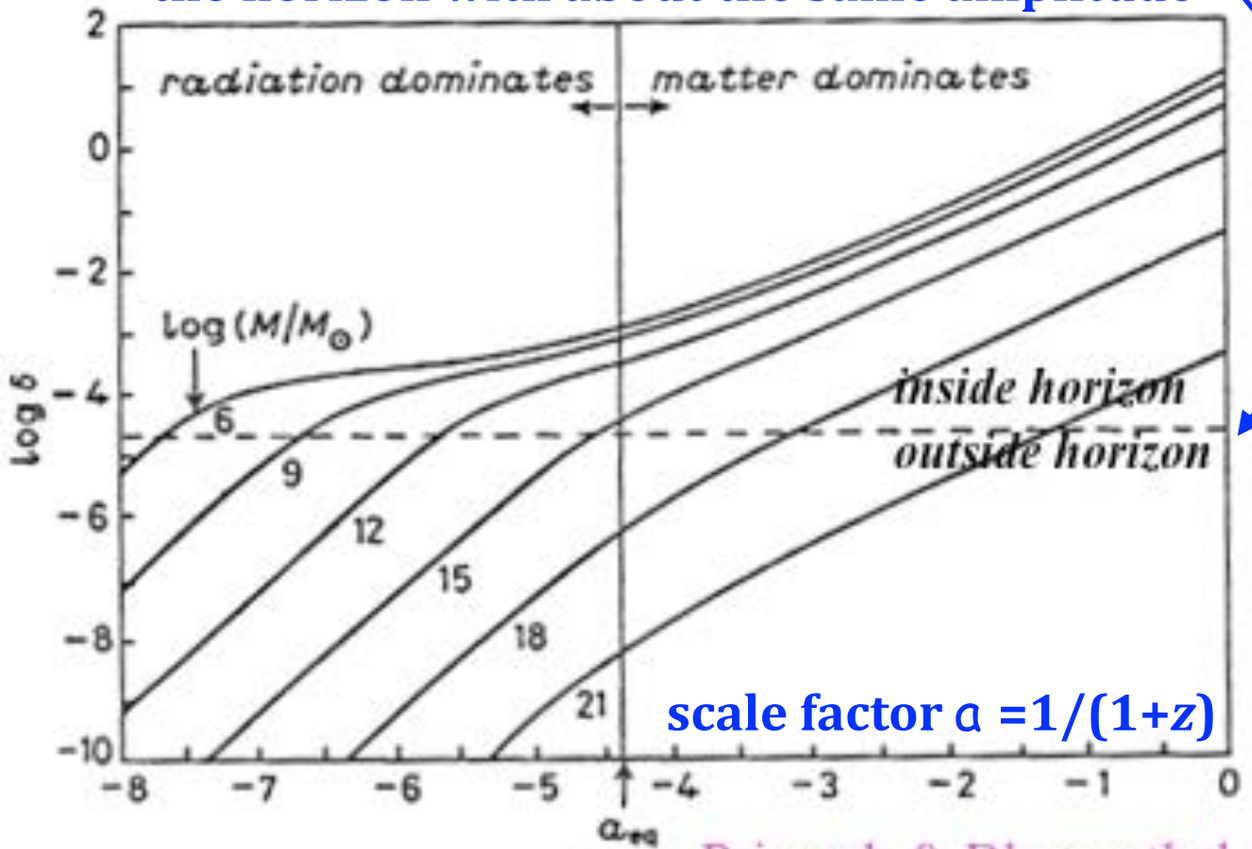

Primack & Blumenthal 1983

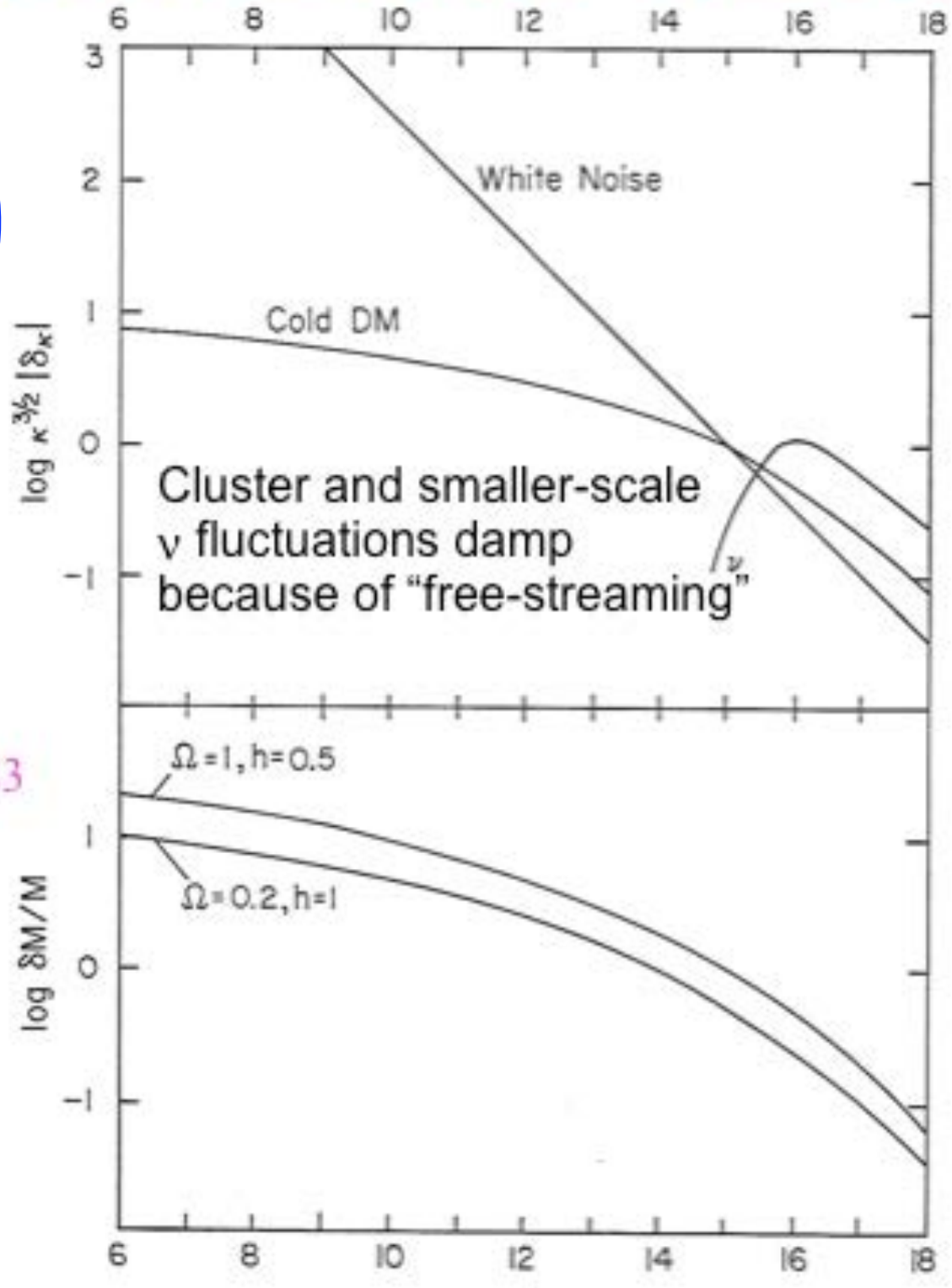

Blumenthal, Faber, Primack, & Rees 1984

Matter fluctuations that enter the horizon during the radiation dominated era, with masses less than about $10^{15} M_\odot$, grow only $\propto \log a$, because they are not in the gravitationally dominant component. But matter fluctuations that enter the horizon in the matter-dominated era grow $\propto a$. This explains the characteristic shape of the CDM fluctuation spectrum, with $\delta(k) \propto k^{-n/2-2} \log k$ for $k >> k_{eq}$.

Matter Distribution Agrees with Double Dark Theory!

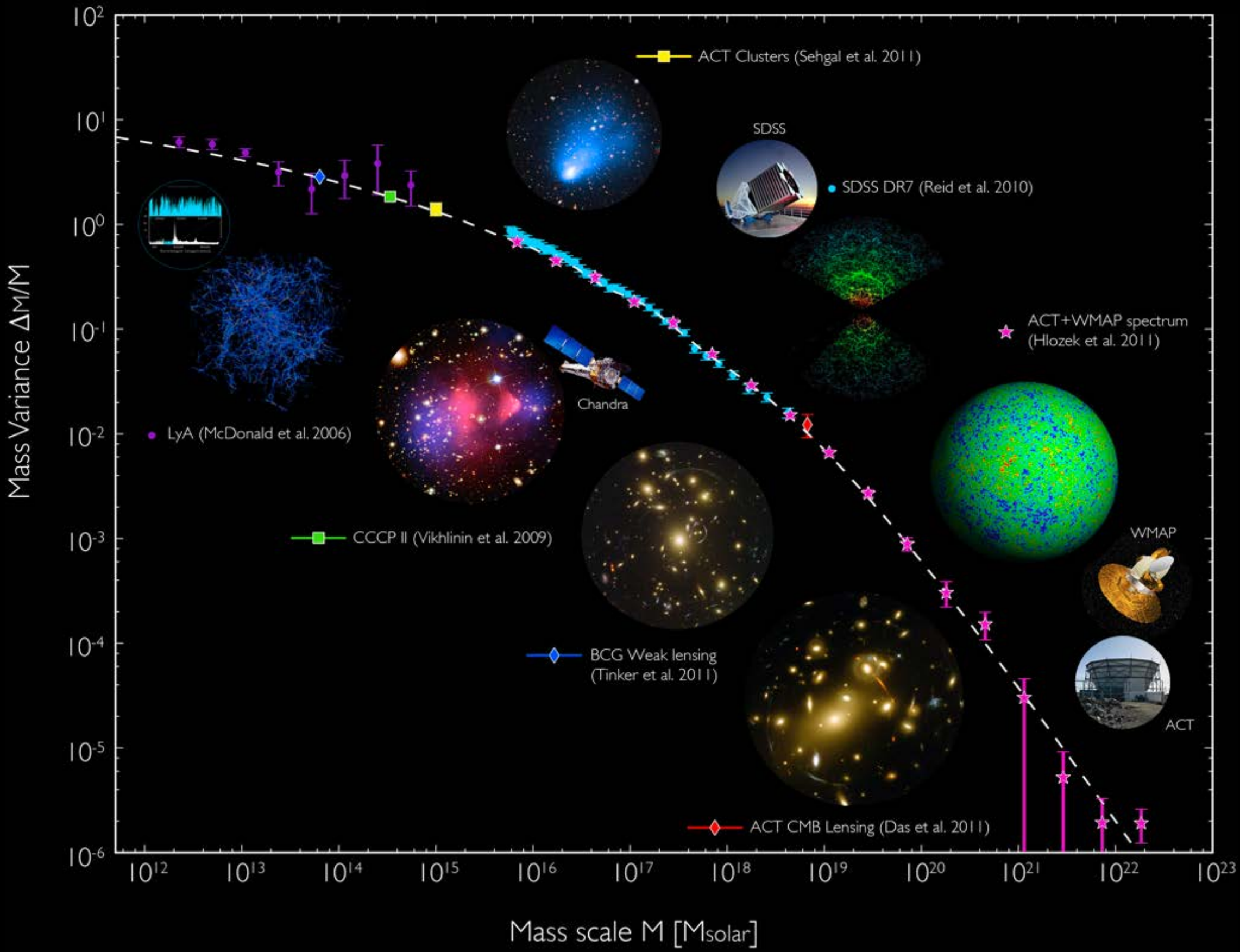

European Space Agency PLANCK Satellite Data

Released February 9, 2015

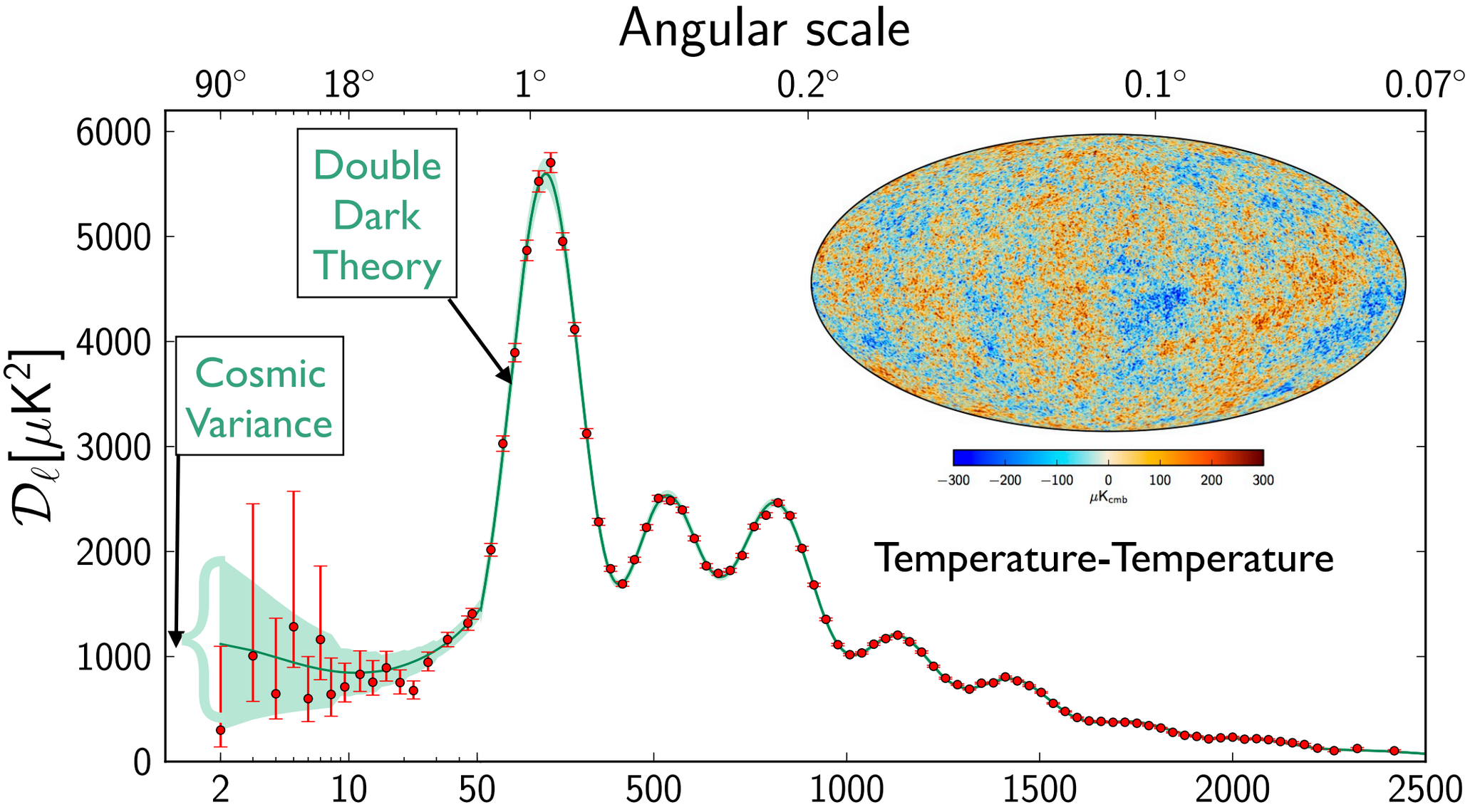

Agrees with Double Dark Theory!

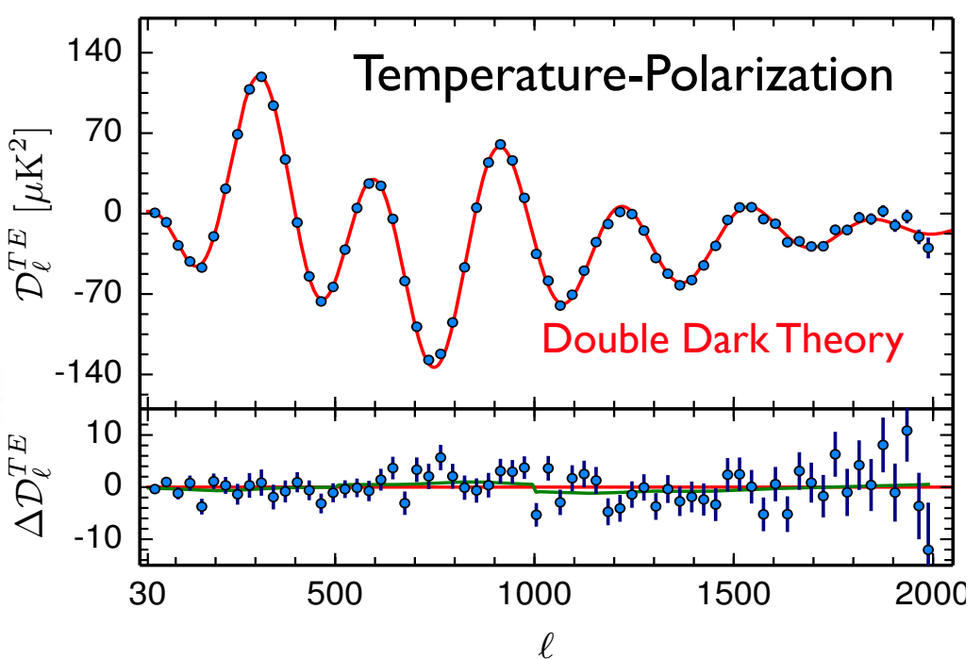

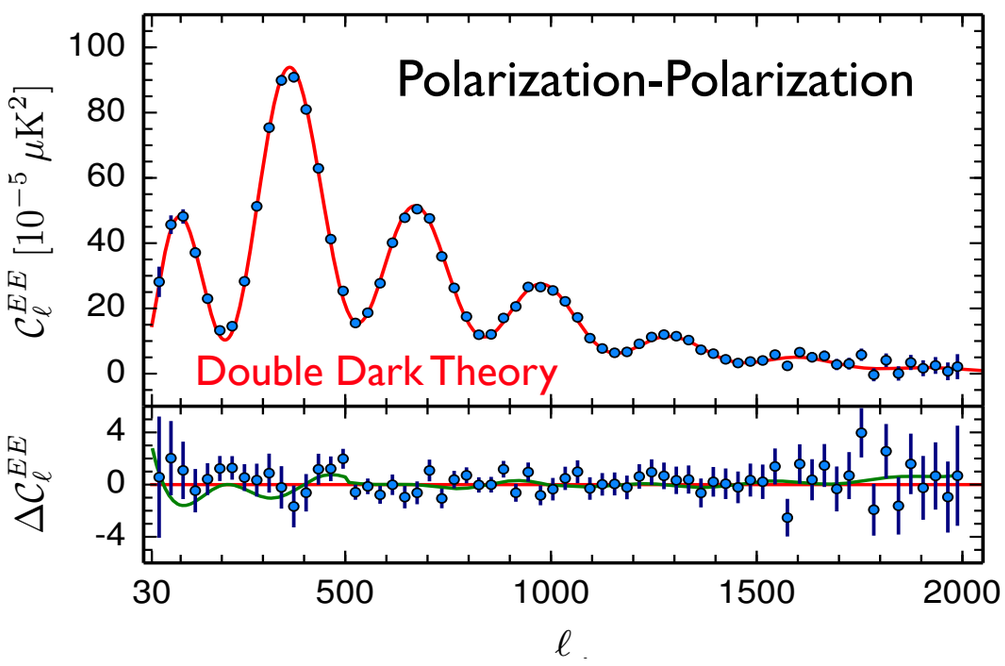

Bolshoi-Planck Cosmological Simulation

Merger Tree of a Large Halo

Peter Behroozi & Christoph Lee

Structure Formation Methodology

- Starting from the Big Bang, we simulate the evolution of a representative part of the universe according to the Double Dark theory to see if the end result matches what astronomers actually observe.
- On the large scale the simulations produce a universe just like the one we observe. We're always looking for new phenomena to predict — every one of which tests the theory!
- But the way individual galaxies form is only partly understood because it depends on the interactions of the ordinary atomic matter as well as the dark matter and dark energy to form stars and super-massive black holes. We need help from observations.

Halo and Subhalo Demographics with Planck Cosmological Parameters: Bolshoi-Planck and MultiDark-Planck Simulations

Aldo Rodrìguez-Puebla, Peter Behroozi, Joel Primack, Anatoly Klypin, Christoph Lee, Doug Hellinger

MNRAS 2016

Cosmological Simulations

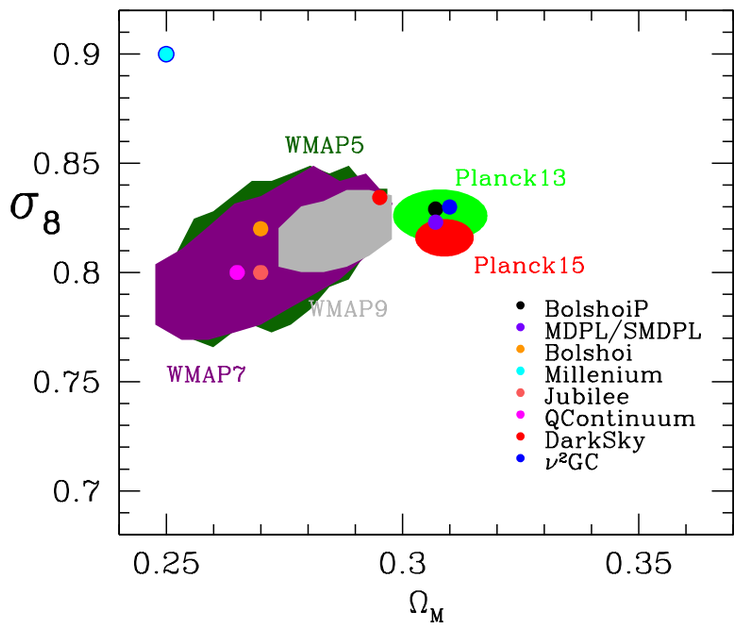

Halo Mass Function and Fits

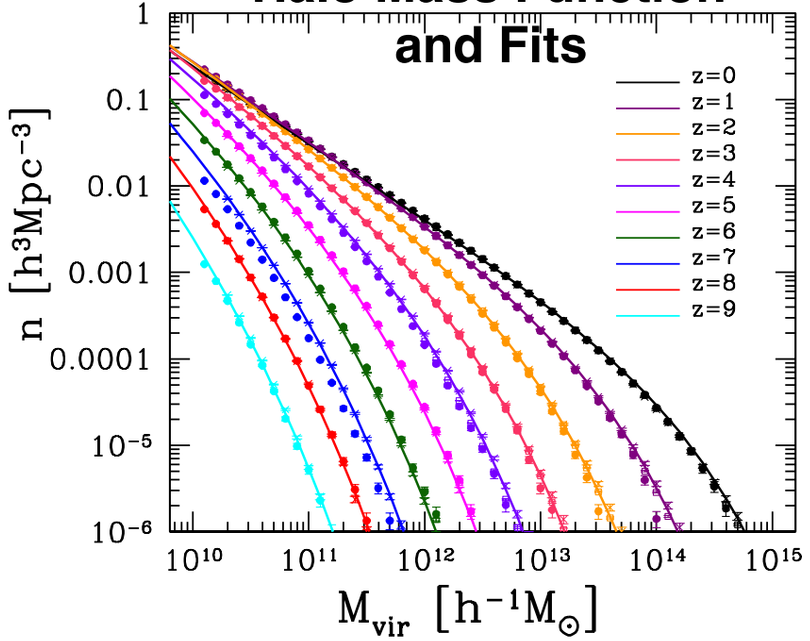

$V_{max}(M_{vir}, z)$

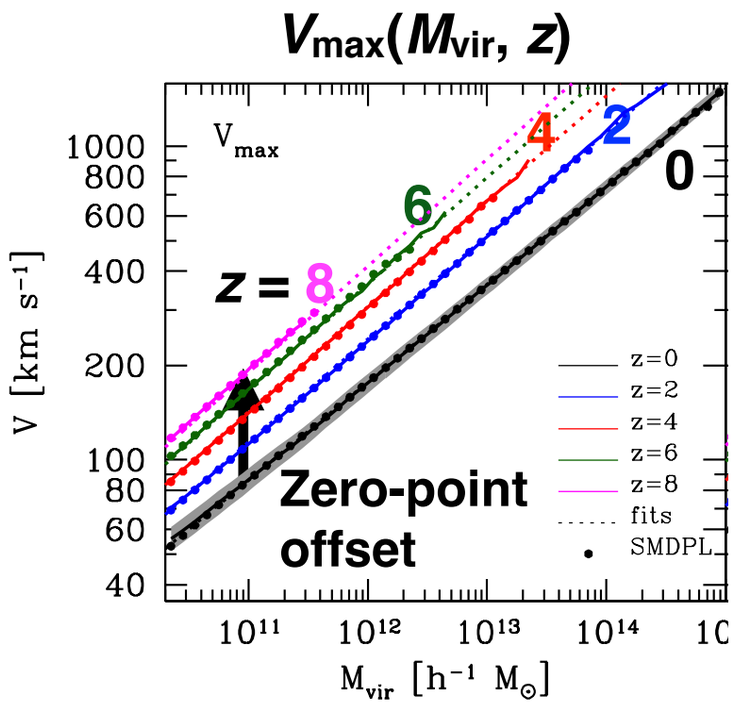

Halo Spin Parameters as a function of M_{vir}

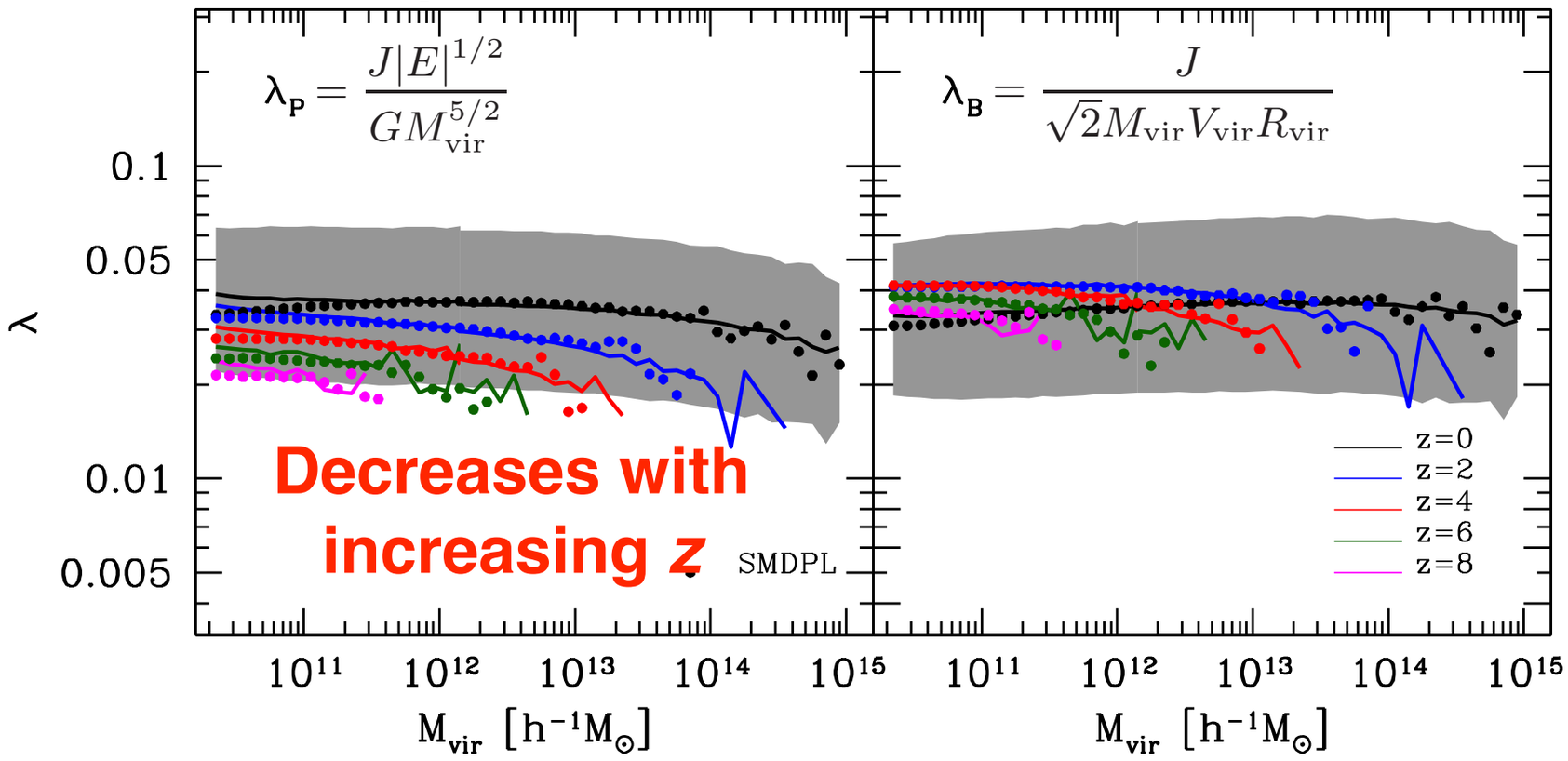

Medians are shown as the solid lines. At z = 0 the grey area is the 68% range.

We have released the halo catalogs and merger trees from Bolshoi-Planck and MultiDark-Planck cosmological simulations. Our paper includes Appendices with instructions for reading these files.

http://hipacc.ucsc.edu/Bolshoi/MergerTrees.html

Two Key Discoveries About Galaxies

Relationship Between Galaxy Stellar Mass and Halo Mass

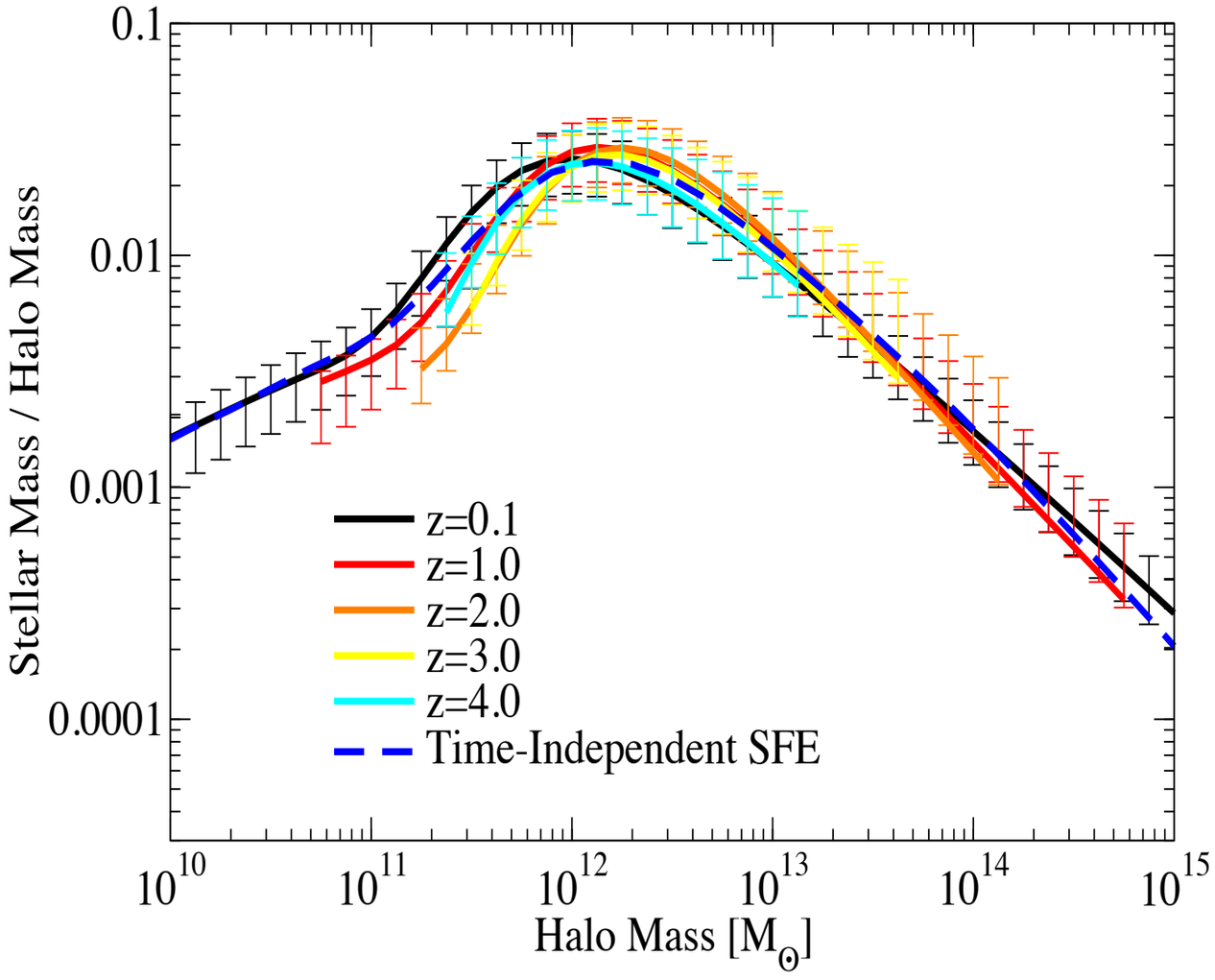

The stellar mass to halo mass ratio at multiple redshifts as derived from observations compared to the Bolshoi cosmological simulation. Error bars show 1σ uncertainties. A time-independent Star Formation Efficiency predicts a roughly **time-independent stellar mass to halo mass relationship**. (Behroozi, Wechsler, Conroy, ApJL 2013)

Star-forming Galaxies Lie on a "Main Sequence"

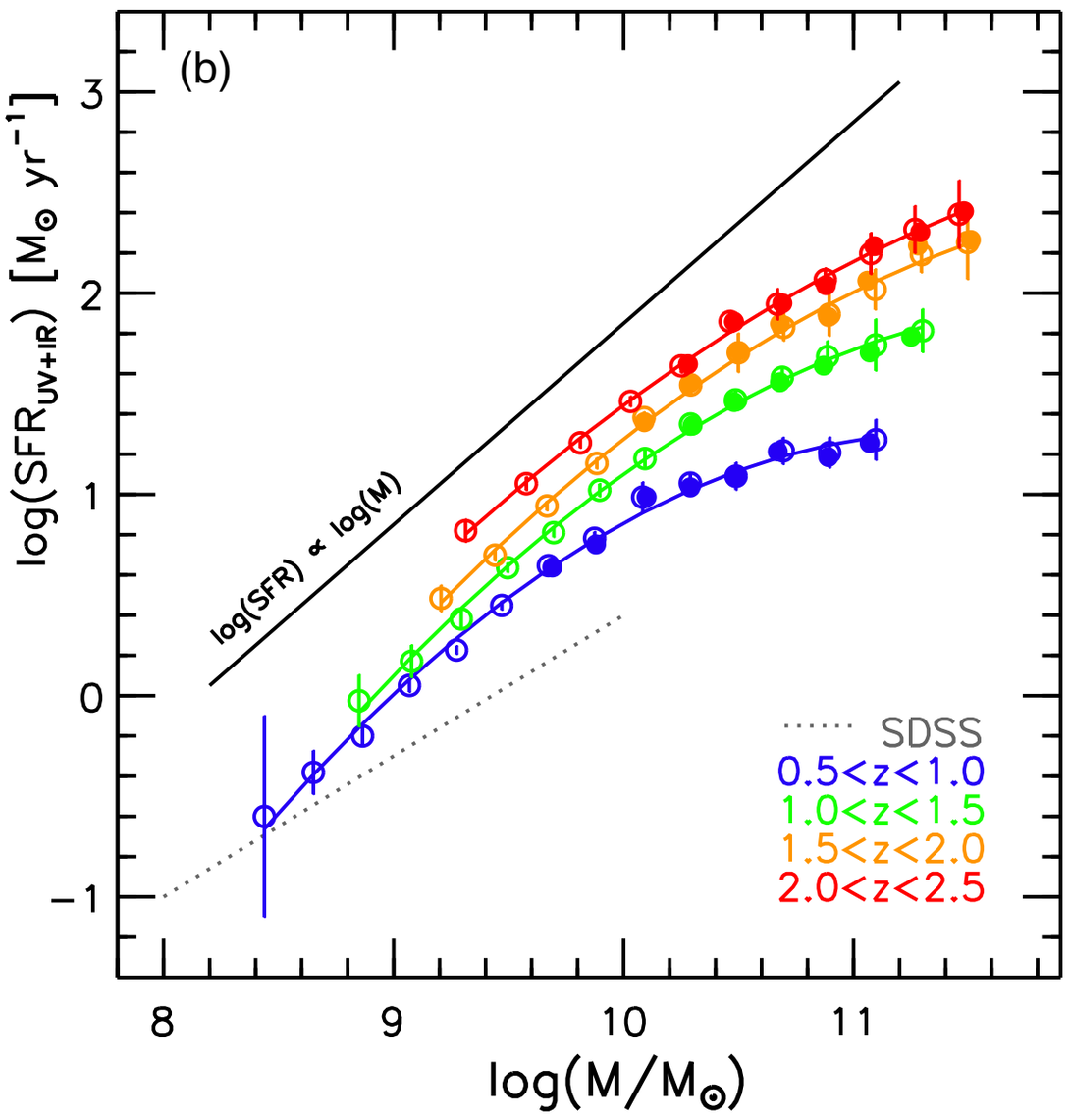

Just as the properties of hydrogen-burning stars are controlled by their mass, **the galaxy star formation rate (SFR) is approximately proportional to the stellar mass**, with the proportionality constant increasing with redshift up to about $z = 2.5$. (Whitaker et al. ApJ 2014)

Is Main Sequence SFR Controlled by Halo Mass Accretion?

by Aldo Rodríguez-Puebla, Joel Primack, Peter Behroozi, Sandra Faber **MNRAS 2016**

Halo mass accretion rates z=0 to 3

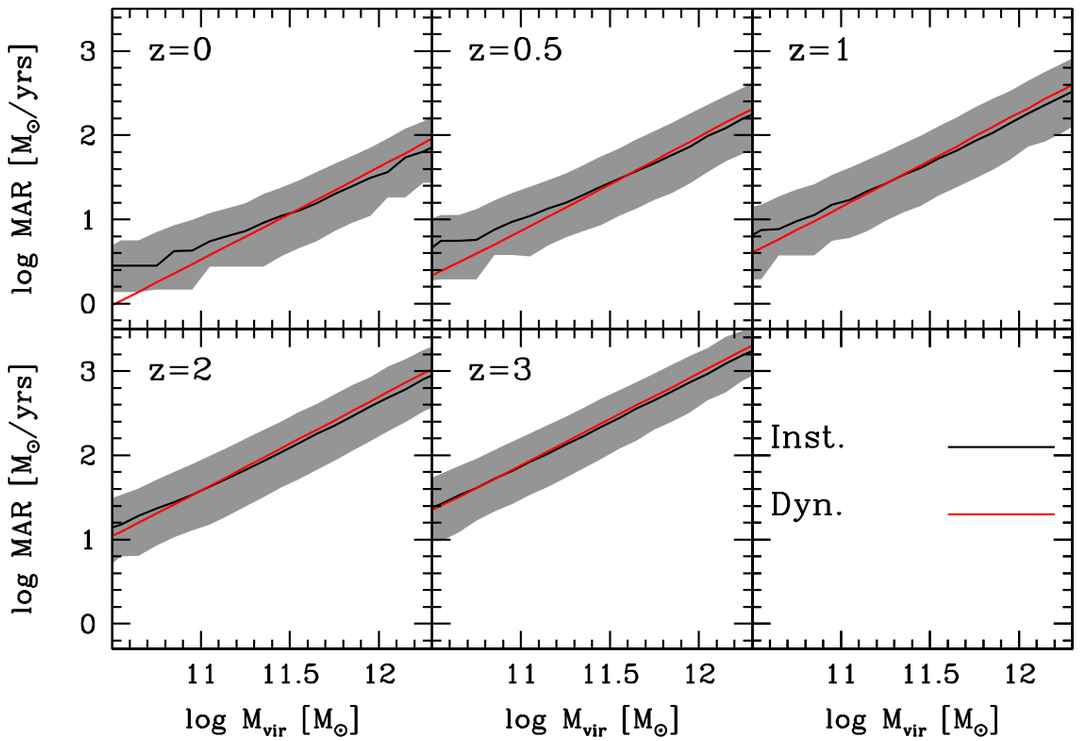

$$\frac{dM_*}{dt} = \frac{\partial M_*(M_{\rm vir}(t),z)}{\partial M_{\rm vir}}\frac{dM_{\rm vir}}{dt} + \frac{\partial M_*(M_{\rm vir}(t),z)}{\partial z}\frac{dz}{dt}$$

but if the M_*–M_{vir} relation is independent of redshift then the stellar mass of a central galaxy formed in a halo of mass $M_{vir}(t)$ is $M_* = M_*(M_{vir}(t))$ and the second term vanishes. From this relation star formation rates are given simply by

$$\frac{dM_*}{dt} = \frac{\partial M_*(M_{\rm vir}(t),z)}{\partial M_{\rm vir}}\frac{dM_{\rm vir}}{dt} = f_*\frac{d\log M_*}{d\log M_{\rm vir}}\frac{dM_{\rm vir}}{dt},$$

where $f_* = M_*/M_{vir}$. We call this **Stellar-Halo Accretion Rate Coevolution (SHARC)** if true halo-by-halo for star-forming galaxies.

Scatter of halo mass accretion rates

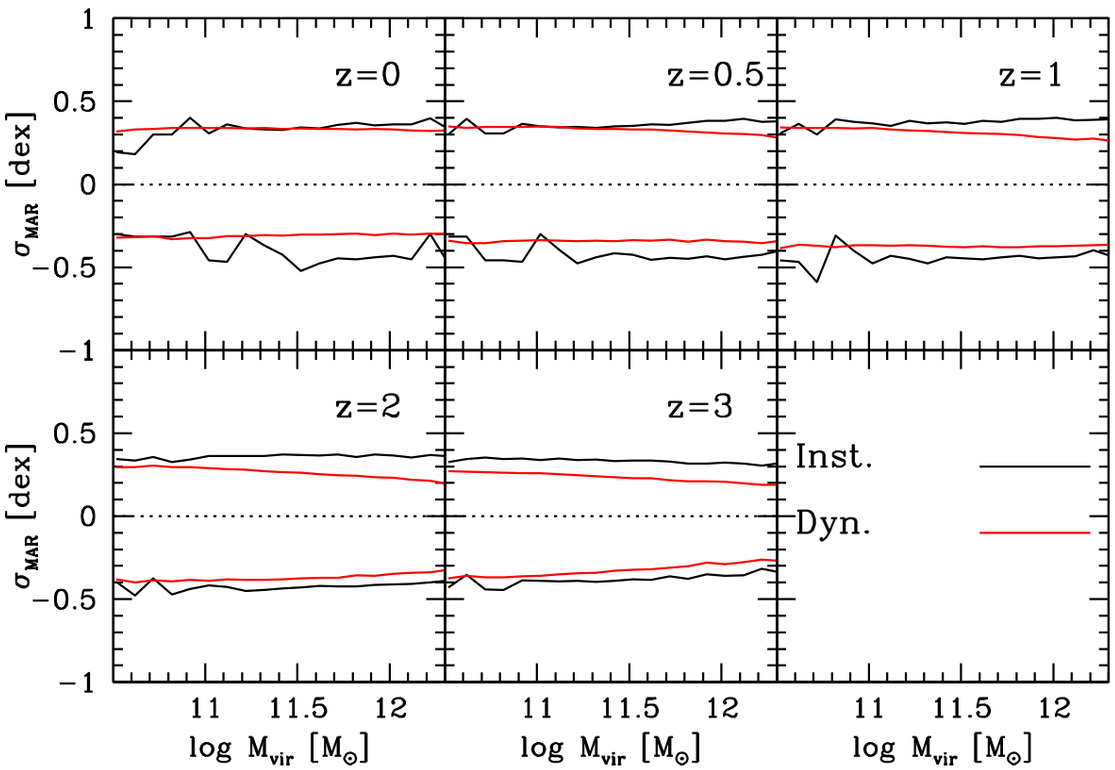

Implied scatter of star formation rates

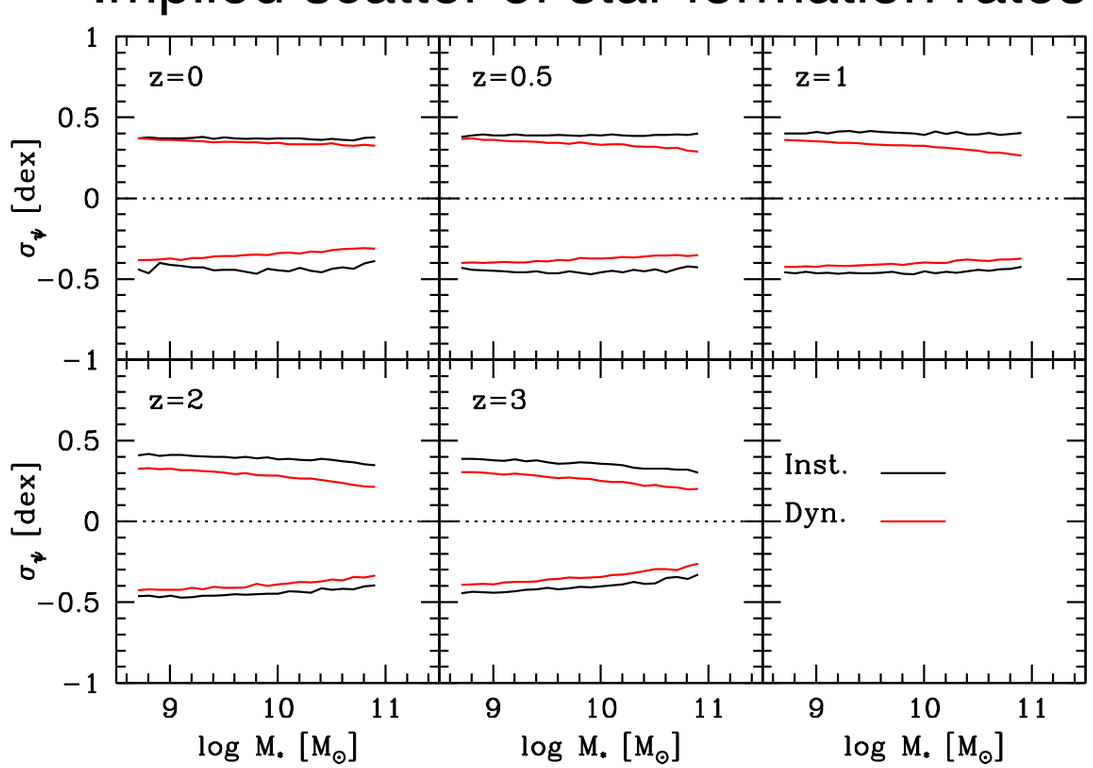

Consistent with observations!

Is Main Sequence SFR Controlled by Halo Mass Accretion?

by Aldo Rodríguez-Puebla, Joel Primack, Peter Behroozi, Sandra Faber **MNRAS 2016**

SHARC correctly predicts star formation rates to z ~ 4

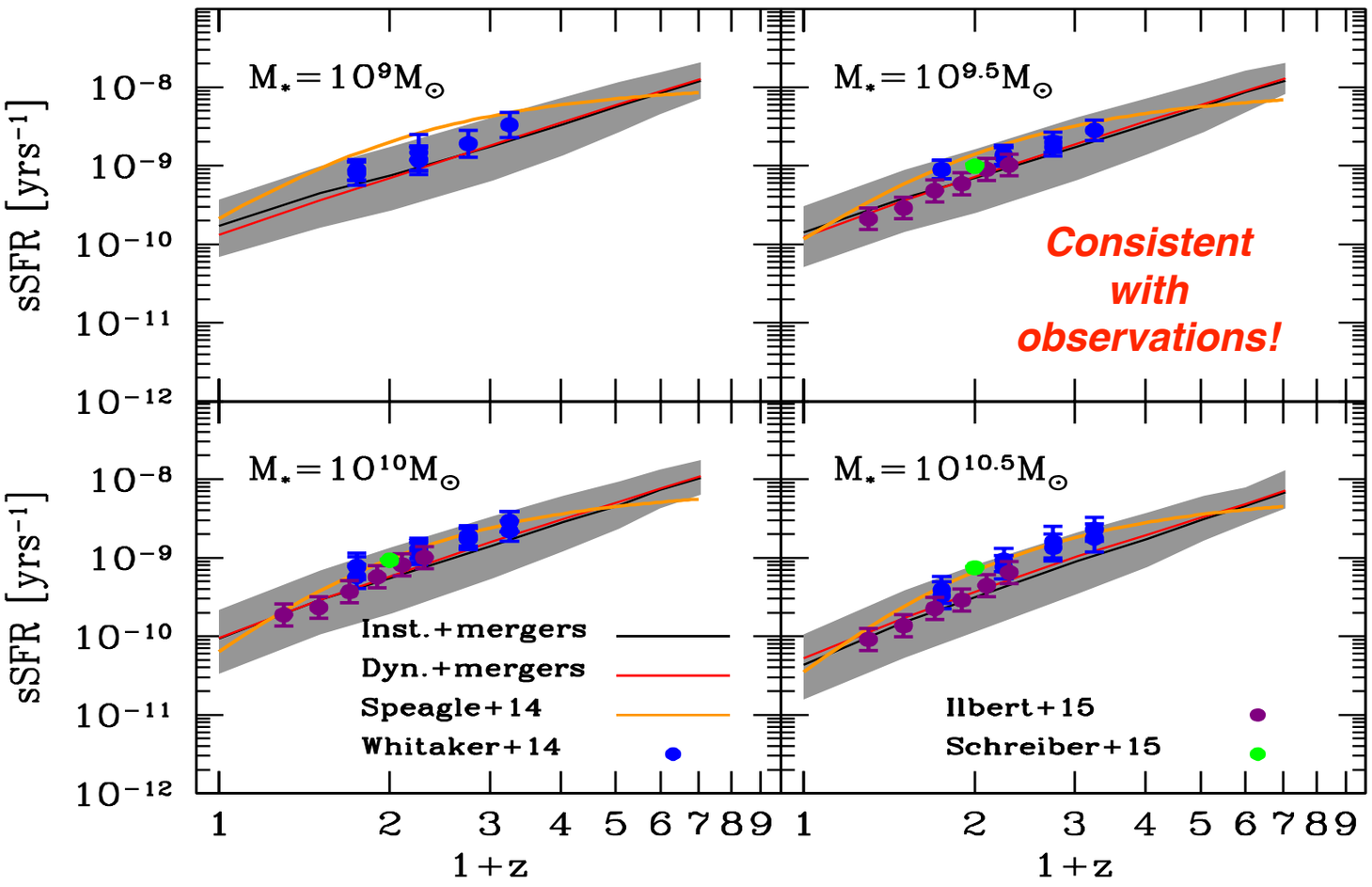

SHARC predicts "Age Matching" (blue galaxies in accreting halos) & "Galaxy SFR Conformity" at low z

Open Questions:

Extend SHARC to higher-mass galaxies

Also take quenching into account

Does SHARC correctly predict the growth rate of central galaxy stellar mass from the accretion rate of their halos? Test this in simulations!

We put **SHARC** in "bathtub" equilibrium models of galaxy formation & predict mass loading and metallicity evolution

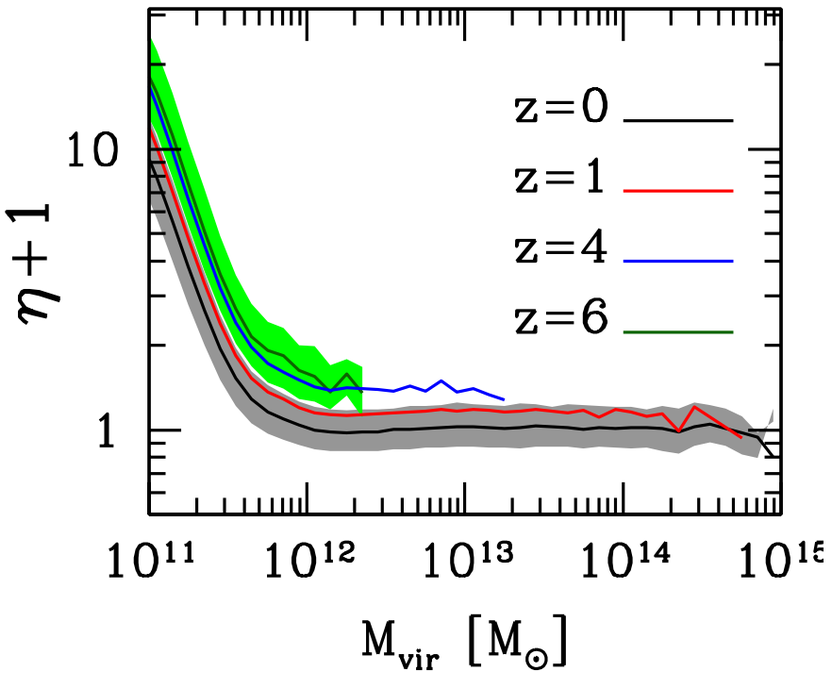

Net mass loading factor η from an equilibrium bathtub model (E+SHARC)

Constraining the Galaxy Halo Connection: Star Formation Histories, Galaxy Mergers, and Structural Properties, by Aldo Rodriguez-Puebla, Joel Primack, Vladimir Avila-Reese, and Sandra Faber MNRAS 470, 651 (2017)

We use results from the Bolshoi-Planck simulation (Aldo Rodriguez-Puebla, Peter Behroozi, Joel Primack, Anatoly Klypin, Christoph Lee, Doug Hellinger 2016, MNRAS 462, 893), including halo and subhalo abundance as a function of redshift and median halo mass growth for halos of given M_{vir} at z = 0. Our semi-empirical approach uses **SubHalo Abundance Matching (SHAM)**, which matches the cumulative galaxy stellar mass function (GSMF) to the cumulative stellar mass function to correlate galaxy stellar mass with (sub)halo mass.

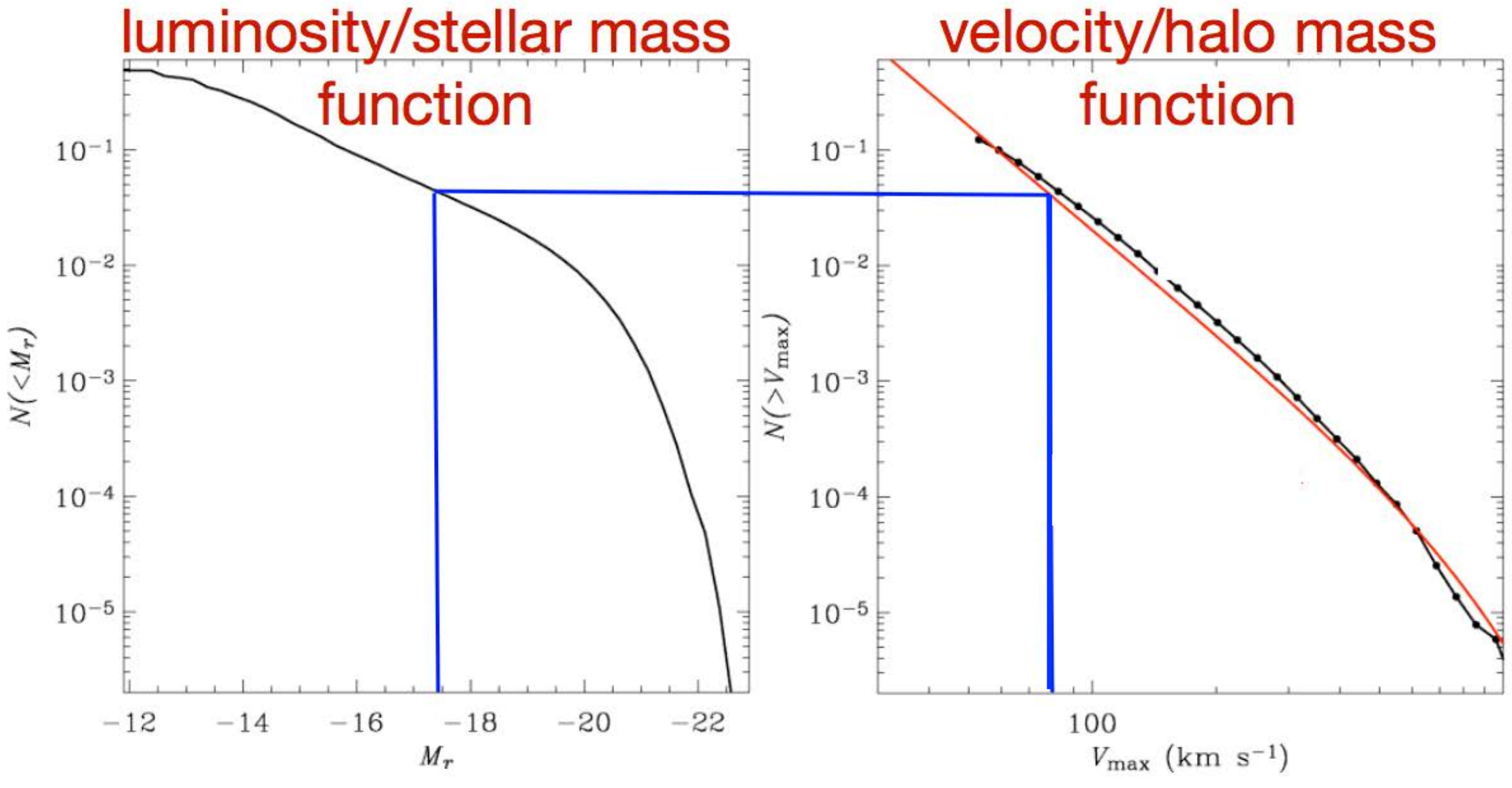

Assumptions: every halo hosts a galaxy, mass growth of galaxies is associated with that of halos

Constraining the Galaxy Halo Connection: Star Formation Histories, Galaxy Mergers, and Structural Properties

Aldo Rodriguez-Puebla, Joel Primack, Vladimir Avila-Reese, Sandra Faber

MNRAS 2017

Author	Redshift[a]	Ω [deg^2]	Corrections
Bell et al. (2003)	$z \sim 0.1$	462	I+SP+C
Yang, Mo & van den Bosch (2009a)	$z \sim 0.1$	4681	I+SP+C
Li & White (2009)	$z \sim 0.1$	6437	I+P+C
Bernardi et al. (2010)	$z \sim 0.1$	4681	I+SP+C
Bernardi et al. (2013)	$z \sim 0.1$	7748	I+SP+C
Rodriguez-Puebla et al. in prep	$z \sim 0.1$	7748	S
Drory et al. (2009)	$0 < z < 1$	1.73	SP+C
Moustakas et al. (2013)	$0 < z < 1$	9	SP+D+C
Pérez-González et al. (2008)	$0.2 < z < 2.5$	0.184	I+SP+D+C
Tomczak et al. (2014)	$0.2 < z < 3$	0.0878	C
Ilbert et al. (2013)	$0.2 < z < 4$	2	C
Muzzin et al. (2013)	$0.2 < z < 4$	1.62	I+C
Santini et al. (2012)	$0.6 < z < 4.5$	0.0319	I+C
Mortlock et al. (2011)	$1 < z < 3.5$	0.0125	I+C
Marchesini et al. (2009)	$1.3 < z < 4$	0.142	I+C
Stark et al. (2009)	$z \sim 6$	0.089	I
Lee et al. (2012)	$3 < z < 7$	0.089	I+SP+C
González et al. (2011)	$4 < z < 7$	0.0778	I+C
Duncan et al. (2014)	$4 < z < 7$	0.0778	C
Song et al. (2015)	$4 < z < 8$	0.0778	I
This paper, Appendix D	$4 < z < 10$	0.0778	–

I=IMF; P= photometry corrections; S=Surface Brightness correction; D=Dust model; NE= Nebular Emissions: SP = SPS Model: C = Cosmology

Author	Redshift[a]	SFR Estimator	Corrections	Type
Chen et al. (2009)	$z \sim 0.1$	H_α/H_β	S	All
Salim et al. (2007)	$z \sim 0.1$	UV SED	S	All
Noeske et al. (2007)	$0.2 < z < 1.1$	UV+IR	S	All
Karim et al. (2011)	$0.2 < z < 3$	1.4 GHz	I+S+E	All
Dunne et al. (2009)	$0.45 < z < 2$	1.4 GHz	I+S+E	All
Kajisawa et al. (2010)	$0.5 < z < 3.5$	UV+IR	I	All
Whitaker et al. (2014)	$0.5 < z < 3$	UV+IR	I+S	All
Sobral et al. (2014)	$z \sim 2.23$	H_α	I+S+SP	SF
Reddy et al. (2012)	$2.3 < z < 3.7$	UV+IR	I+S+SP	SF
Magdis et al. (2010)	$z \sim 3$	FUV	I+S+SP	SF
Lee et al. (2011)	$3.3 < z < 4.3$	FUV	I+SP	SF
Lee et al. (2012)	$3.9 < z < 5$	FUV	I+SP	SF
González et al. (2012)	$4 < z < 6$	UV+IR	I+NE	SF
Salmon et al. (2015)	$4 < z < 6$	UV SED	I+NE+E	SF
Bouwens et al. (2011)	$4 < z < 7.2$	FUV	I+S	SF
Duncan et al. (2014)	$4 < z < 7$	UV SED	I+NE	SF
Shim et al. (2011)	$z \sim 4.4$	H_α	I+S+SP	SF
Steinhardt et al. (2014)	$z \sim 5$	UV SED	I+S	SF
González et al. (2010)	$z = 7.2$	UV+IR	I+NE	SF
This paper, Appendix D	$4 < z < 8$	FUV	I+E+NE	SF

I=IMF; S=Star formation calibration; E=Extinction; NE= Nebular Emissions; SP=SPS Model

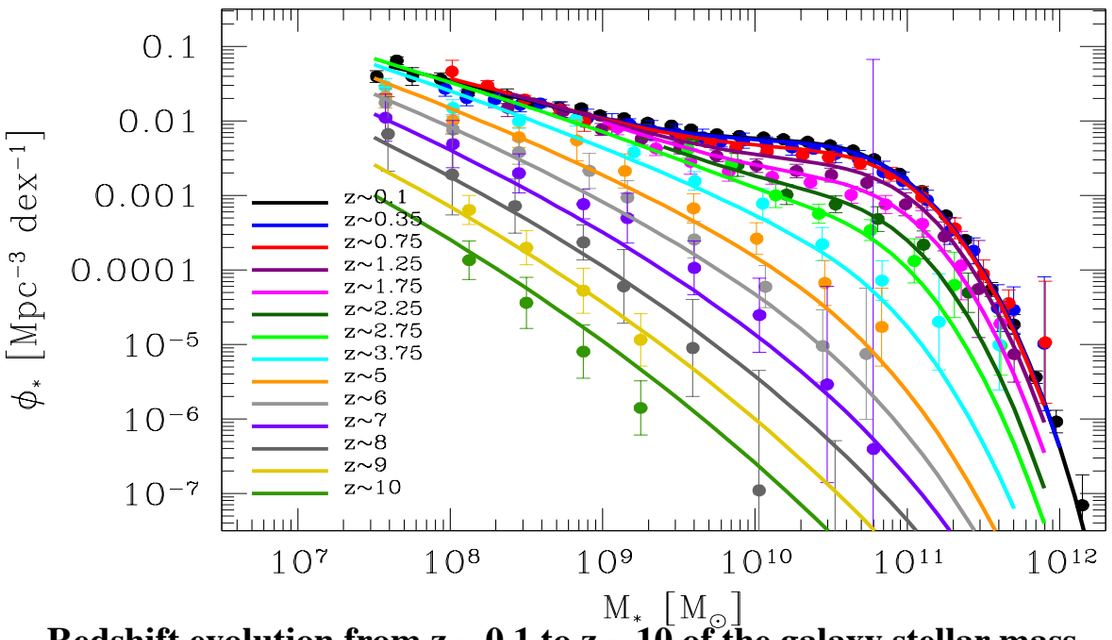

Redshift evolution from z ~ 0.1 to z ~ 10 of the galaxy stellar mass function derived by using 20 observational samples from the literature and represented by filled circles with error bars. The various data has been corrected for potential systematics that could affect our results. Solid lines are the best fit model from a set of 3×10^5 MCMC trials.

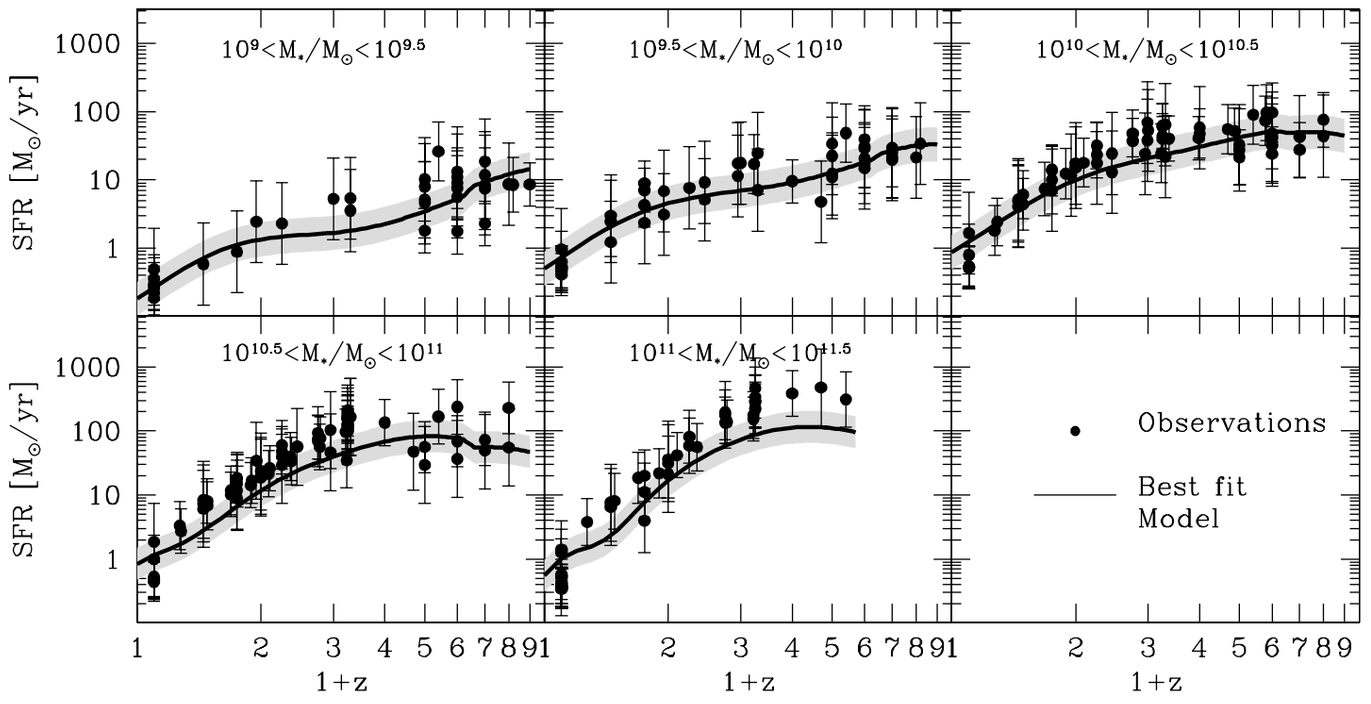

Star formation rates as a function of redshift z in five stellar mass bins. Filled circles with error bars show the observed data. Black solid lines show our best fit model to the SFRs.

Constraining the Galaxy Halo Connection: Star Formation Histories, Galaxy Mergers, and Structural Properties

Aldo Rodriguez-Puebla, Joel Primack, Vladimir Avila-Reese, Sandra Faber

MNRAS 2017

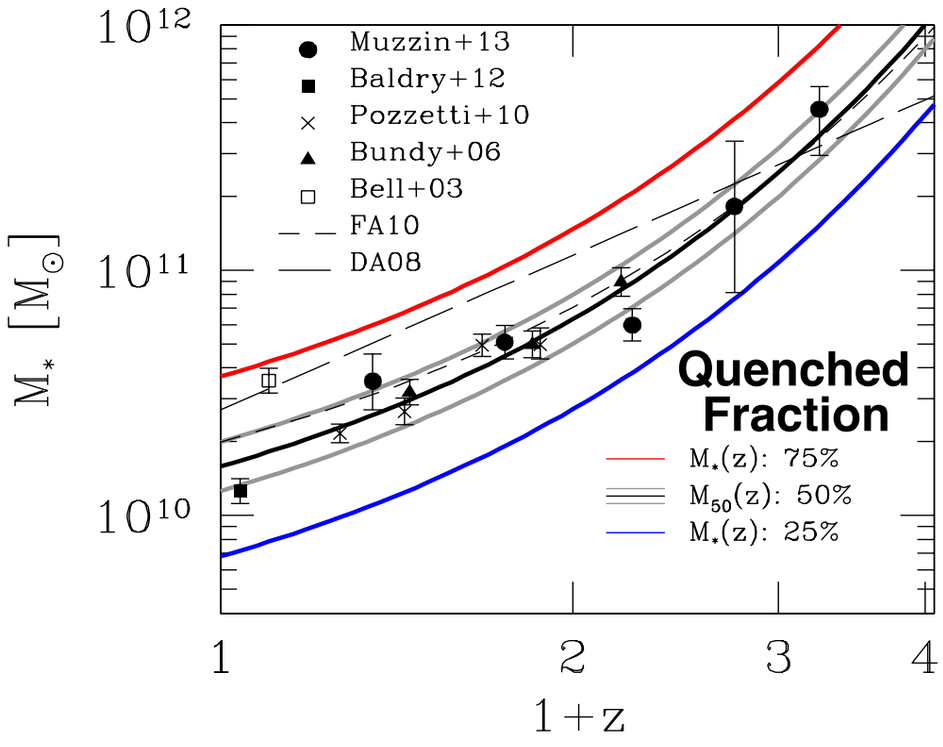

Average Stellar Mass Halo Mass Relation

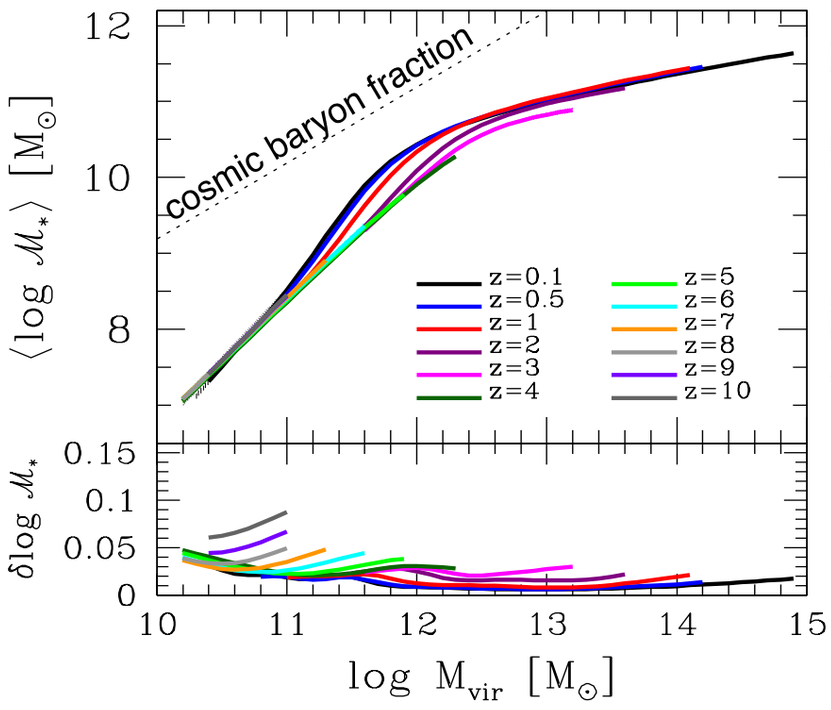

Star Formation Rate Density

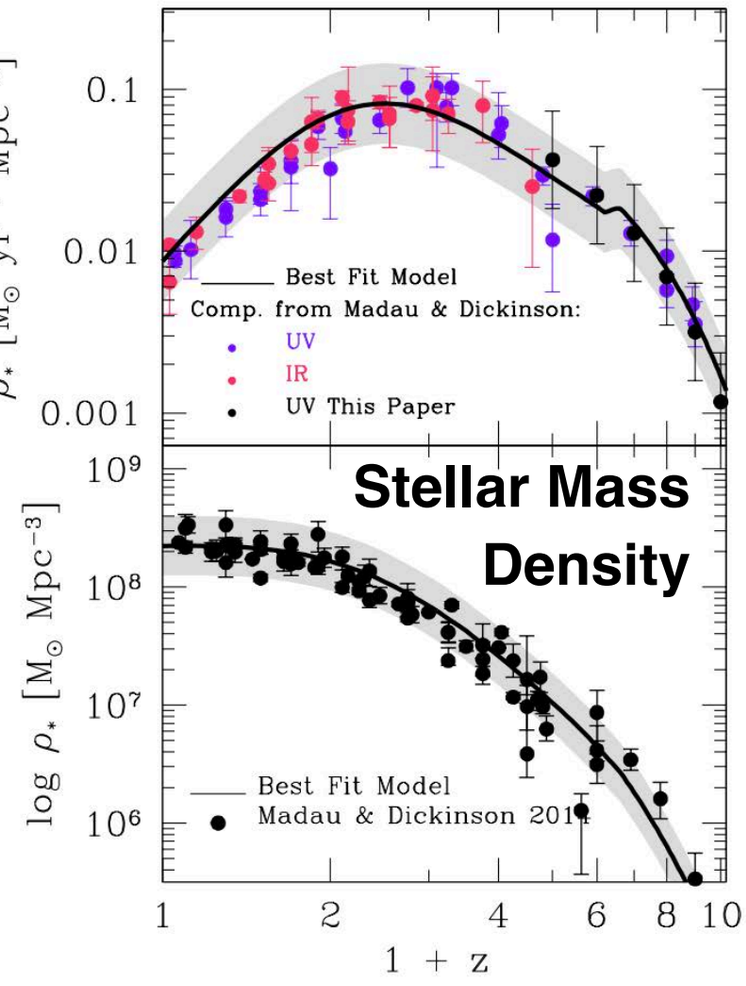

Median Halo Growth

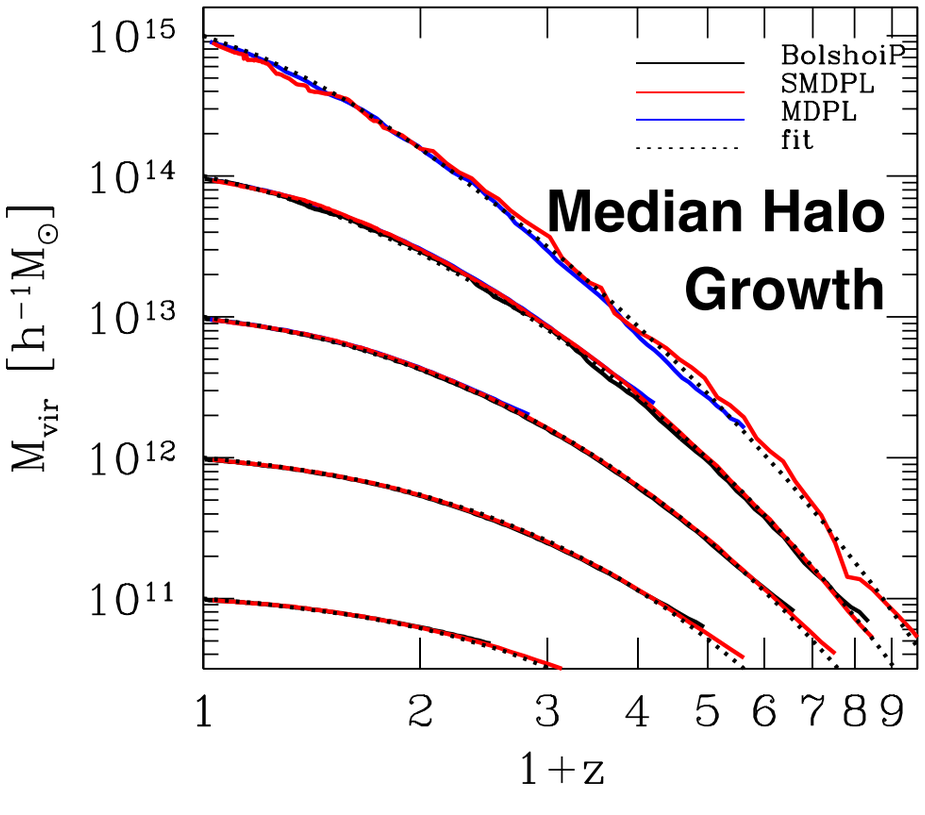

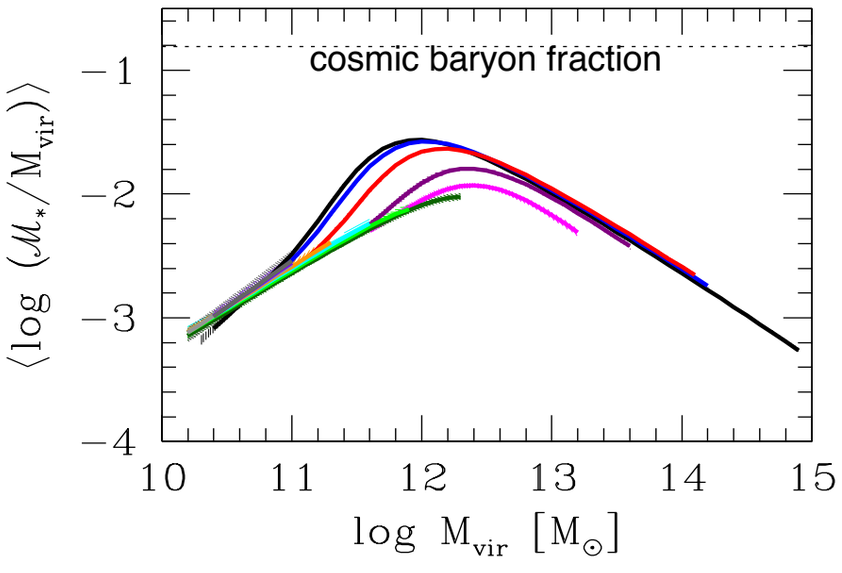

Constraining the Galaxy Halo Connection: Star Formation Histories, Galaxy Mergers, and Structural Properties

Aldo Rodriguez-Puebla, Joel Primack, Vladimir Avila-Reese, Sandra Faber **MNRAS 2017**

SFR vs. M*, M_{vir}, and *z*

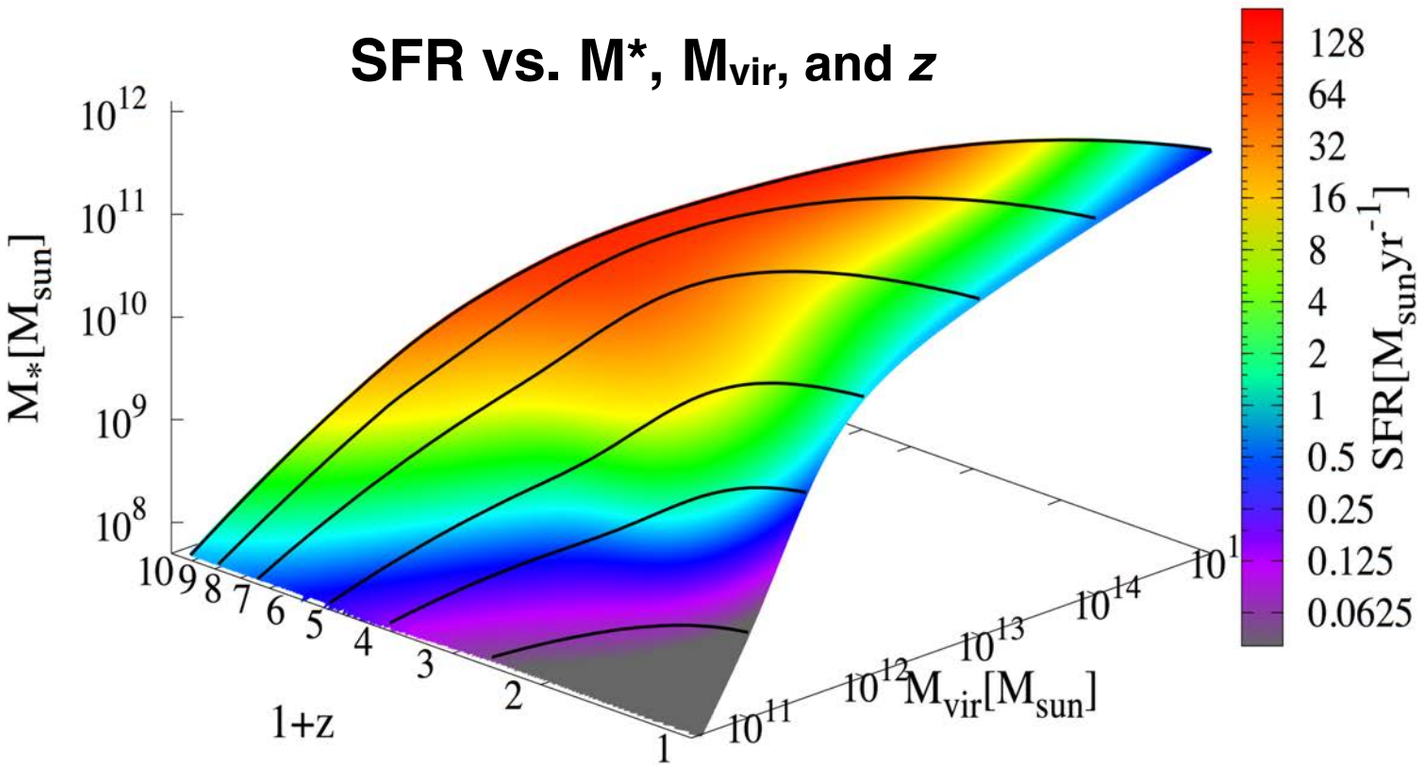

Stellar Mass-Halo Mass Relation

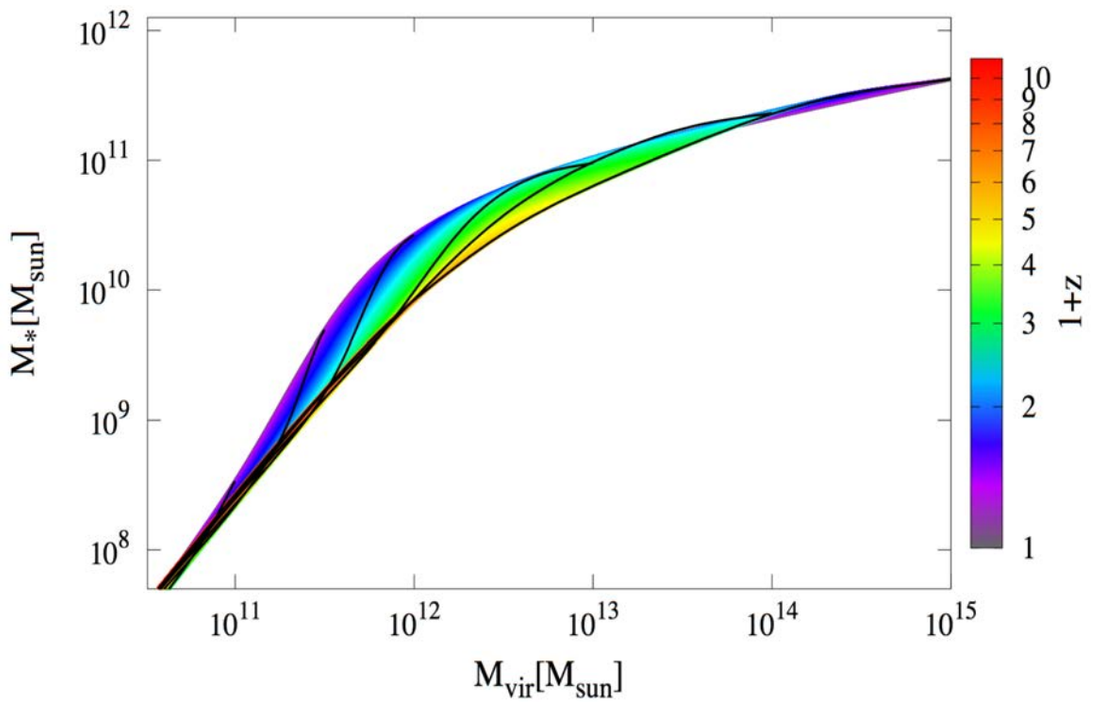

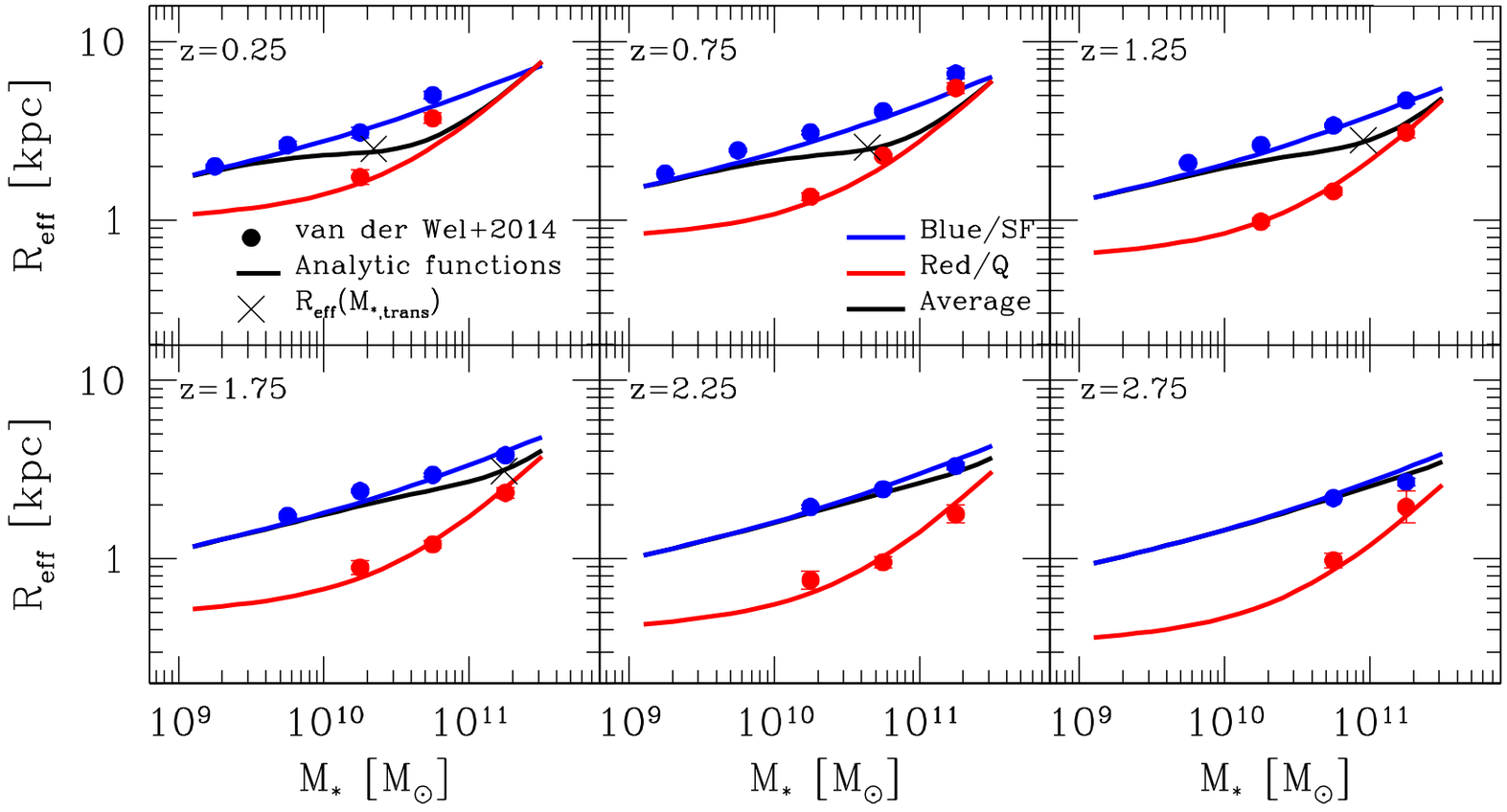

Galaxy Radial Stellar Mass Distribution

Solid lines show the CANDELS redshift *z* dependence of R_e vs. M_* for blue and red galaxies, which matches the local relation by Mosleh, Williams & Franx (2013) based on the MPA-JHU SDSS DR7. The black solid lines show the average circularized effective radius as a function of stellar mass. The crosses show the effective radius at M_{50}, the stellar mass at which the quenched fraction of galaxies is 50%. We utilize the plotted redshift dependences as an input to derive the average galaxy's radial mass distribution as a function of stellar mass by assuming that blue/star-forming galaxies have a Sersic index n = 1 while red/ quenched galaxies have a Sersic index n = 4.

Constraining the Galaxy Halo Connection: Star Formation Histories, Galaxy Mergers, and Structural Properties

Aldo Rodriguez-Puebla, Joel Primack, Vladimir Avila-Reese, Sandra Faber **MNRAS 2017**

We infer galaxy merger rates from halo mergers

Change in slope in R_{eff} - M_* diagram after quenching, consistent with uptick in minor merger rate and galaxy minor merger simulations

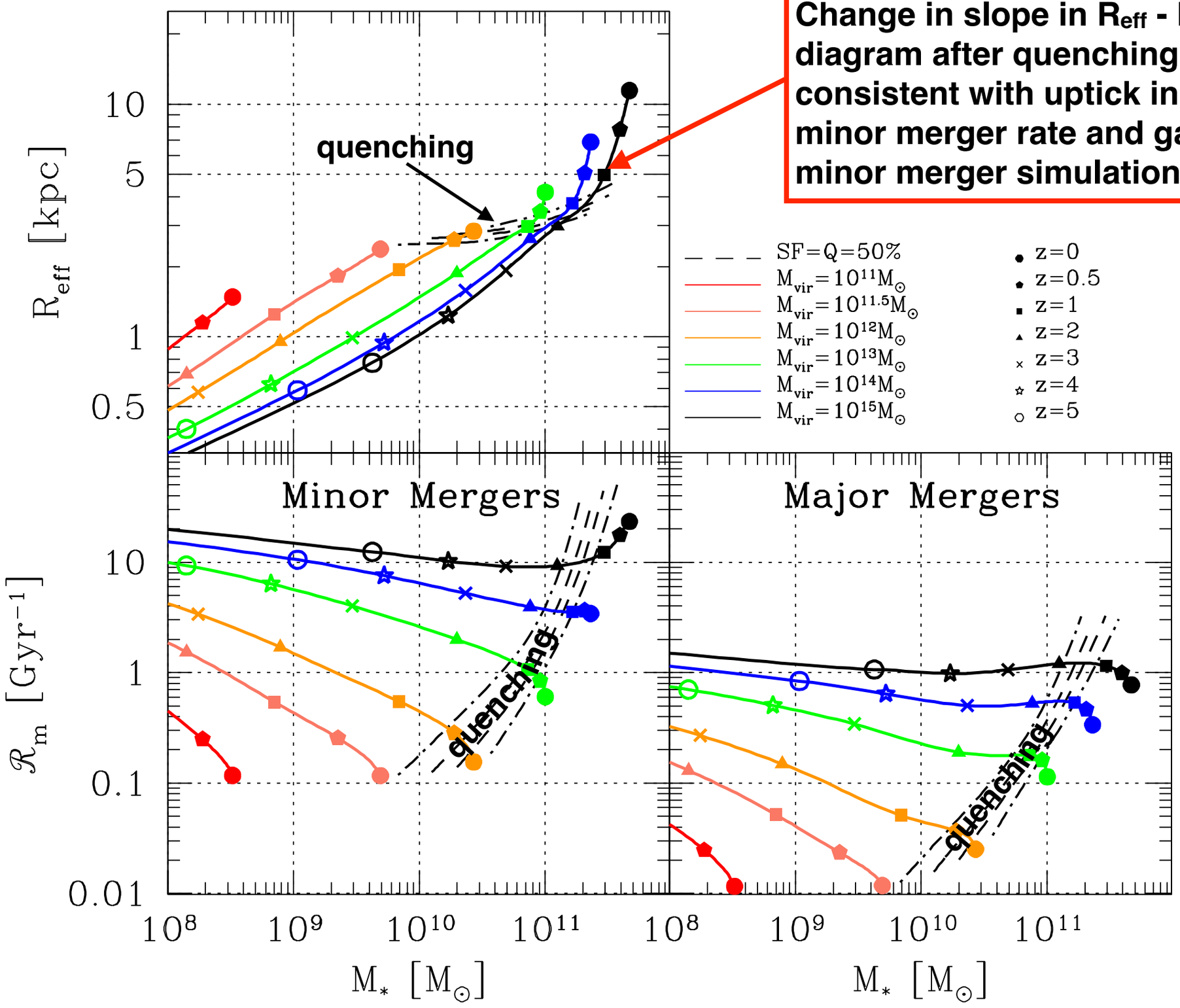

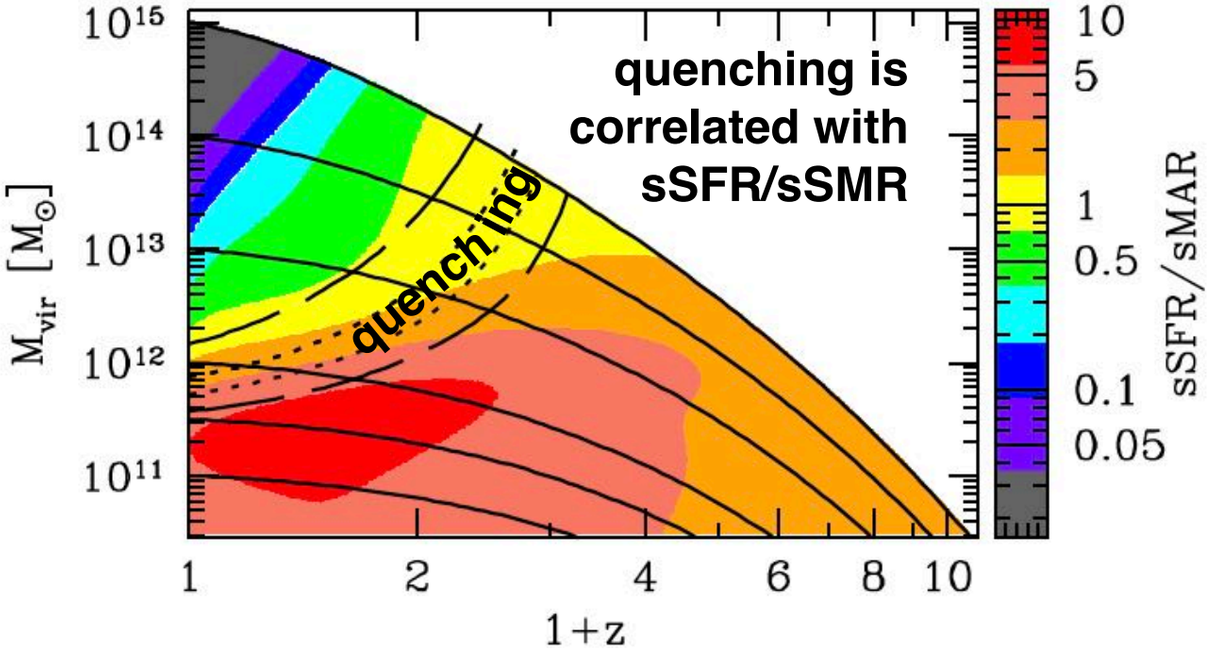

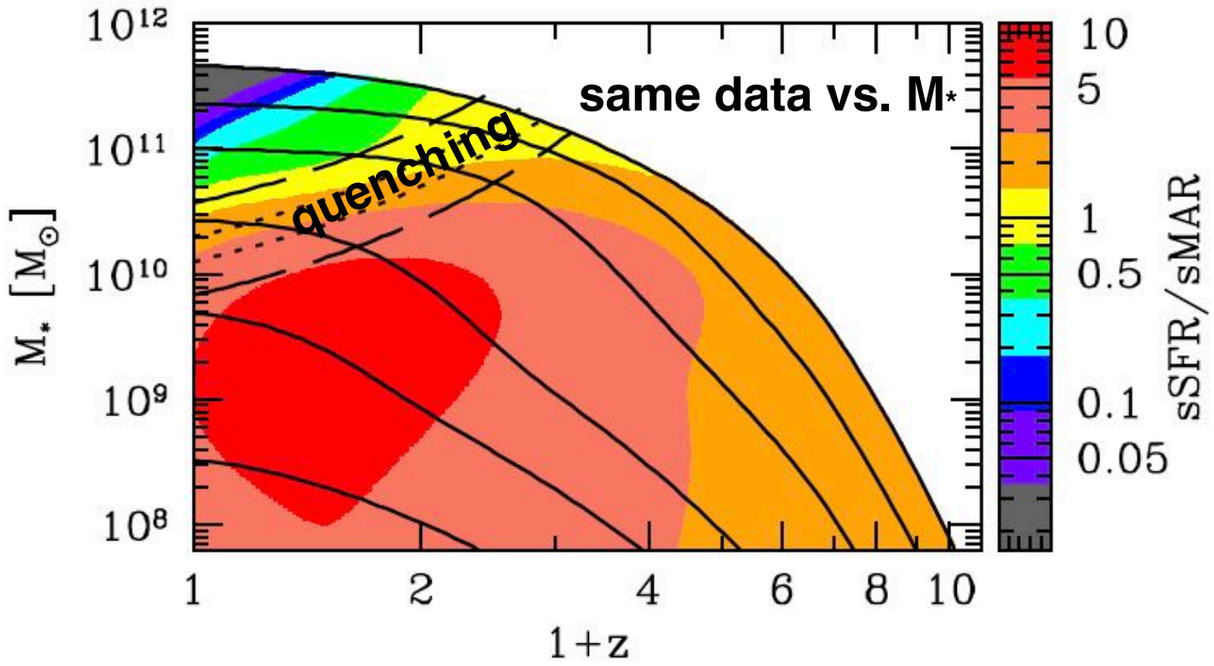

This figure shows that quenching is correlated with sSFR/sSMR = t_{halo}/t_*, since sSFR/sSMR and quenching curves are nearly parallel. sSFR/sSMR
- first rises, reaching a peak ~2 at z ~ 3 for 10^{13} halos, a peak ~7 for 10^{12} halos at z~1.5, and 10^{11} halos are still at peak sSFR/sSMR ~ 10
- then declines along all Mvir and M* progenitor tracks toward z=0.

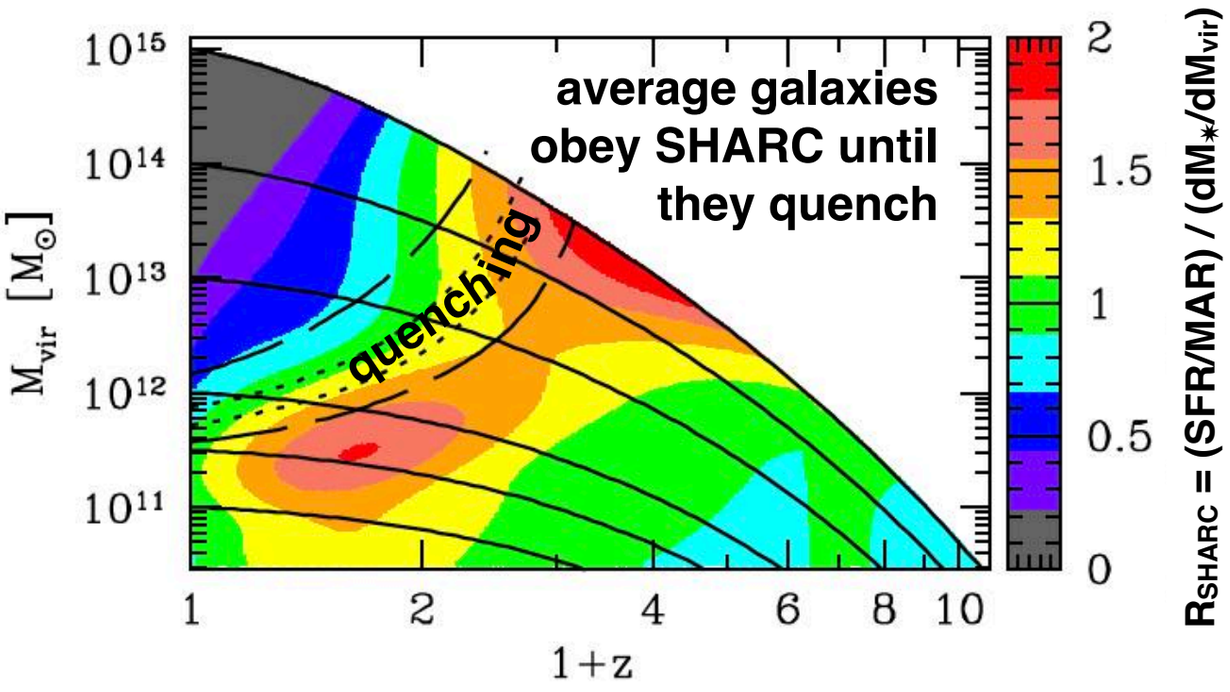

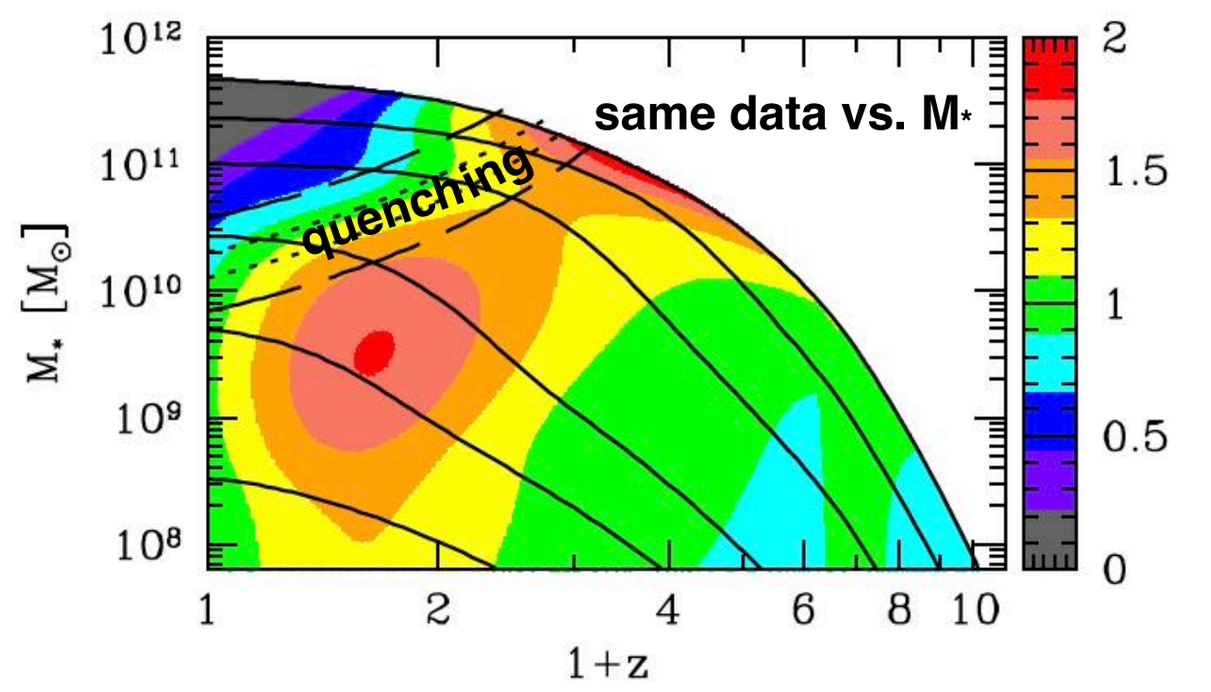

This figure shows that the SHARC approximation is rather well satisfied until quenching, the SHARC ratio R_{SHARC} = (SFR / MAR) / (dM_{vir}/dlog M*) having a value of about 1 to 2 along the progenitor trajectories, and then dropping after quenching. This shows quenching is correlated with R_{SHARC} :

- **the fraction of quenched galaxies is ~ 50% when R_{SHARC} ~ 1 to 1.5, and the quenched fraction is > 75% when R_{SHARC} drops to ~1**
- **like sSFR/sSMR, R_{SHARC} first rises along all progenitor curves, reaches a peak at higher z for higher mass (Mvir or M*), and then declines**
- **unlike sSFR/sSMR, the peak SHARC ratio is nearly constant between 1.5 and 2 (the SHARC ratio peaks at about 2 for both $10^{11.5}$ halos at z ~ 0.5 and 10^{15} halos at z ~ 3, and at about 1.5 for intermediate mass halos).**

Note: the SHARC formula is SFR = (dM_*/dM_{vir}) MAR where MAR = dM_{vir}/dt. Define R_{SHARC} = (SFR / MAR) / (dM_*/dM_{vir}), so SHARC ==> R_{SHARC} = 1.

Constraining the Galaxy Halo Connection: Star Formation Histories, Galaxy Mergers, and Structural Properties

Aldo Rodriguez-Puebla, Joel Primack, Vladimir Avila-Reese, Sandra Faber **MNRAS 2017**

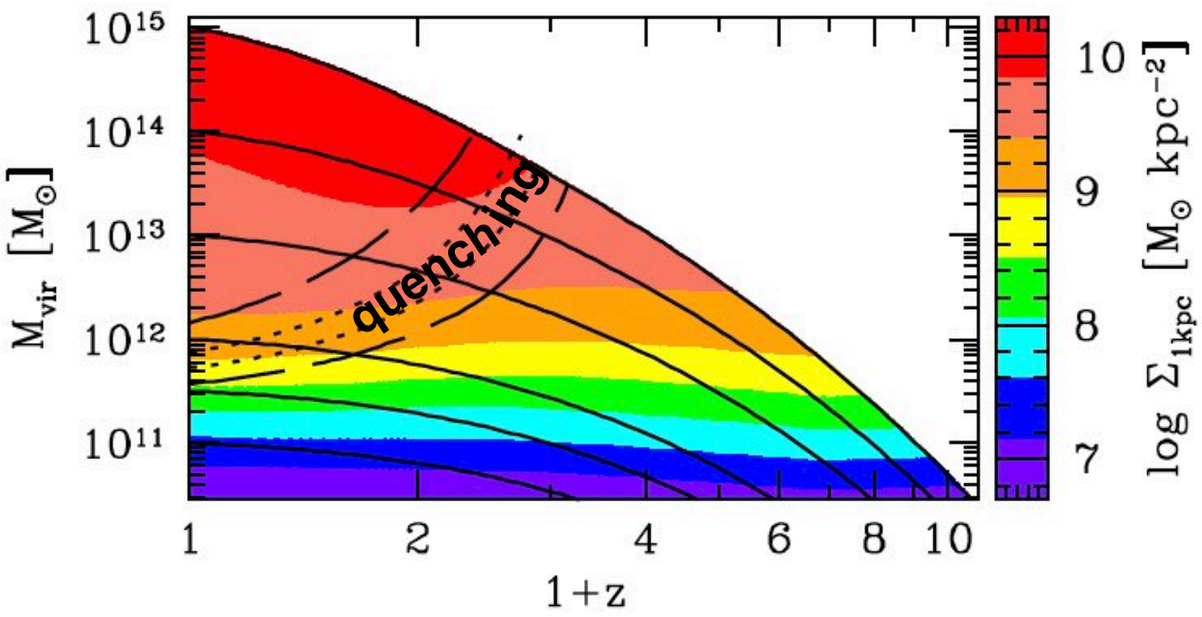

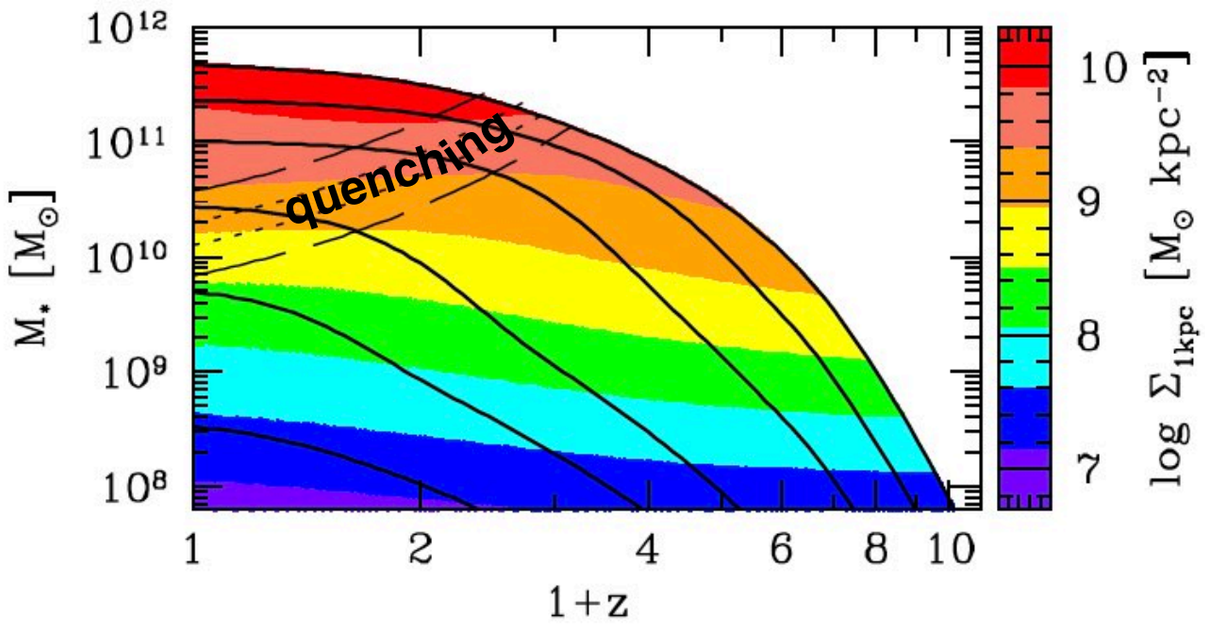

This figure (and the left panel below) shows that Σ_1 reaching a maximum correlates with quenching:

- **Σ_1 at the quenching transition rises steadily with M_{vir} and reaches maximum at lower z for lower M_{vir} — "quenching downsizing"**
- **That the progenitor tracks are parallel to the trajectory curves shows that Σ_1 remains constant after it reaches its maximum**

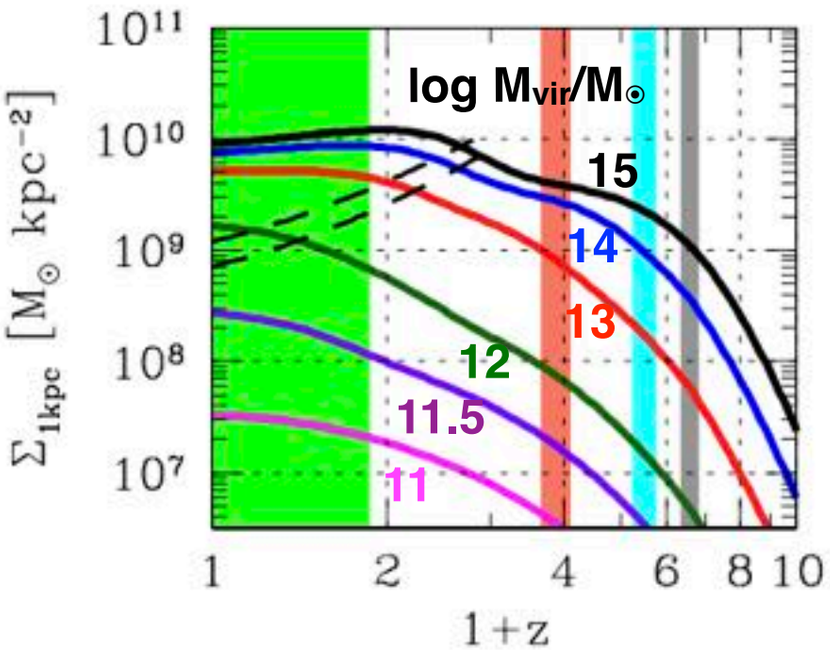

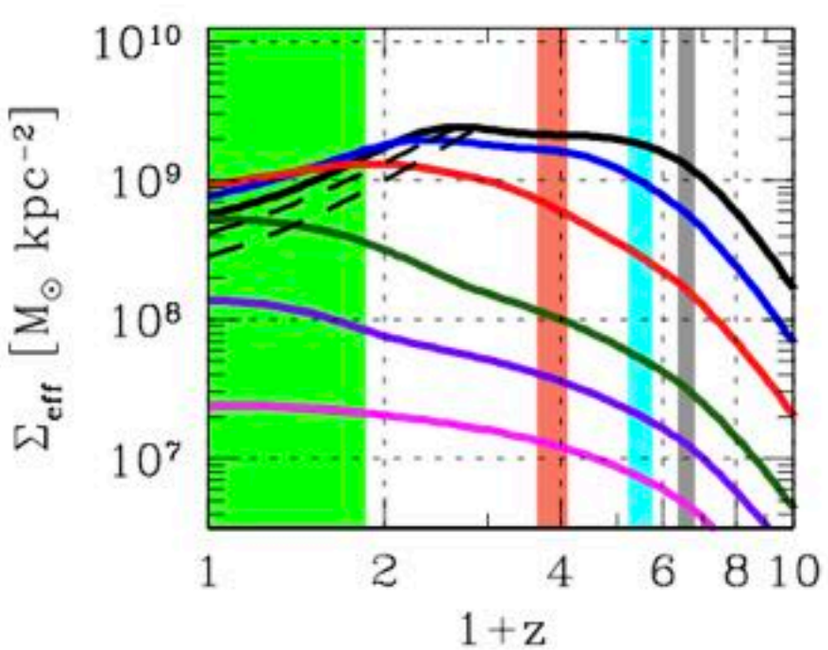

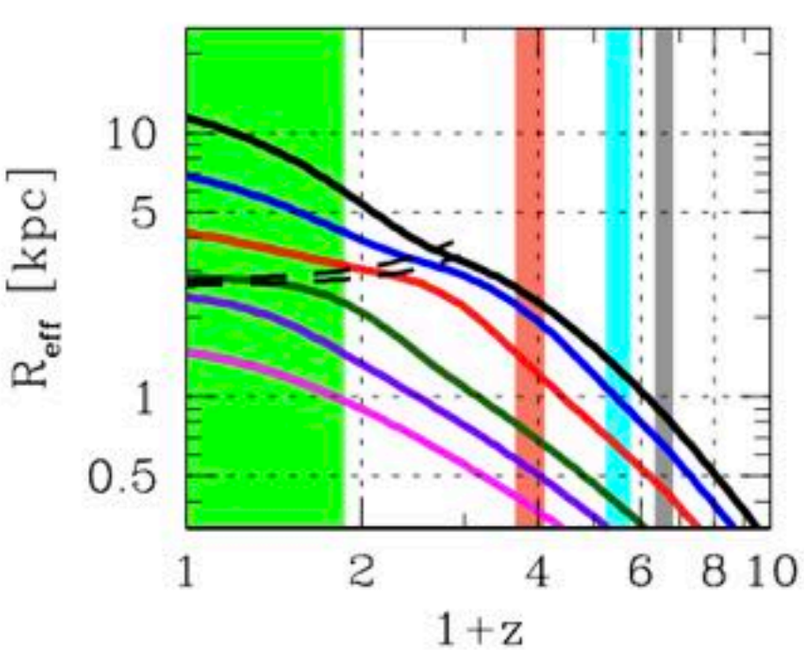

The right panel shows that R_{eff} steadily rises along halo trajectories, and quenching typically occurs when $R_{eff} \approx 3$ kpc. Although Σ_1 is flat after quenching, the middle panel shows that Σ_{eff} declines after quenching as R_{eff} increases.

https://132.248.1.39/galaxy/galaxy_halo.html

The Galaxy-Halo Connection Project

How can I help you?

Does the Galaxy-Halo Connection Vary with Environment?

Radu Dragomir[1⋆], Aldo Rodríguez-Puebla[2,3]†, Joel R. Primack[1]‡, Christoph T. Lee[1]§
[1] *Physics Department, University of California, Santa Cruz, CA 95064, USA*
[2] *Department of Astronomy & Astrophysics, University of California at Santa Cruz, Santa Cruz, Ca 95064, USA*
[3] *Instituto de Astronomía, Universidad Nacional Autónoma de México, A. P. 70-264, 04510, México, D.F., México*

MNRAS 2018

ABSTRACT SubHalo Abundance Matching (SHAM) assumes that one (sub)halo property, such as mass M_{vir} or peak circular velocity V_{peak}, determines properties of the galaxy hosted in each (sub)halo such as its luminosity or stellar mass. This assumption implies that the dependence of Galaxy Luminosity Functions (GLFs) and the Galaxy Stellar Mass Function (GSMF) on environmental density is determined by the corresponding halo density dependence. In this paper, we test this by determining from an SDSS sample the observed dependence with environmental density of the *ugriz* GLFs and GSMF for all galaxies, and for central and satellite galaxies separately. We then show that the SHAM predictions are in remarkable agreement with these observations, even when the galaxy population is divided between central and satellite galaxies. However, we show that SHAM fails to reproduce the correct dependence between environmental density and color for all galaxies and central galaxies, although it correctly reproduces the color dependence on environmental density of satellite galaxies.

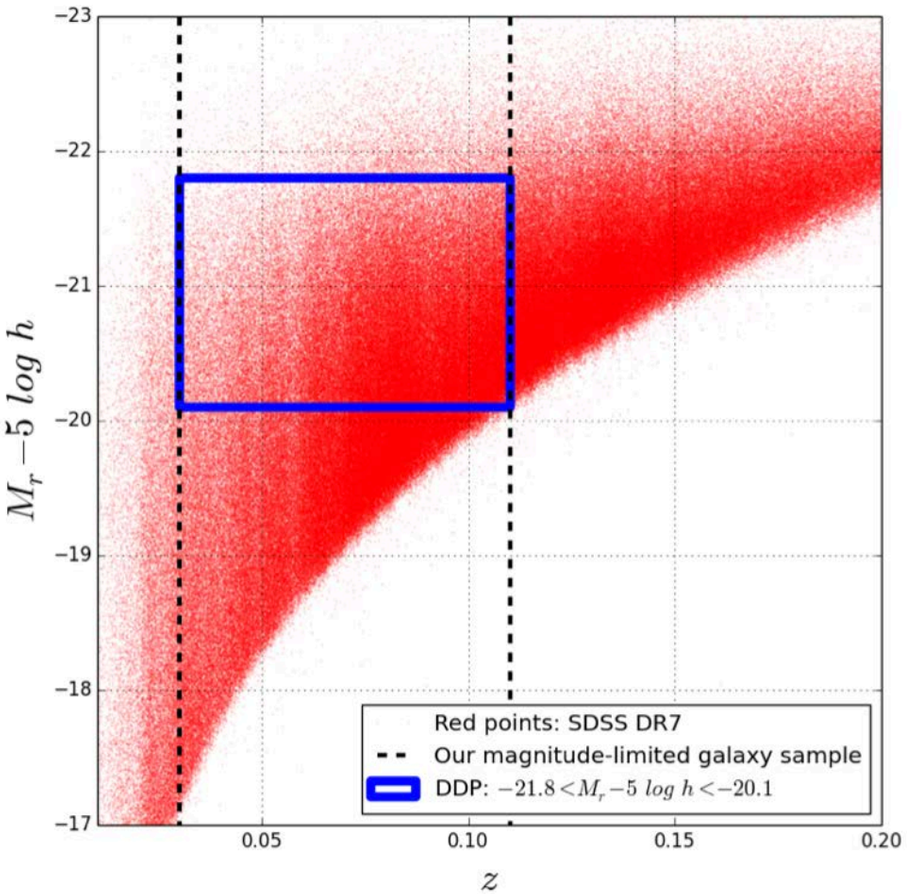

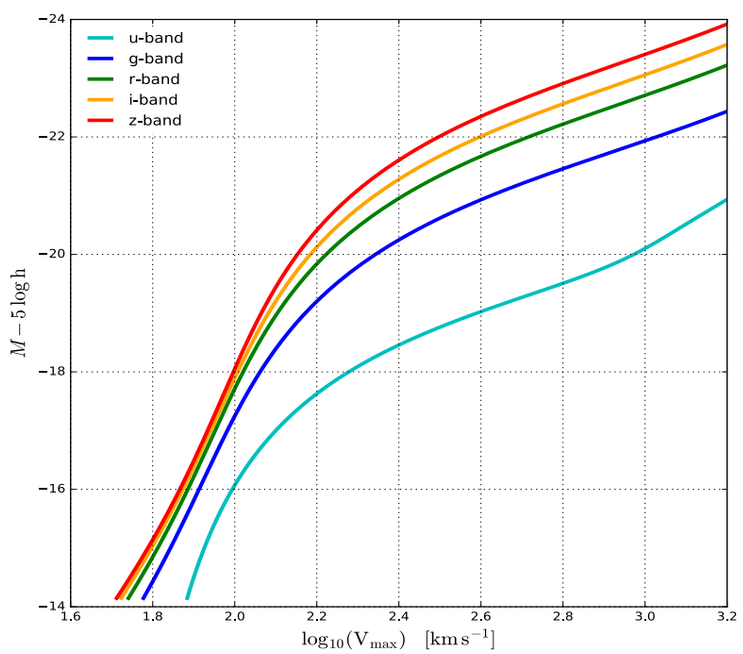

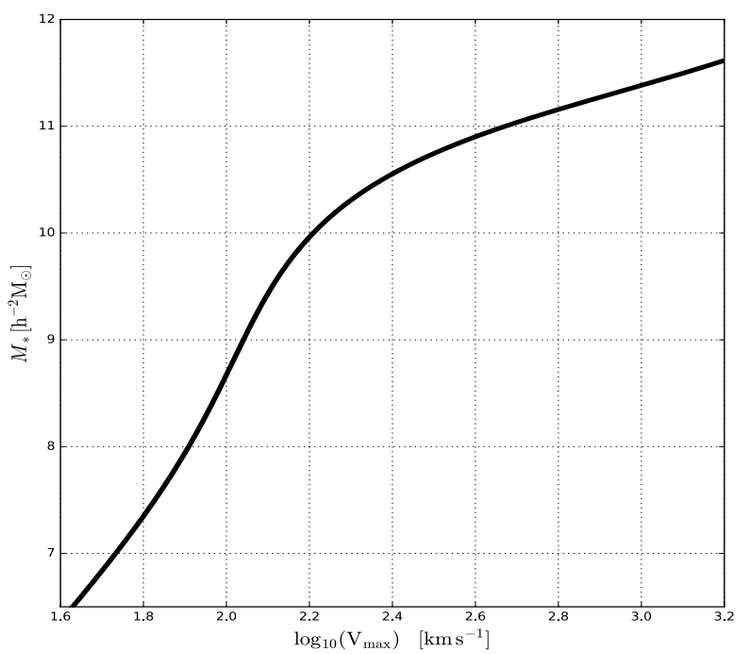

Figure 3. Left Panel: Luminosity-to-$V_{\rm max}$ relation from SHAM. The different colors indicate the band utilized for the match. **Right Panel:** Stellar mass-to-$V_{\rm max}$ relation. Recall that SHAM assumes that these relations are valid for centrals as well as for satellites. We report these values in Table A1.In the case of centrals $V_{\rm max}$ refers to the halo maximum circular velocity, while for satellites $V_{\rm max}$ represents the highest maximum circular velocity ($V_{\rm peak}$) reached along the subhalo's main progenitor branch. SHAM assumes that $V_{\rm max}$ fully determines these statistical properties of the galaxies.

Does the Galaxy-Halo Connection Vary with Environment?

Radu Dragomir, Aldo Rodriguez-Puebla, Joel Primack, Christoph Lee

MNRAS 2018

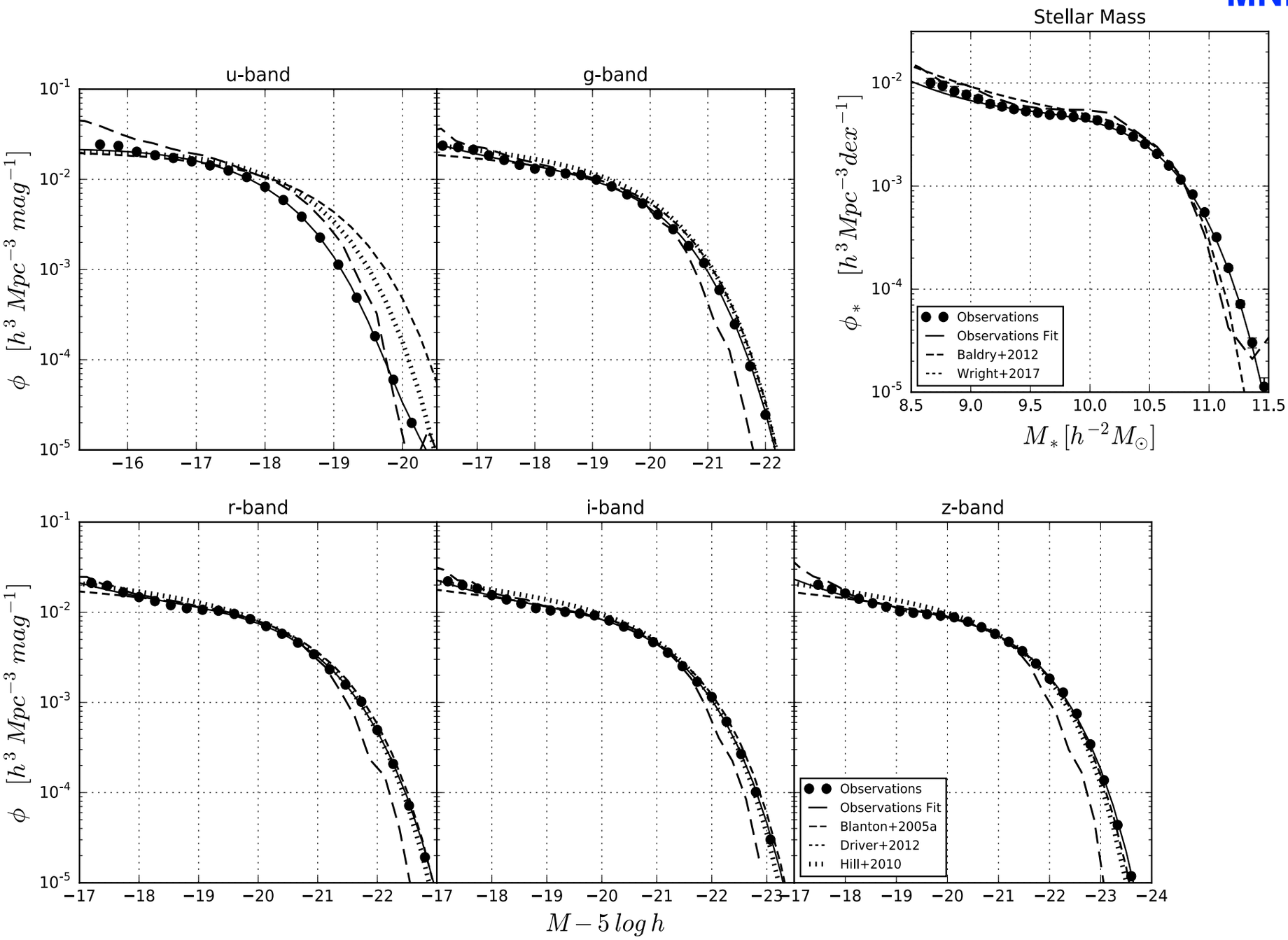

Figure 1. The global *ugriz* galaxy luminosity function. Our derived *ugriz* GLFs and GSMF are shown with the black circles with error bars. For comparison we reproduce the *ugriz* GLFs from Blanton et al. (2005a, black long dashed lines) based on the SDSS DR2; Hill et al. (2010, dotted lines) by combining the MGC, SDSS DR5 and the UKIDSS surveys; and Driver et al. (2012, short dashed lines) based on the GAMA survey. As for the stellar masses we compare with the GSMF from Baldry et al. (2012) and Wright et al. (2017), black long and short dashed lines, respectively.

Does the Galaxy-Halo Connection Vary with Environment?

Radu Dragomir, Aldo Rodriguez-Puebla, Joel Primack, Christoph Lee **MNRAS 2018**

r-Band Luminosity Function

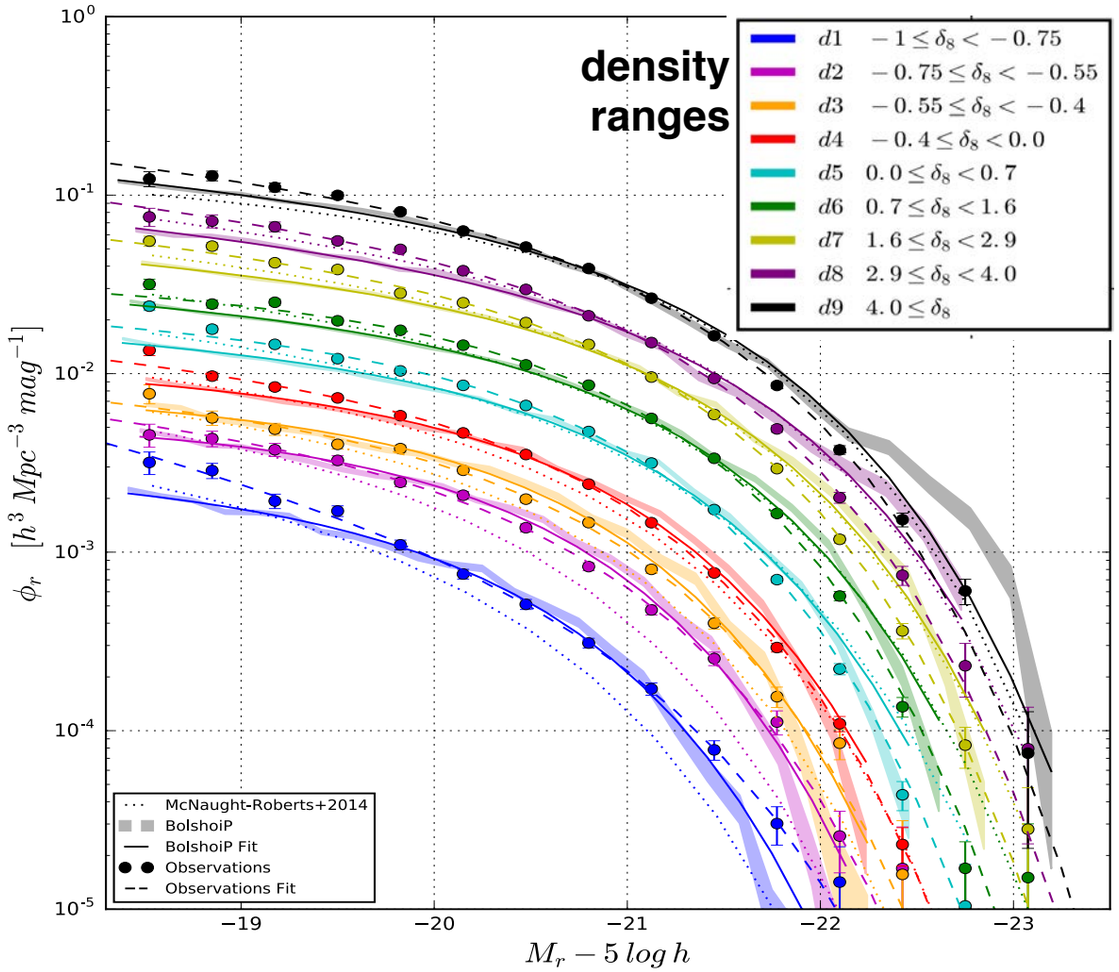

Stellar Mass Function

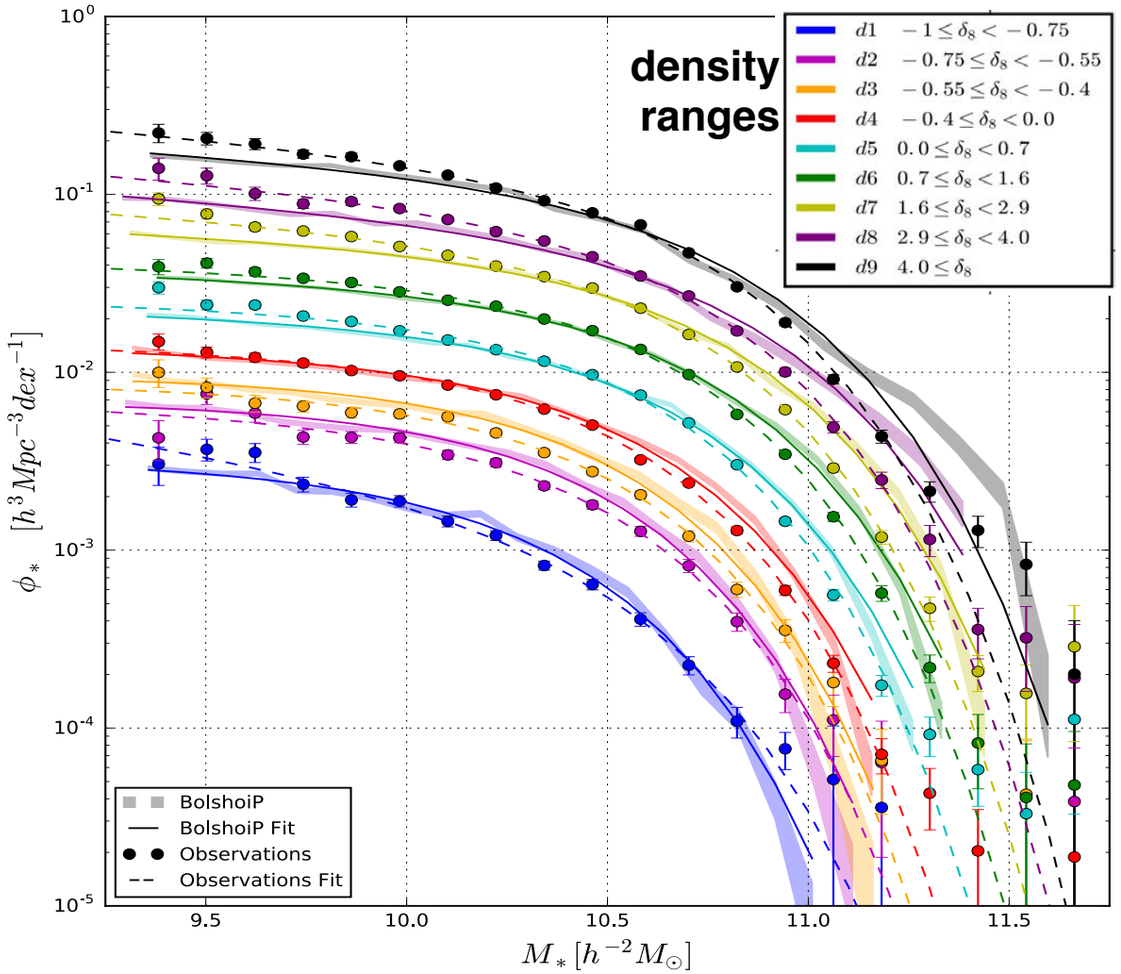

Figure 7. Left Panel: Comparison between the observed $r-$band GLF with environmental density in spheres of 8 h^{-1}Mpc, filled circles with error bars, and the ones predicted based on the BolshoiP simulation from SHAM, shaded regions. The dashed lines show the best fitting Schechter functions to the r-band GLFs from the GAMA survey (McNaught-Roberts et al. 2014). **Right Panel:** Similar to the left panel but for the GSMF with environmental density. Here again the dashed lines are the best fitting Schechter functions.

Does the Galaxy-Halo Connection Vary with Environment?

Radu Dragomir, Aldo Rodriguez-Puebla, Joel Primack, Christoph Lee **MNRAS 2018**

Luminosity Functions

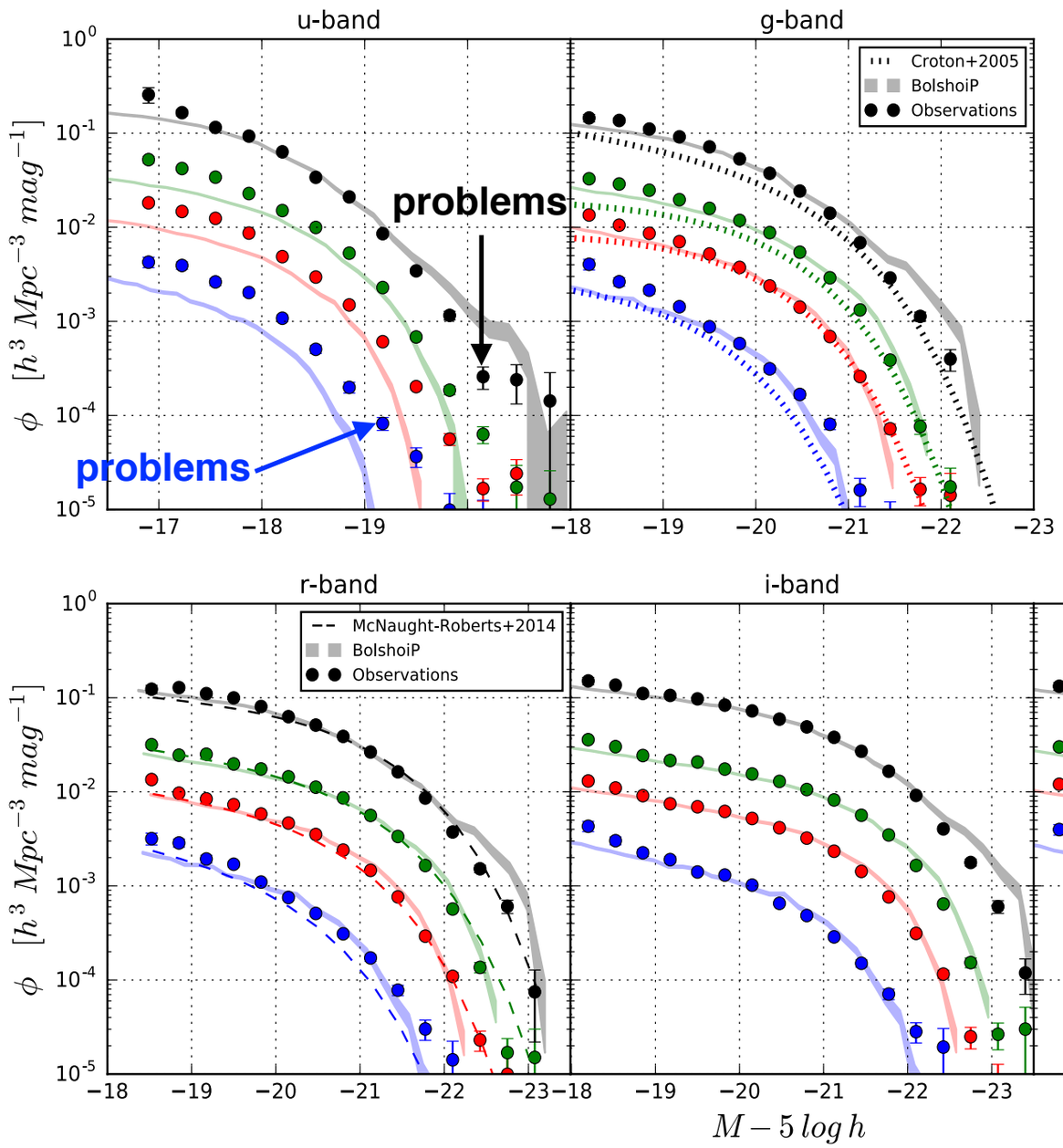

Mass Function

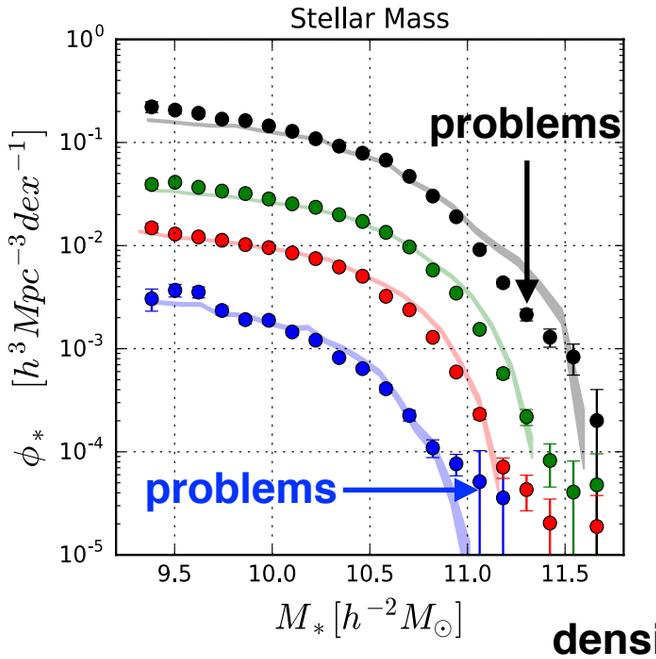

density ranges

$d1 \quad -1 \leq \delta_8 < -0.75$

$d4 \quad -0.4 \leq \delta_8 < 0.0$

$d6 \quad 0.7 \leq \delta_8 < 1.6$

$d9 \quad 4.0 \leq \delta_8$

Figure 6. Comparison between the observed SDSS DR7 *ugriz* GLFs and GSMF, filled circles with error bars, and the ones predicted based on the BolshoiP simulation from SHAM, shaded regions, at four environmental densities in spheres of radius 8 h^{-1}Mpc. We also reproduce the best fitting Schechter functions to the r-band GLFs from the GAMA survey (McNaught-Roberts et al. 2014). Observe that SHAM predictions are in excellent agreement with observations, especially for the longest wavelength bands.

Does the Galaxy-Halo Connection Vary with Environment?

Radu Dragomir, Aldo Rodriguez-Puebla, Joel Primack, Christoph Lee MNRAS 2018

All, Central, & Satellite *r*-Band Luminosity Functions vs. Density

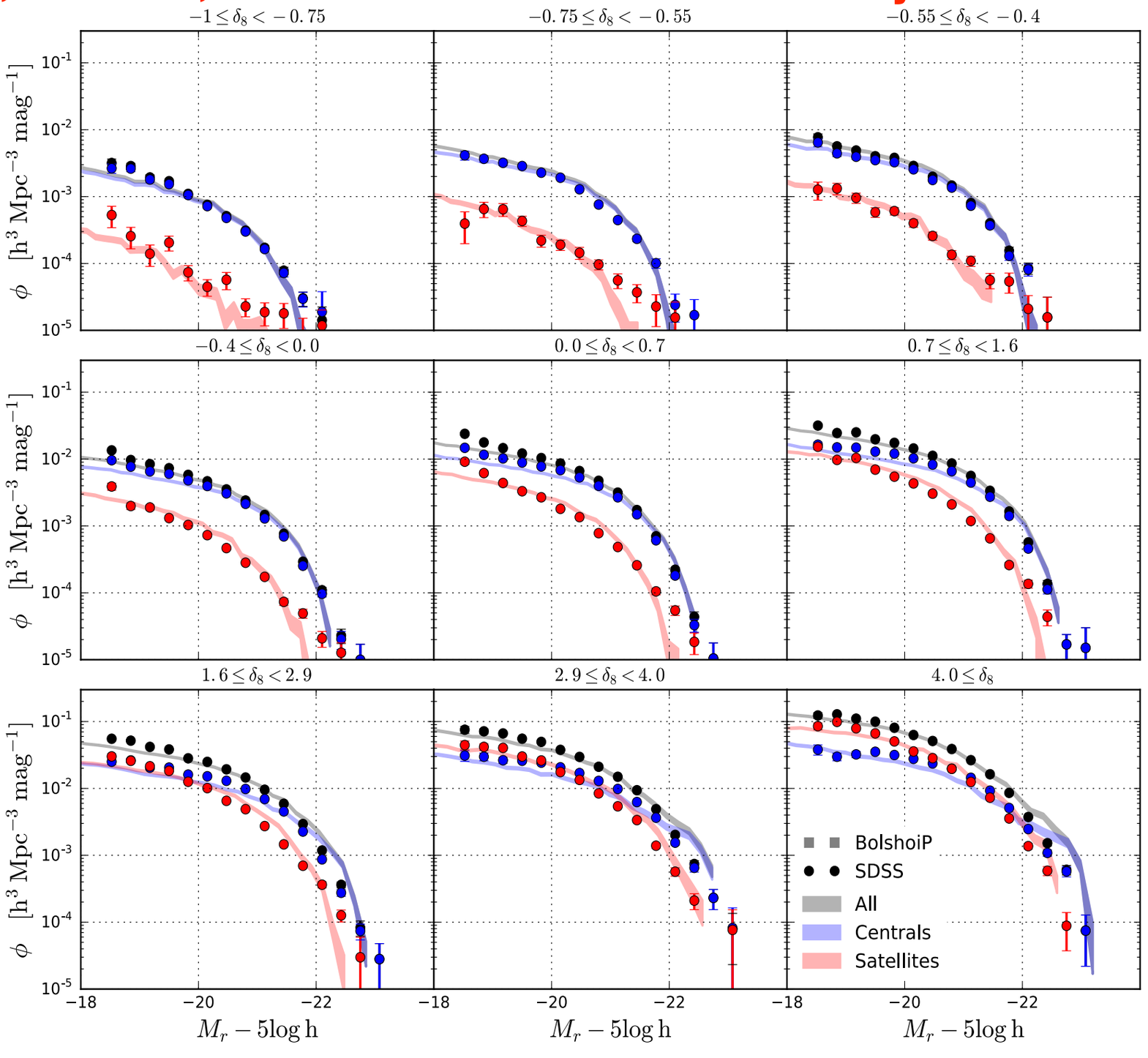

Figure 9. The dependence on r-band magnitude of the GLFs in nine bins of environmental density for all galaxies, central galaxies, and satellite galaxies. Filled circles with error bars show the results from the SDS DR7 while shaded areas show the SHAM predictions from the BolshoiP simulation. There is a remarkable agreement between observations and SHAM predictions, even when dividing between centrals and satellites.

Abundance Matching

M* with V_{max}/V_{peak} as in

Does the Galaxy-Halo Connection Vary with Environment? 2018

Radu Dragomir,
Aldo Rodriguez-Puebla,
Joel Primack, Christoph Lee

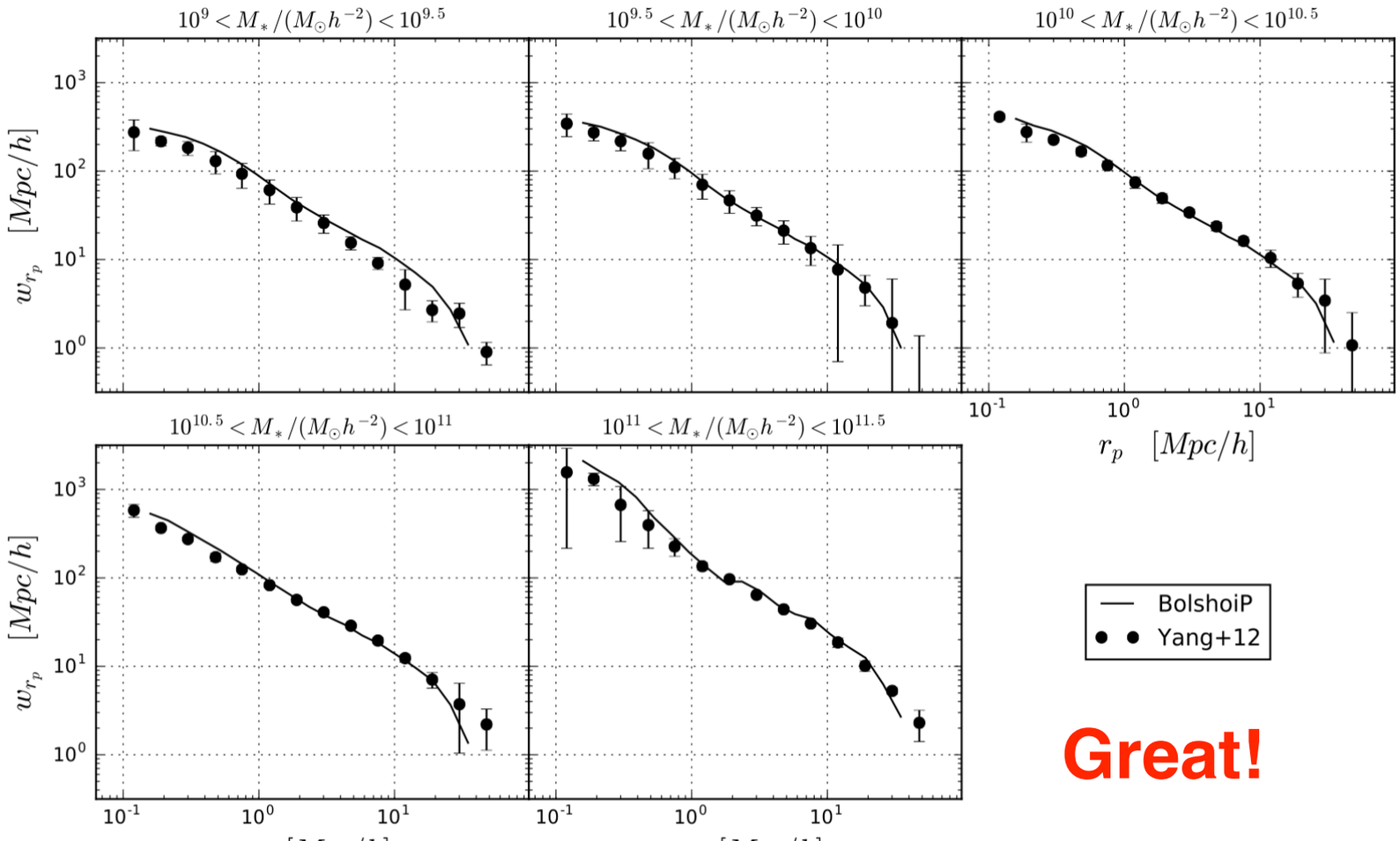

Great!

Abundance Matching

M* with M_{halo} as in

Constraining the Galaxy Halo Connection 2017

Aldo Rodriguez-Puebla,
Joel Primack, Vladimir Avila-Reese, Sandra Faber

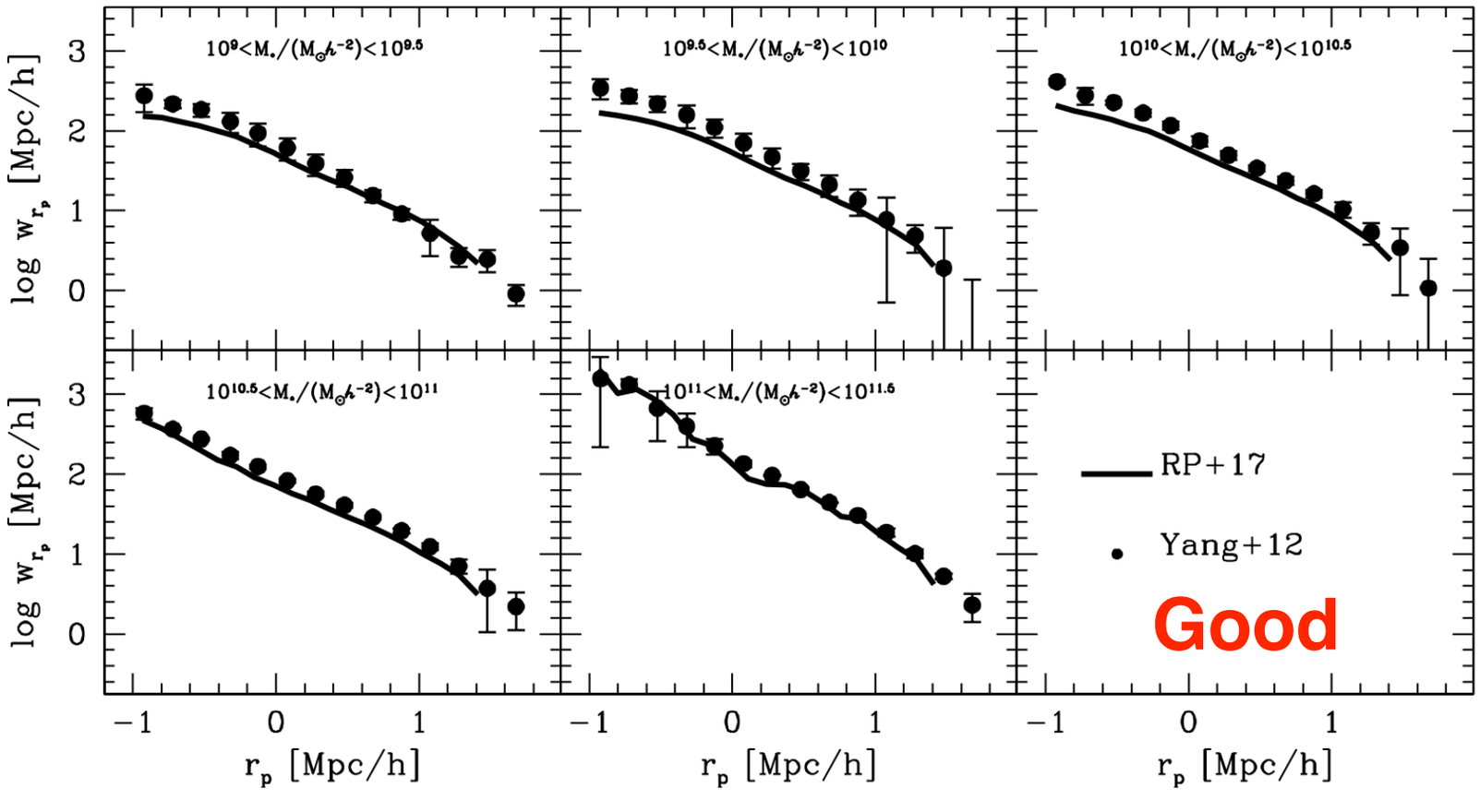

Good

Properties of Dark Matter Haloes: Local Environment Density

Christoph T. Lee, Joel R. Primack, Peter Behroozi, Aldo Rodríguez-Puebla, Doug Hellinger, Avishai Dekel MNRAS 2017

Low Mass	Intermediate Mass		High Mass
$\log_{10} M_{vir}/(h^{-1}M_\odot) = 11.200\pm0.375$	11.95 ± 0.375	12.70 ± 0.375	13.45 ± 0.375

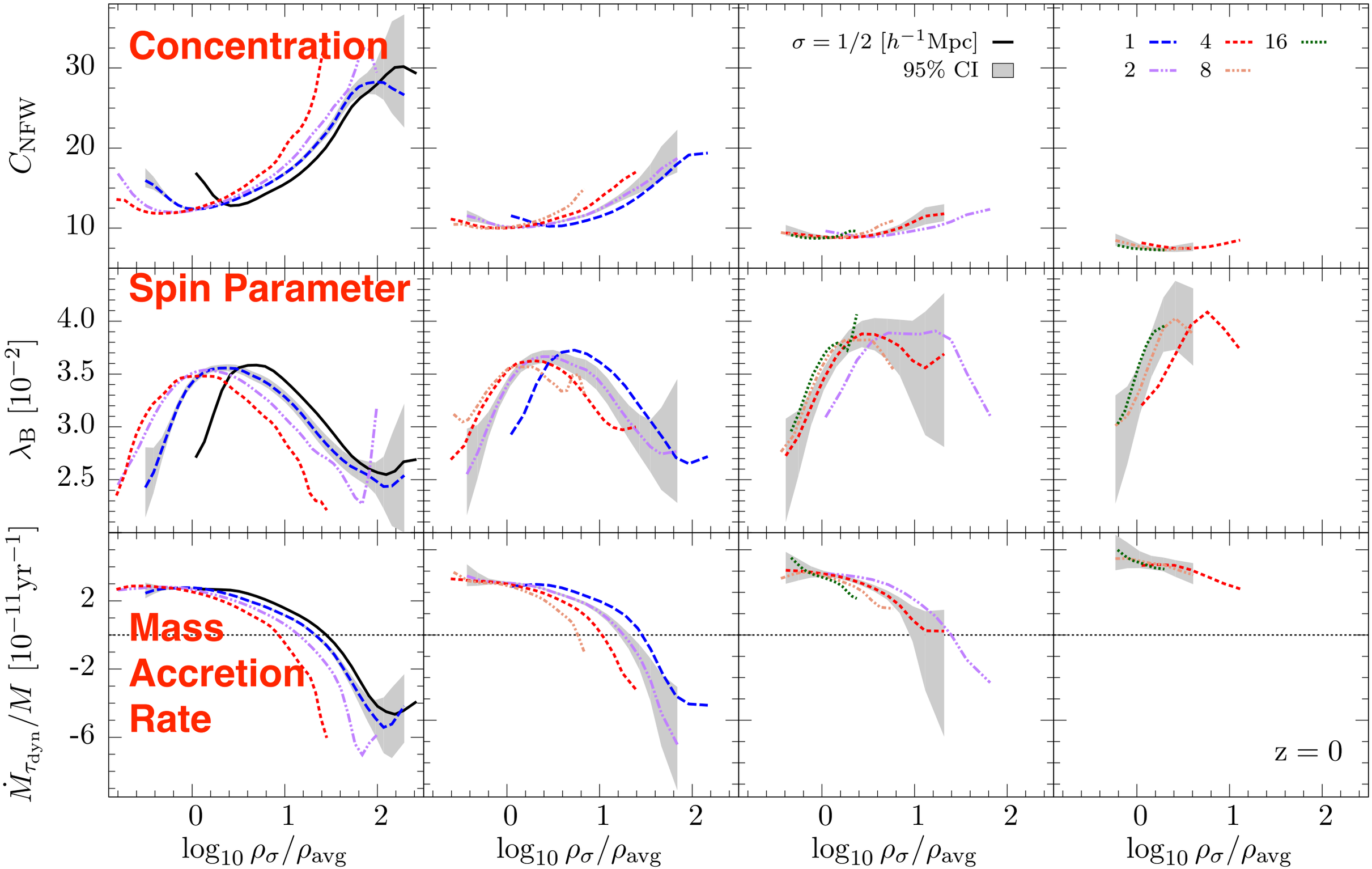

Is galaxy stellar radius R* controlled by its halo's spin

$R^*_{3D} \propto \lambda R_{halo}$?

This predicts that galaxy size R^*_{3D} declines with decreasing ρ_σ/ρ_{ave} but galaxy size is not lower in low-density regions!

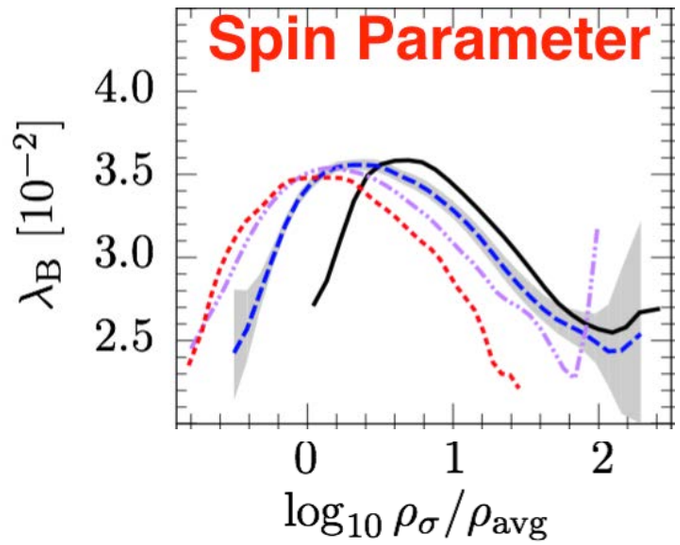

Huertas-Company+ 2013 found no difference in galaxy size vs. density. Cebrian & Trujillo 2014; Pranger, Trujillo, Kelvin, Cebrian 2017; Yoon, Im, and Kim 2017; and Zhang & Yang 2017 find that galaxies in low-density regions are perhaps slightly larger at the same stellar mass. We are finding similar results.

Kravtsov 2013 found that $\langle R^*_{3D} \rangle \approx 0.02\ R_{halo}$ at z~0. Somerville+2017 agreed at z~0 using GAMA, and found that $\langle R^*_{3D} \rangle \approx 0.02\ R_{halo}$ out to z~3. But the papers listed above did not attempt to measure R^*_{3D} nor did they measure density around low-mass galaxies carefully in low-density regions.

We are measuring R^*_{3D} vs. local density in SDSS using several methods (galaxy counts within 2, 4, 8 Mpc projected, distance to n^{th} nearest galaxy, Voronoi volume), and spin λ_B, NFW scale radius R_s, and $(C_{NFW}/7)^{0.4} R_s$ vs. density by the exact same methods in mock catalogs from our Bolshoi-Planck cosmological simulation.

We are also determining how to measure R^*_{3D} from the optical images using simulations.

Halo Properties Independent of Web Location at the Same Density

Tze Ping Goh, Christoph T. Lee, Joel R. Primack, Miguel Aragon Calvo, Peter Behroozi, Aldo Rodríguez-Puebla, Doug Hellinger, Avishai Dekel, Kathryn Johnston (in preparation)

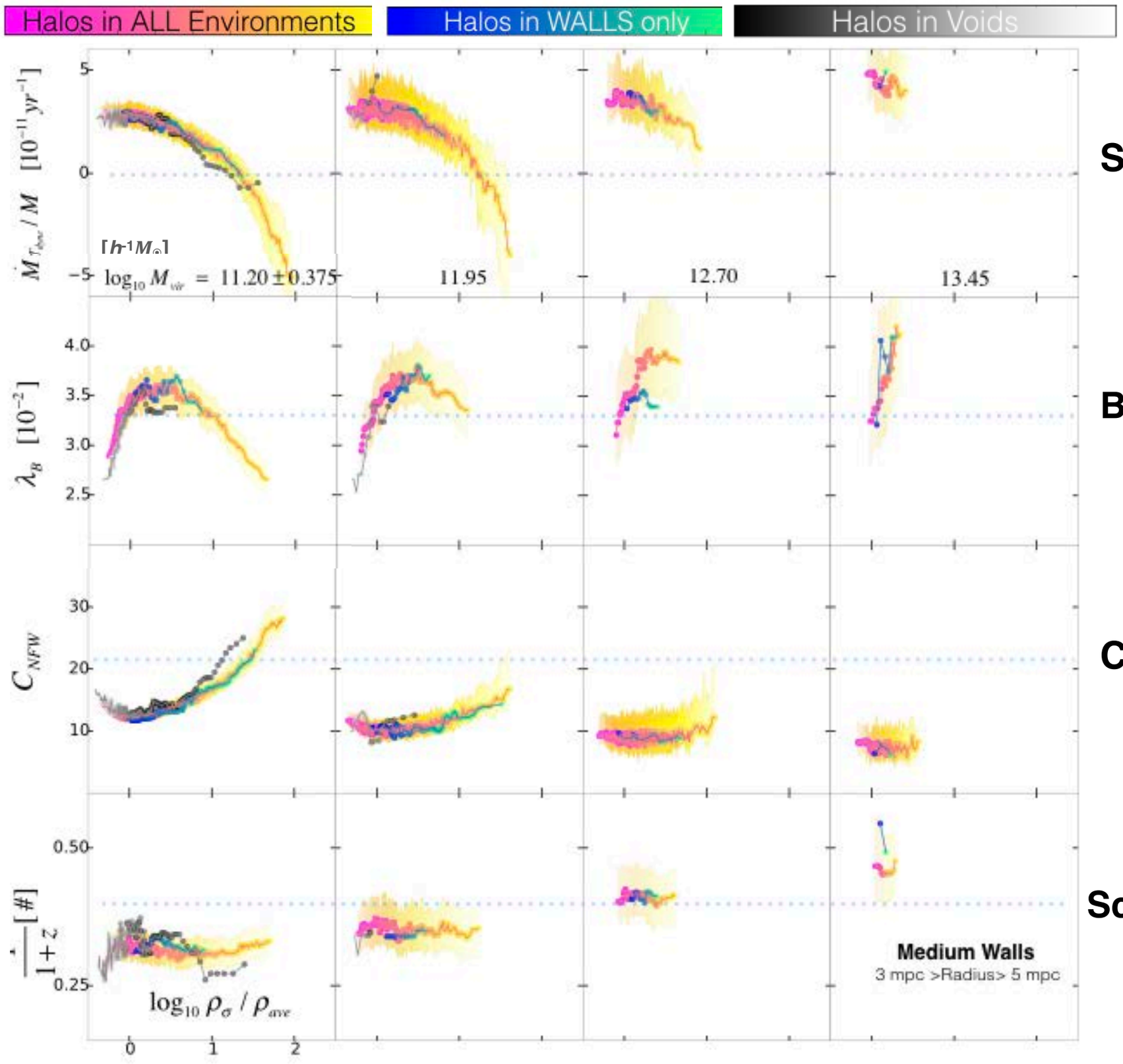

Specific Mass Accretion Rate

Bullock+2001 Spin Parameter λ_B

Concentration $C_{NFW} = R_{vir}/R_s$

Scale Factor of Last Major Merger

Halo Properties Independent of Web Location at the Same Density

Tze Ping Goh, Christoph T. Lee, Joel R. Primack, Miguel Aragon Calvo, Peter Behroozi, Aldo Rodríguez-Puebla, Doug Hellinger, Avishai Dekel, Kathryn Johnston (in preparation)

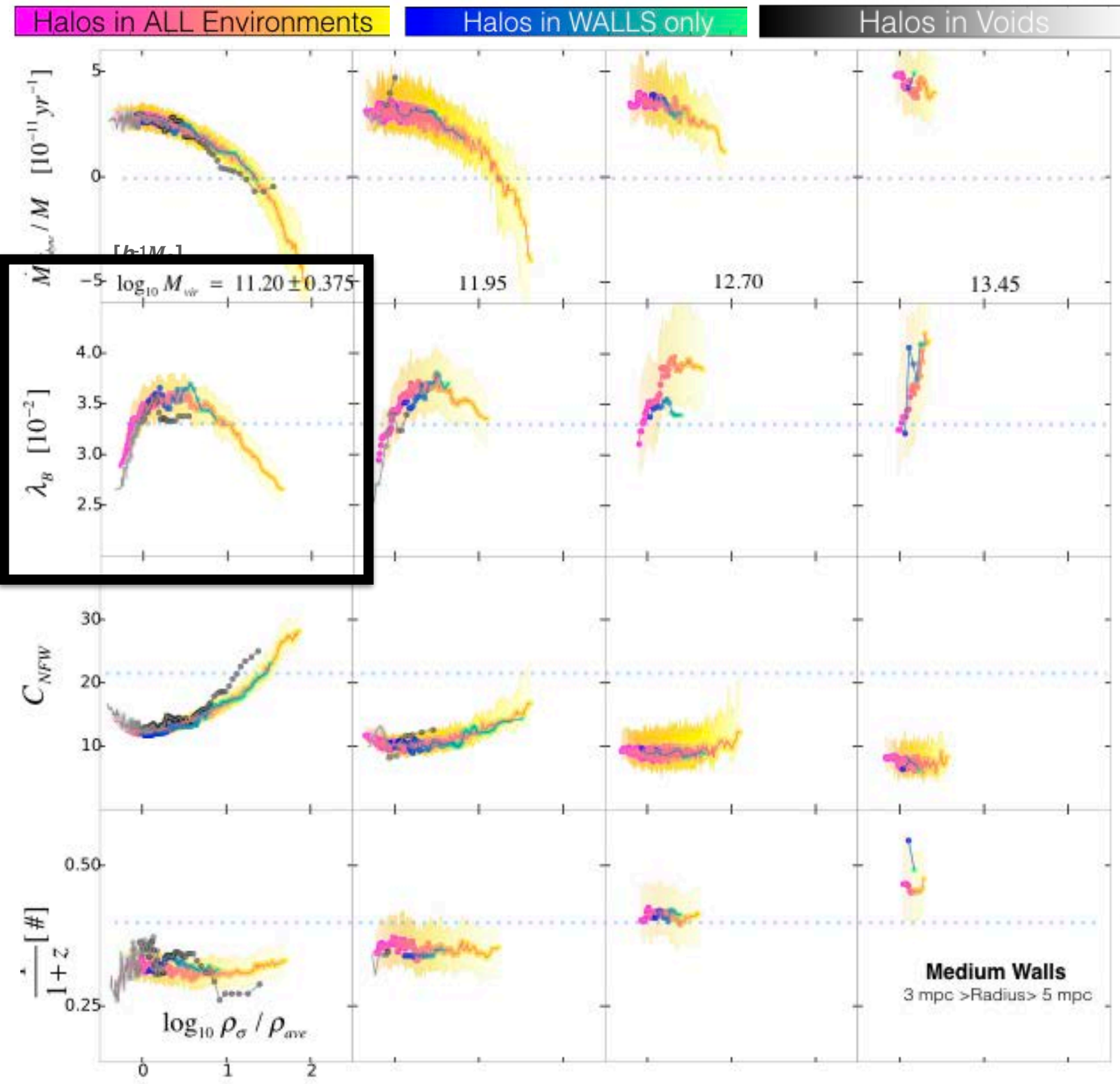

Specific Mass Accretion Rate

Bullock+2001 Spin Parameter λ_B

Concentration $C_{NFW} = R_{vir}/R_s$

Scale Factor of Last Major Merger

Halo Properties Independent of Web Location at the Same Density

Tze Ping Goh, Christoph T. Lee, Joel R. Primack, Miguel Aragon Calvo, Peter Behroozi, Aldo Rodríguez-Puebla, Doug Hellinger, Avishai Dekel, Kathryn Johnston (in preparation)

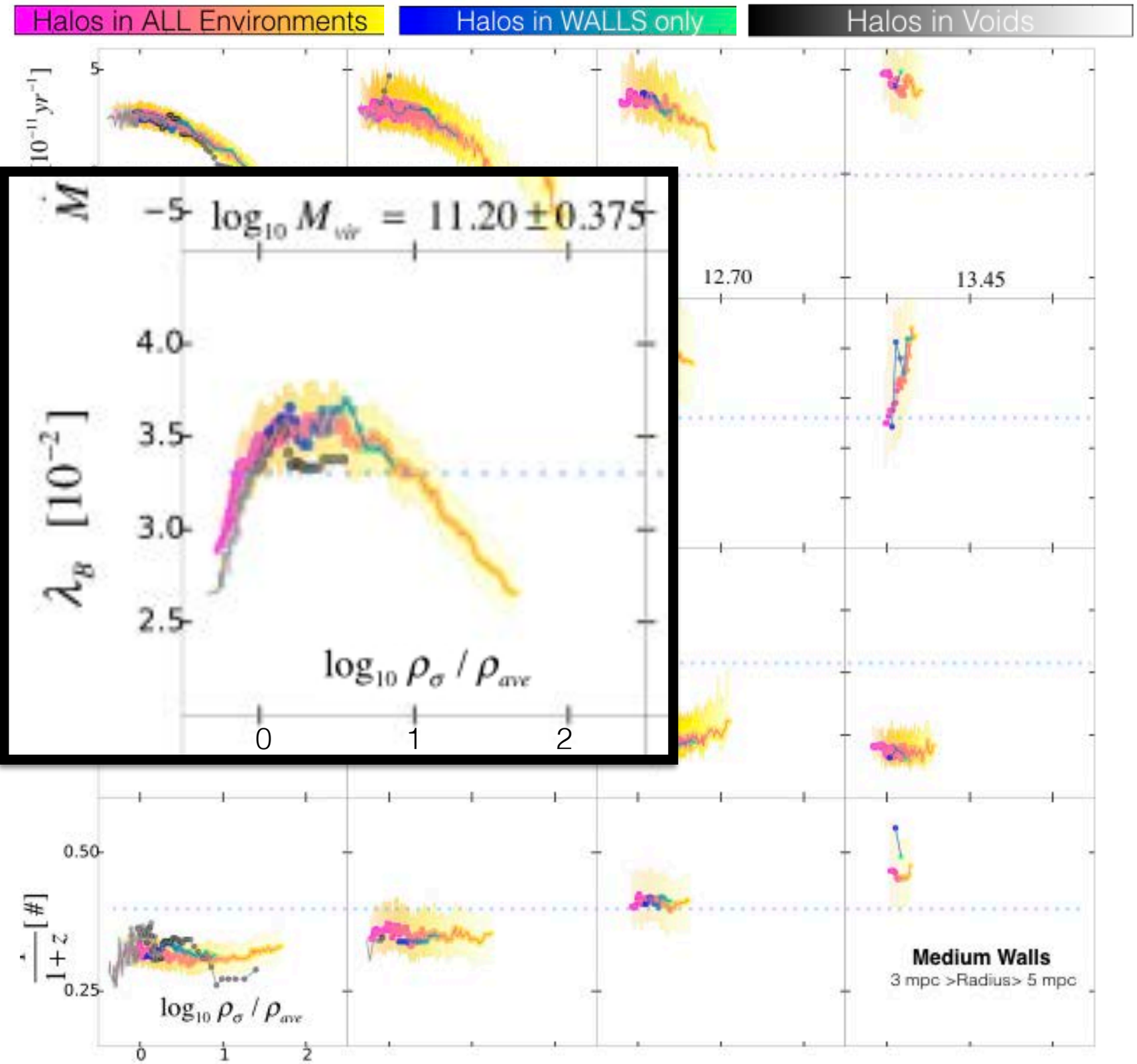

Halo Properties Independent of Web Location at the Same Density

Tze Ping Goh, Christoph T. Lee, Joel R. Primack, Miguel Aragon Calvo, Peter Behroozi, Aldo Rodríguez-Puebla, Doug Hellinger, Avishai Dekel, Kathryn Johnston (in preparation)

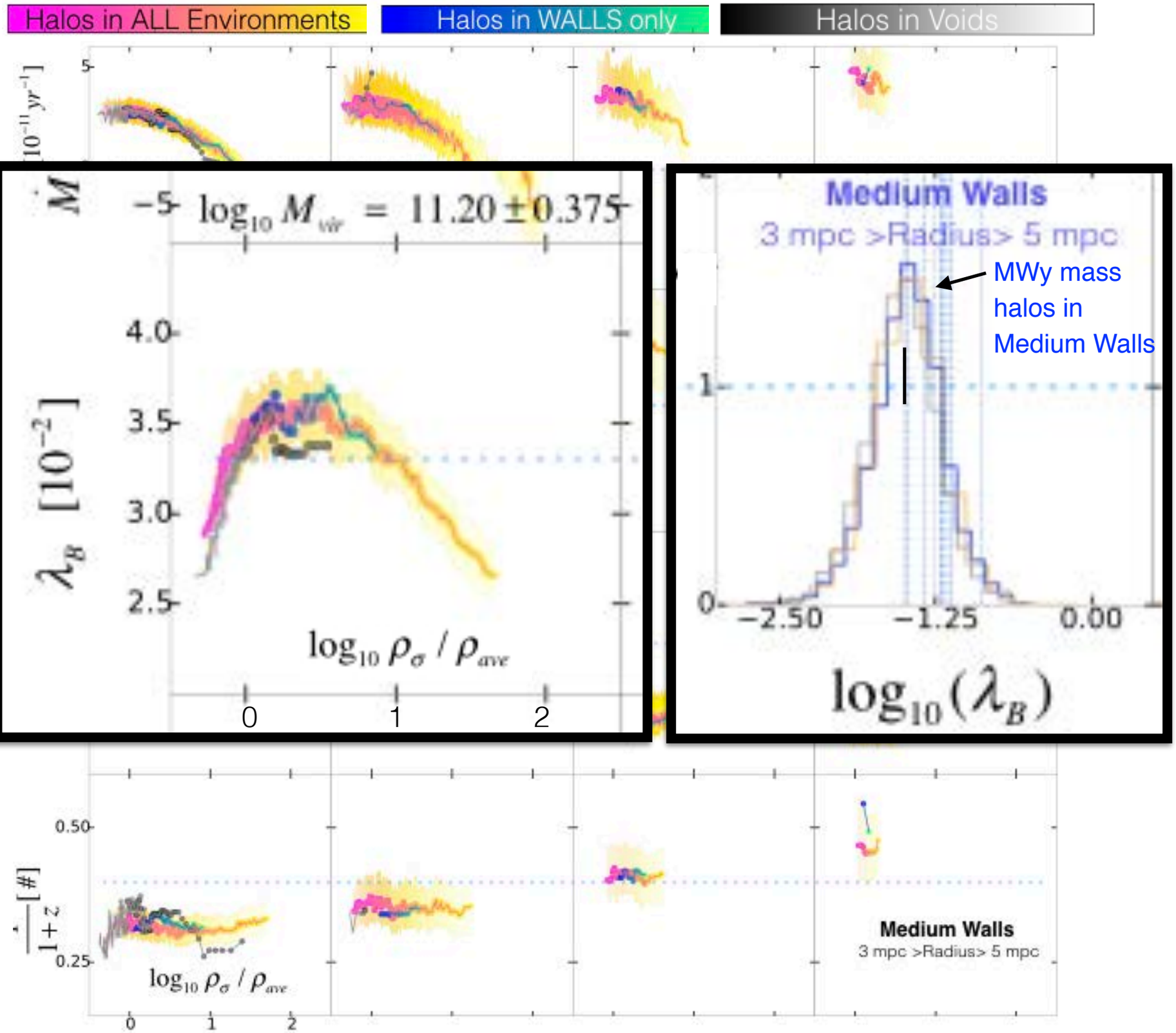

Halo Properties Independent of Web Location at the Same Density

Tze Ping Goh, Christoph T. Lee, Joel R. Primack, Miguel Aragon Calvo, Peter Behroozi, Aldo Rodríguez-Puebla, Doug Hellinger, Avishai Dekel, Kathryn Johnston (in preparation)

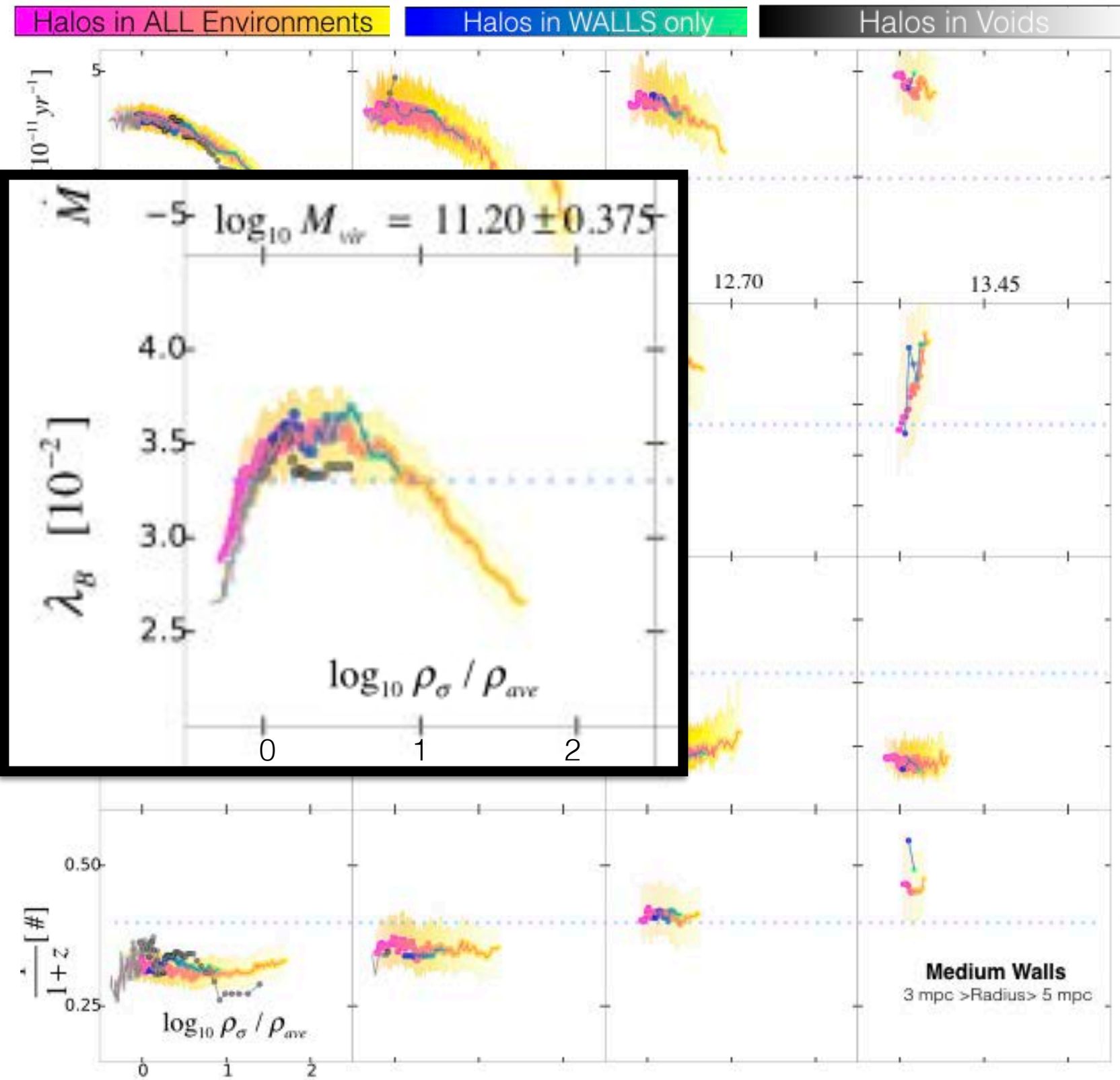

Specific Mass Accretion Rate

Bullock+2001 Spin Parameter λ_B

Concentration $C_{NFW} = R_{vir}/R_s$

Scale Factor of Last Major Merger

Halo Properties Independent of Web Location at the Same Density

Tze Ping Goh, Christoph T. Lee, Joel R. Primack, Miguel Aragon Calvo, Peter Behroozi, Aldo Rodríguez-Puebla, Doug Hellinger, Avishai Dekel, Kathryn Johnston (in final prep.)

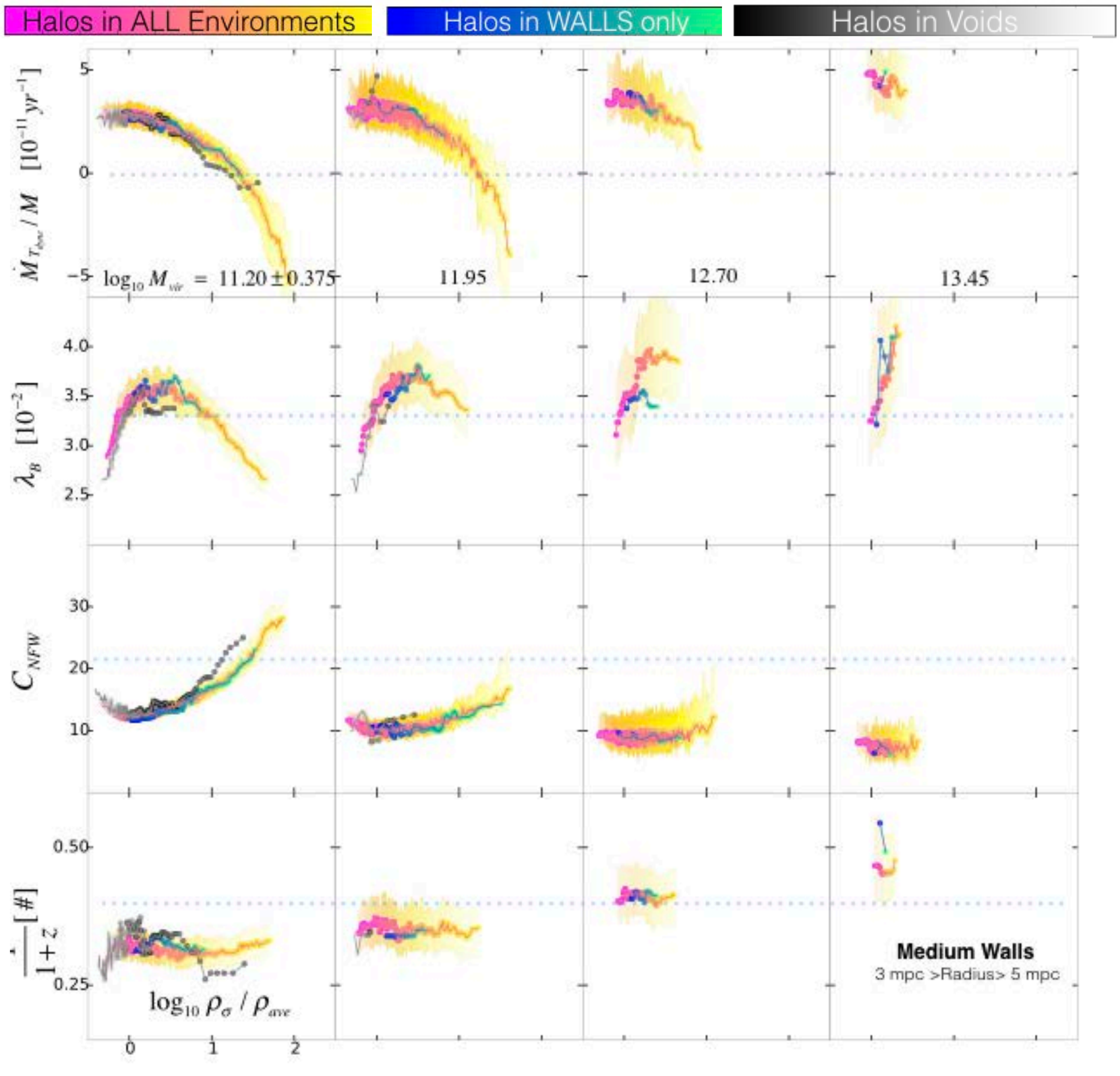

At the same environmental density, halo properties are independent of cosmic web location. It doesn't matter whether a halo is in a cosmic void, wall, or filament, what matters is the halos's environmental density. The properties studied are mass accretion rate, spin, halo concentration, scale factor of the last major merger, half-mass scale factor, and prolateness. We had expected that a web's cosmic web location would matter for at least some of these halo properties. That it does not is a discovery.

SDSS galaxy mass and size are independent of web environment at fixed density (Yan, Fan, White 2013). GAMA data show that the galaxy luminosity function is also independent of web environment at fixed density (Eardley et al. MNRAS 2015). This contrasts with the finding that the halo mass function is dependent on web location at the same density using the v-web (Metuki, Liebeskind, Hoffman 2016).

Astronaut Andrew Feustel
installing WFC3 on the
last visit to HST in 2009

The infrared capabilities of
Wide Field Camera 3
allow us to see the full stellar
populations of forming galaxies
out to redshift $z \sim 2$

The CANDELS Survey

candels.ucolick.org

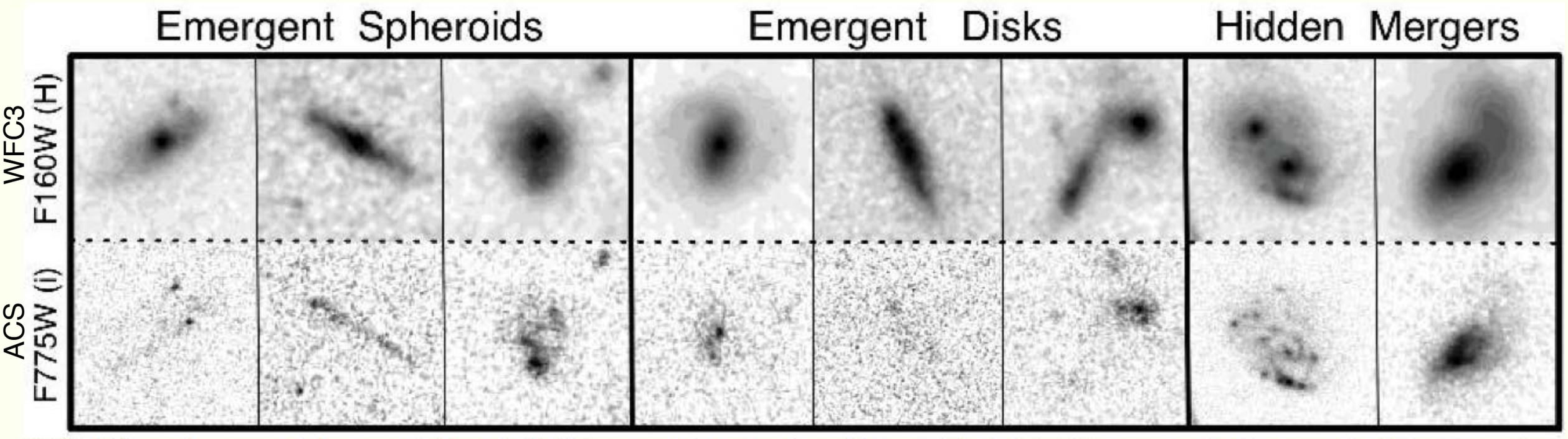

(blue 0.4 μm)(1+z) = 1.6 μm @ z = 3

(red 0.7 μm)(1+z) = 1.6 μm @ z = 2.3

CANDELS: A Cosmic Odyssey

CANDELS is a powerful imaging survey of the distant Universe being carried out with two cameras on board the Hubble Space Telescope.

- CANDELS is the largest project in the history of Hubble, with 902 assigned orbits of observing time. This is the equivalent of four months of Hubble time if executed consecutively, but in practice CANDELS will take three years to complete (2010-2013).
- The core of CANDELS is the revolutionary near-infrared WFC3 camera, installed on Hubble in May 2009. WFC3 is sensitive to longer, redder wavelengths, which permits it to follow the stretching of lightwaves caused by the expanding Universe. This enables CANDELS to detect and measure objects much farther out in space and nearer to the Big Bang than before. CANDELS also uses the visible-light ACS camera, and together the two cameras give unprecedented panchromatic coverage of galaxies from optical wavelengths to the near-IR.
- CANDELS will exploit this new lookback power to construct a "cosmic movie" of galaxy evolution that follows the life histories of galaxies from infancy to the present time. This work will cap Hubble's revolutionary series of discoveries on cosmic evolution and bequeath a legacy of precious data to future generations of astronomers.

Redshift

9 6 4 3 2 1 0.5 0.2 0

CANDELS

CANDELS
Cosmic Assembly Near-infrared Deep Extragalactic Legacy Survey

Star-formation rate
(solar masses/year/megaparsecs^3 × 10^{-2})

10
5
0

Cosmic dawn

Cosmic high noon

0 1 2 3 4 5 6 7 8 9 10 11 12 13

Time since Big Bang (billions of years)

Big Bang

Now
13.7

Most astronomers used to think

(1) that galaxies form as disks,

(2) that forming galaxies are pretty smooth, and

(3) that galaxies generally grow in radius as they grow in mass.

But CANDELS and other HST observations show that all these statements are wrong!

(1) The majority of low-mass star-forming galaxies at z > 1 apparently have mostly elongated (prolate) stellar distributions rather than disks or spheroids, and our simulations may explain why.

(2) A large fraction of star-forming galaxies at redshifts 1 < z < 3 are found to have massive stellar clumps; these originate from phenomena including mergers and disk instabilities in our simulations.

(3) These phenomena also help to create compact stellar spheroidal galaxies ("nuggets") through galaxy compaction (rapid inflow of gas to galaxy centers, where it forms stars).

- **3 Aspects of Star-Forming Galaxies Seen in CANDELS**
  - **Compaction**
  - **Elongation**
  - **Clumps**

  } **Challenge for Observers & Simulators!**

Our hydroART cosmological zoom-in simulations produce all of these phenomena!

Galaxy Hydro Simulations: 2 Approaches

1. Low resolution (~ kpc)

Advantages: it's possible to simulate many galaxies and study galaxy populations and their interactions with CGM & IGM.
Disadvantages: since feedback &winds are "tuned," we learn little about how galaxies themselves evolve, and cannot compare in detail with high-*z* galaxy images and spectra.
Examples: Overwhelmingly Large Simulations (OWLs, EAGLE), AREPO simulations in large boxes (Illustris, TNG).

2. High resolution (~10s of pc) ← THIS TALK

Advantages: it's possible to compare in detail with high-z galaxy images and spectra, to discover how galaxies evolve, morphological drivers (e.g., galaxy shapes, clumps and other instabilities, origins of galactic spheroids, quenching). Radiative pressure & AGN feedbacks essential?
Disadvantages: statistical galaxy samples take too much computer time; can we model galaxy population evolution using simulation insights in semi-analytic models (SAMs)?
Examples: ART/VELA and FIRE simulation suites, AGORA simulation comparison project.

Prolate Galaxies Dominate at High Redshifts & Low Masses

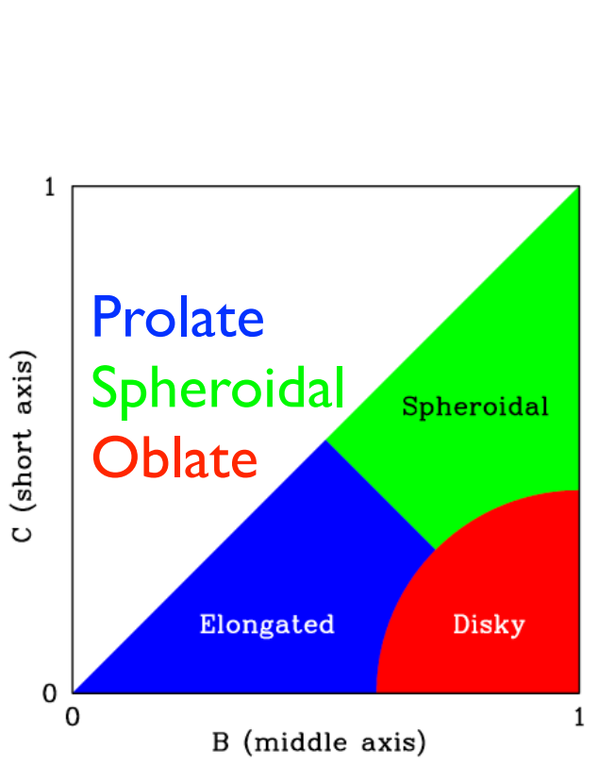

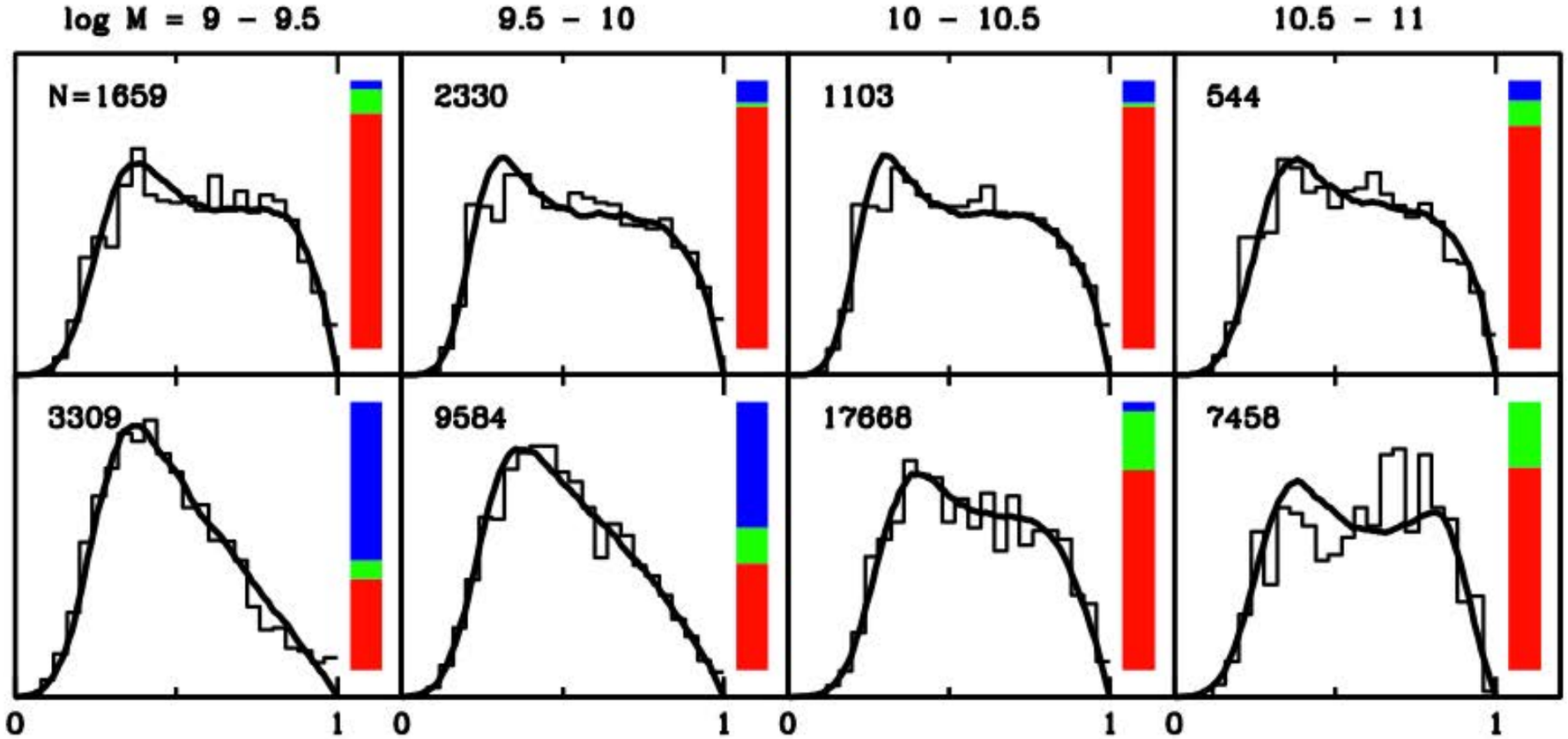

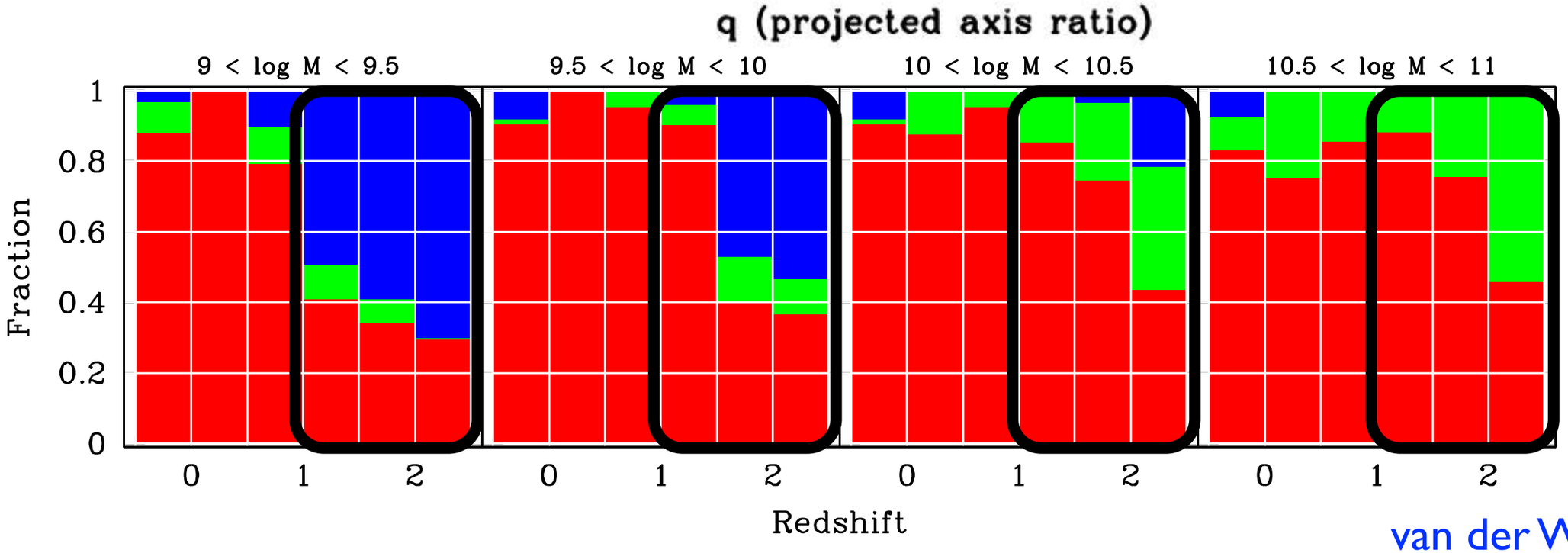

van der Wel+2014

See also Morphological Survey of Galaxies z=1.5-3.6 Law, Steidel+ ApJ 2012

When Did Round Disk Galaxies Form? T. M. Takeuchi+ ApJ 2015

The Evolution of Galaxy Shapes in CANDELS: from Prolate to Oblate

Haowen Zhang, Joel R. Primack, S. M. Faber, David C. Koo, Avishai Dekel, Zhu Chen, Daniel Ceverino, Yu-Yen Chang, Jerome J. Fang, Yicheng Guo, Lin Lin, and Arjen van der Wel **MNRAS submitted**

ABSTRACT

We model the projected b/a – $\log a$ distributions of CANDELS main sequence star-forming galaxies, where a (b) is the semi-major (semi-minor) axis of the galaxy images. We find that smaller-a galaxies are rounder at all stellar masses M_* and redshifts, so we include a when analyzing b/a distributions. Approximating intrinsic shapes of the galaxies as triaxial ellipsoids and assuming a multivariate normal distribution of galaxy size and two shape parameters, we construct their intrinsic shape and size distributions to obtain the fractions of prolate, oblate, and spheroidal galaxies in each redshift and mass bin. We find that galaxies tend to be prolate at low M_* and high redshifts, and oblate at high M_* and low redshifts, qualitatively consistent with van der Wel et al. (2014), implying that galaxies tend to evolve from prolate to oblate. These results are consistent with the predictions from simulations (Ceverino et al. 2015, Tomassetti et al. 2016) that the transition from prolate to oblate is caused by a compaction event at a characteristic mass range, making the galaxy center baryon dominated. We give probabilities of a galaxy's being prolate, oblate, or spheroidal as a function of its M_*, redshift, and projected b/a and a, which can facilitate target selections of galaxies with specific shapes at high redshifts. We also give predicted optical depths of galaxies, which are qualitatively consistent with the expected correlation that A_V should be higher for edge-on disk galaxies in each $\log a$ slice at low redshift and high mass bins.

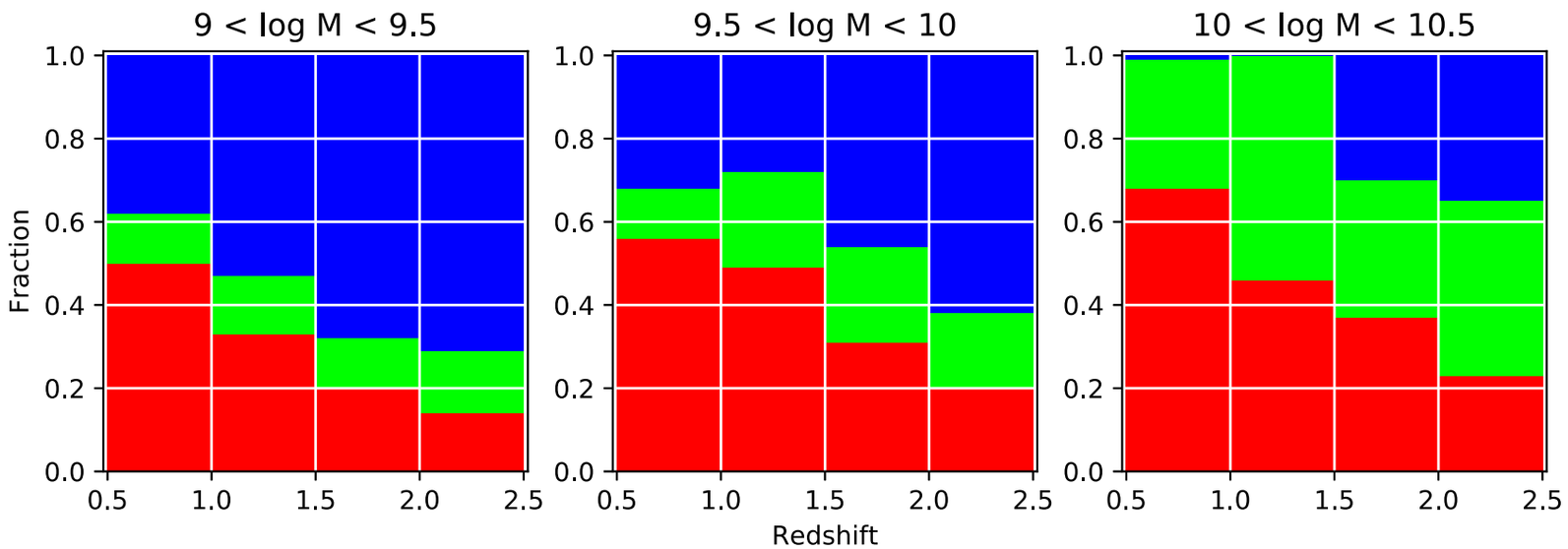

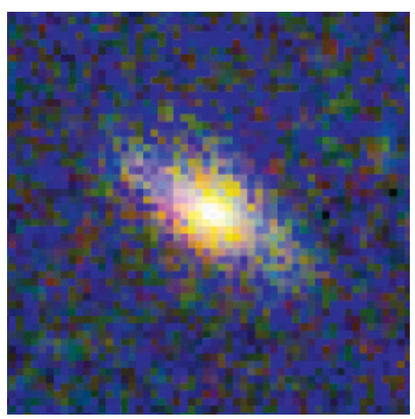

(a) CANDELS galaxy

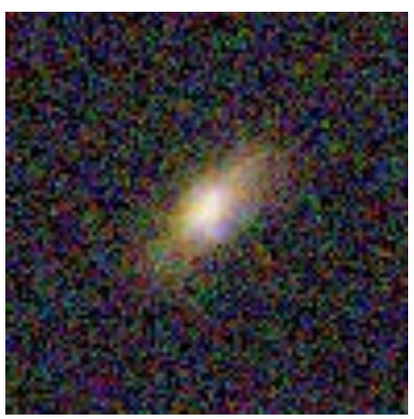

(b) VELA galaxy

The Evolution of Galaxy Shapes in CANDELS: from Prolate to Oblate

Projected b/a - log a distributions of CANDELS galaxies in redshift-mass bins

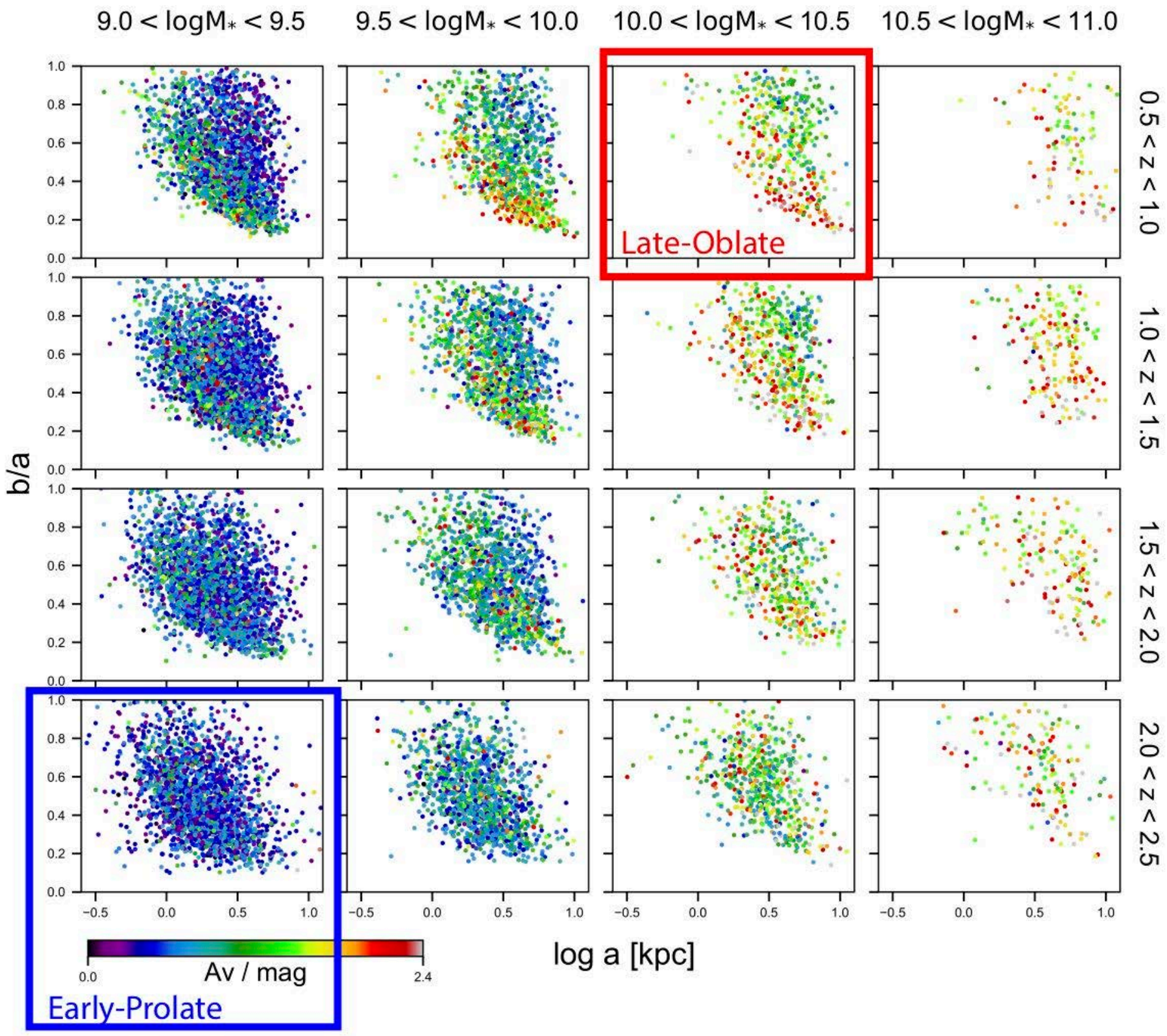

The Evolution of Galaxy Shapes in CANDELS: from Prolate to Oblate

b/a - log a distribution modeling to determine the shape distribution statistics

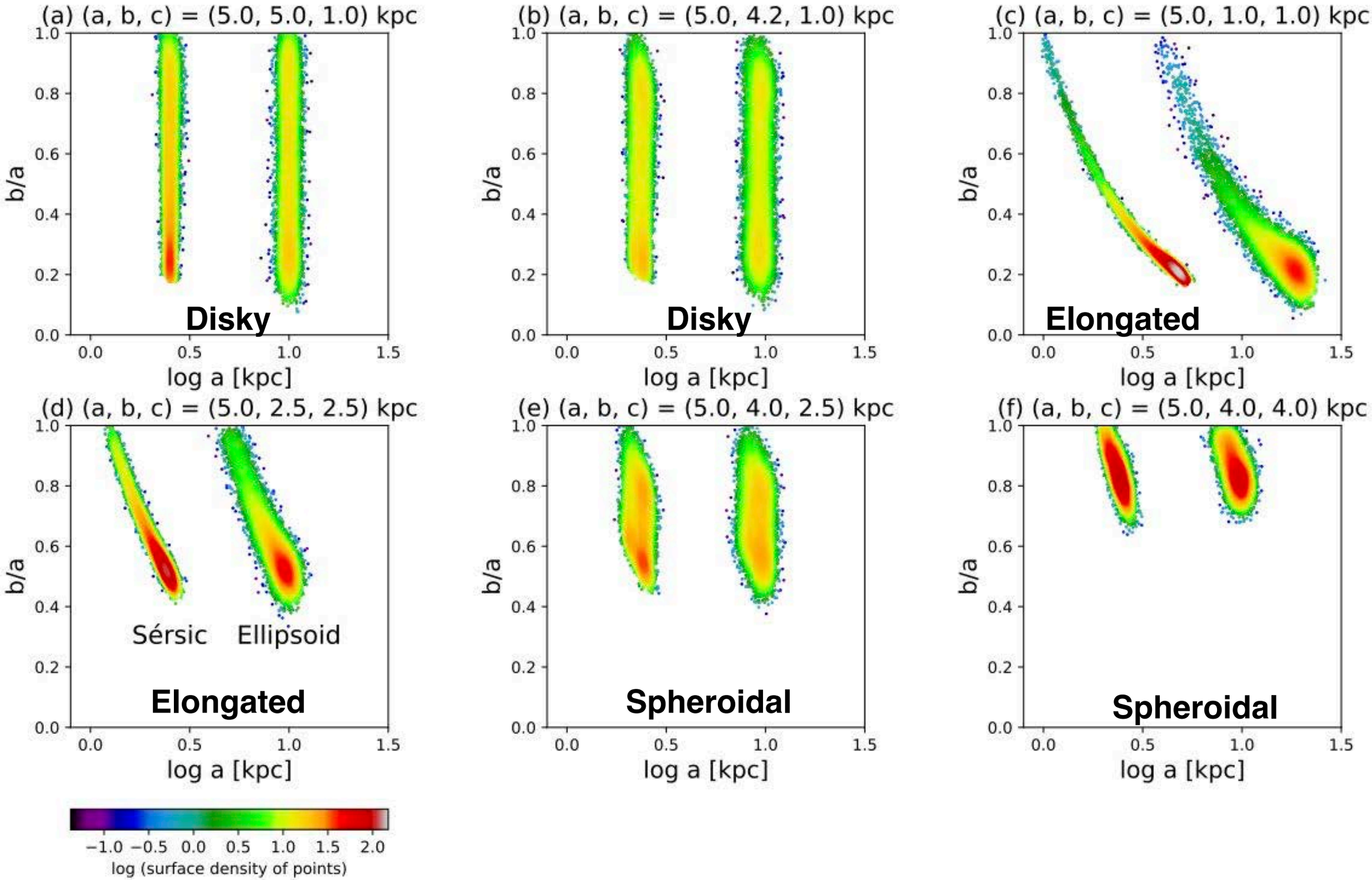

The Evolution of Galaxy Shapes in CANDELS: from Prolate to Oblate

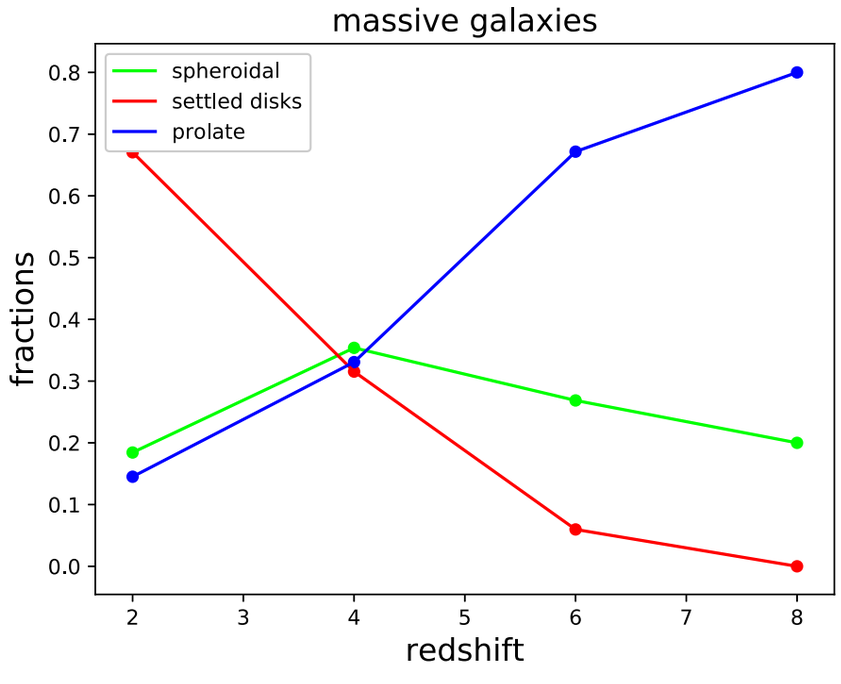

(a)

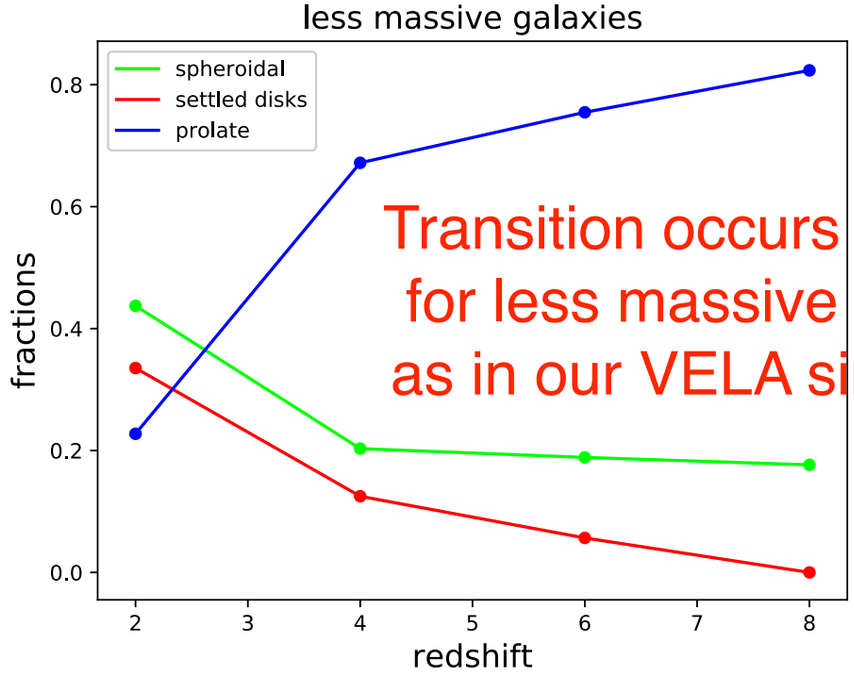

(b)

Transition occurs at lower z for less massive galaxies, as in our VELA simulations

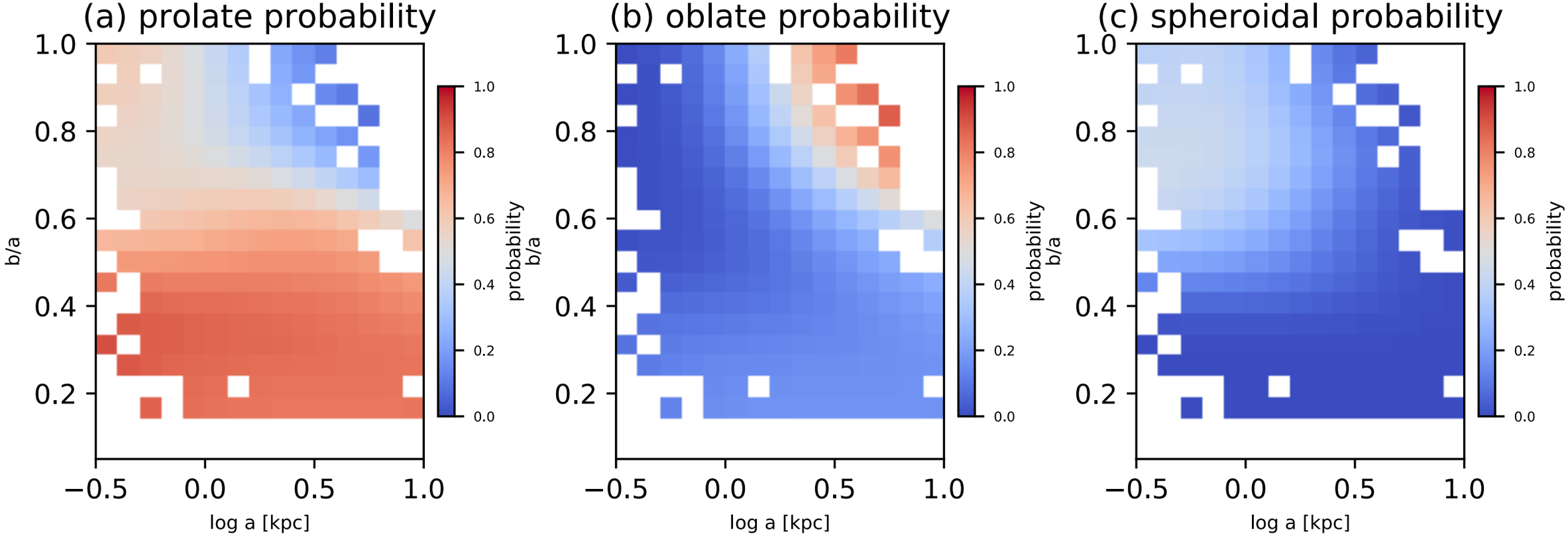

The probability distribution of a CANDELS galaxy's being prolate, oblate or spheroidal over the b/a - log a plane for the early-prolate bin. Probabilities are only calculated in the bins containing at least one observed galaxy.

Our cosmological zoom-in simulations often produce elongated galaxies like observed ones. The elongated stellar distribution follows the elongated inner dark matter halo.

Prolate DM halo → elongated galaxy

DM VELA28 stars

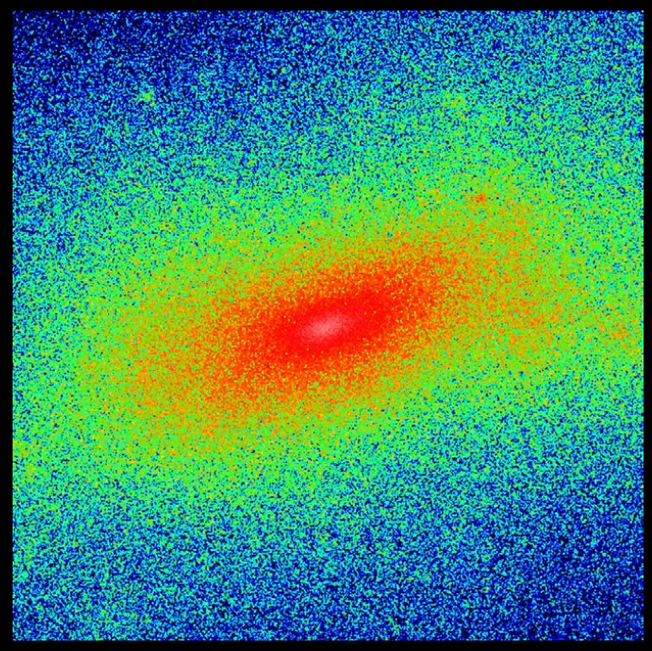

30 kpc

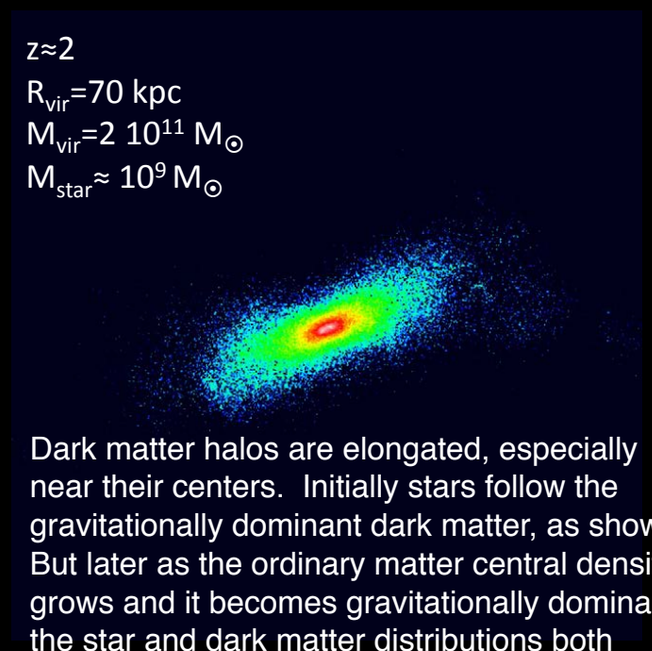

z≈2
R_{vir}=70 kpc
M_{vir}=2 10^{11} $M_\odot$
M_{star}≈ 10^9 $M_\odot$

Dark matter halos are elongated, especially near their centers. Initially stars follow the gravitationally dominant dark matter, as shown. But later as the ordinary matter central density grows and it becomes gravitationally dominant, the star and dark matter distributions both become disky — as observed by Hubble Space Telescope (van der Wel+ ApJL Sept 2014).

Monthly Notices of the ROYAL ASTRONOMICAL SOCIETY

MNRAS **453,** 408–413 (2015)

Formation of elongated galaxies with low masses at high redshift

Daniel Ceverino, Joel Primack and Avishai Dekel

ABSTRACT

We report the identification of elongated (triaxial or prolate) galaxies in cosmological simulations at z ~ 2. These are preferentially low-mass galaxies ($M_* \leq 10^{9.5}$ $M_\odot$), residing in dark matter (DM) haloes with strongly elongated inner parts, a common feature of high-redshift DM haloes in the cold dark matter cosmology. A large population of elongated galaxies produces a very asymmetric distribution of projected axis ratios, as observed in high-z galaxy surveys. This indicates that the majority of the galaxies at high redshifts are not discs or spheroids but rather galaxies with elongated morphologies

Nearby large galaxies are mostly disks and spheroids — but they start out looking more like pickles.

Evolution of Stellar Distribution in VELA 28 Simulation

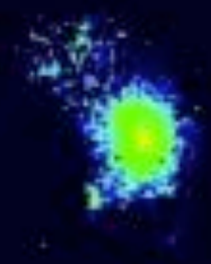

Formation of elongated galaxies with low masses at high redshift

Daniel Ceverino, Joel Primack and Avishai Dekel

MNRAS 2015

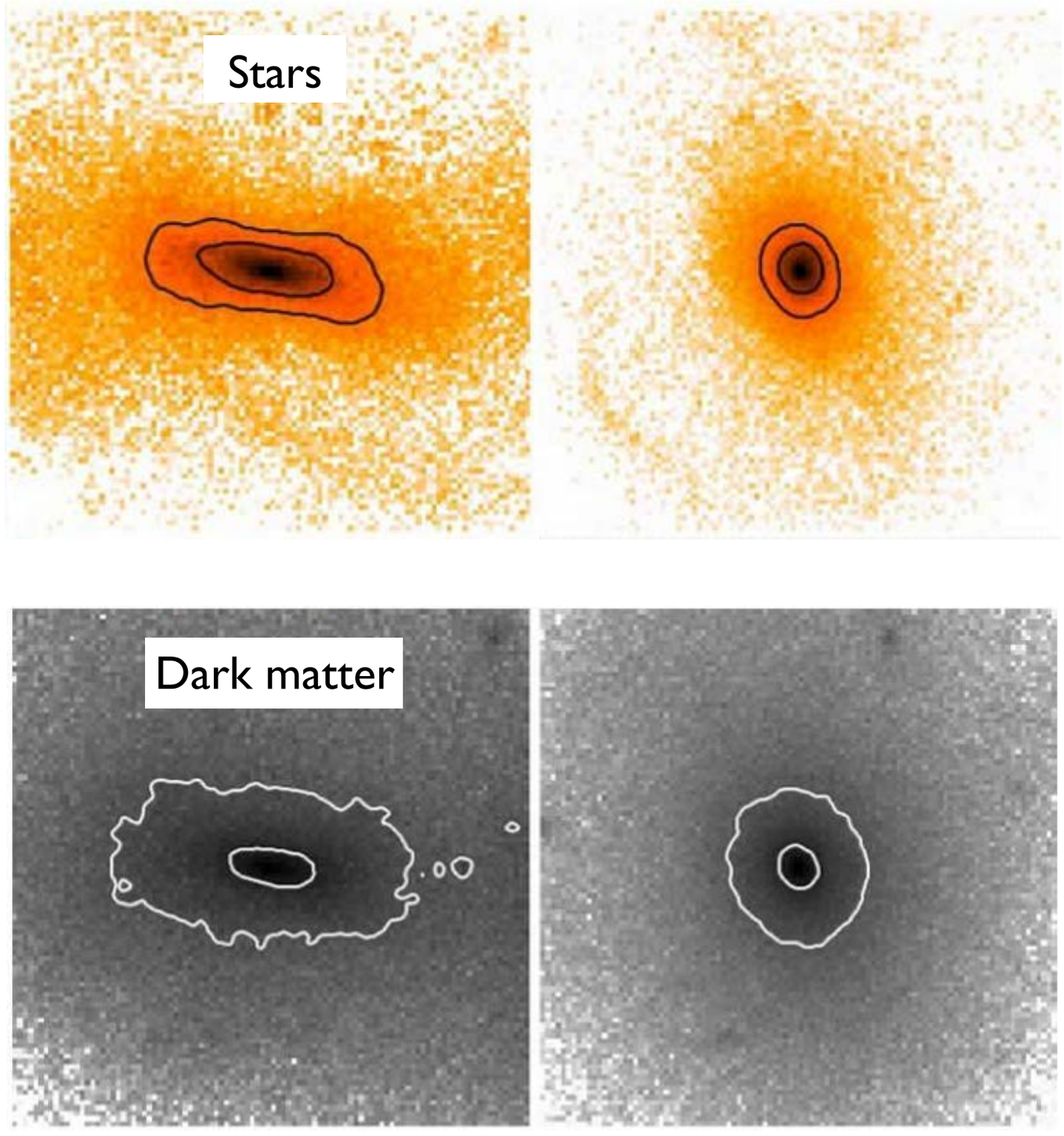

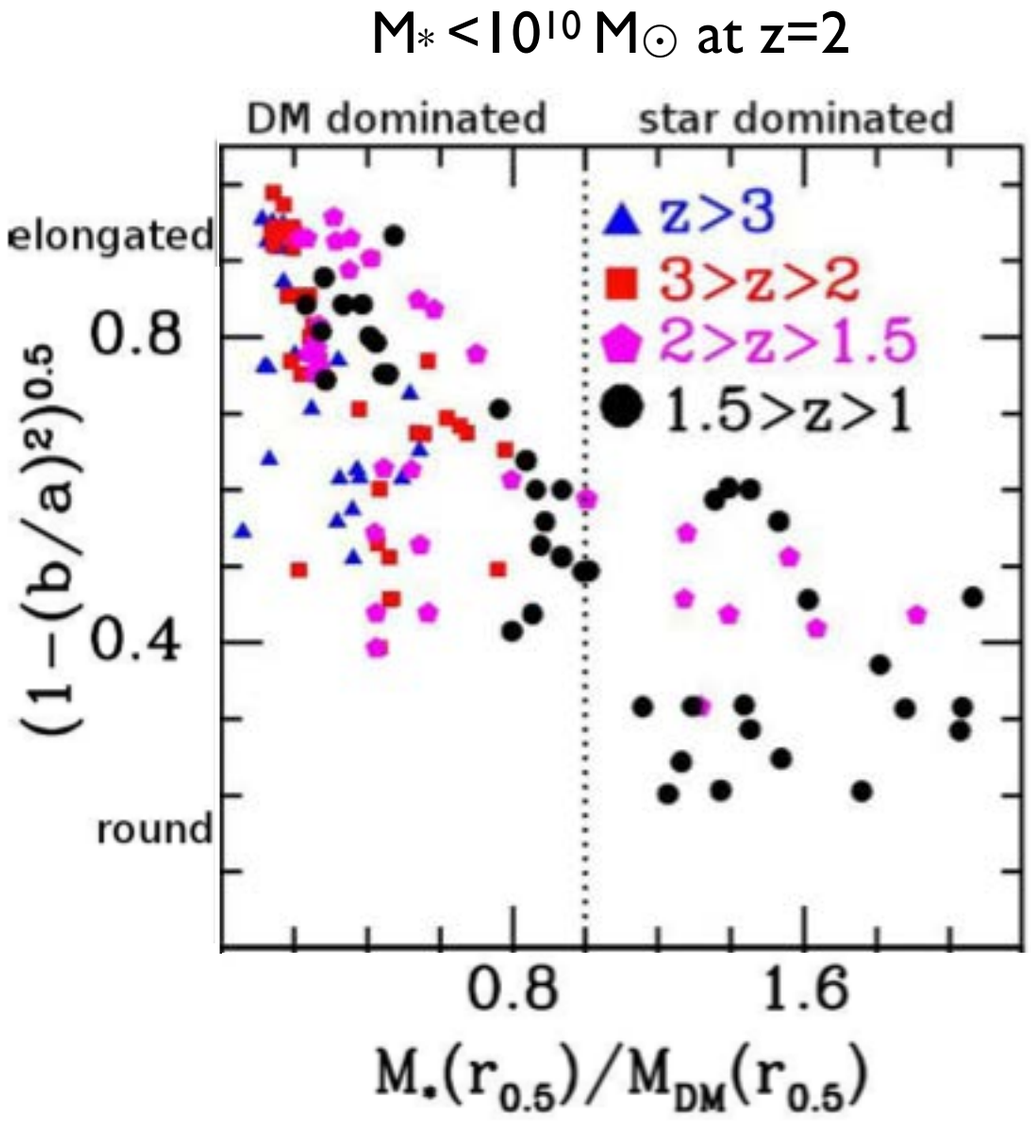

Also Tomassetti et al. 2016 MNRAS

Simulated elongated galaxies are aligned with cosmic web filaments, become round after compaction (gas inflow fueling central starburst)

CLUMPS in CANDELS - Yicheng Guo

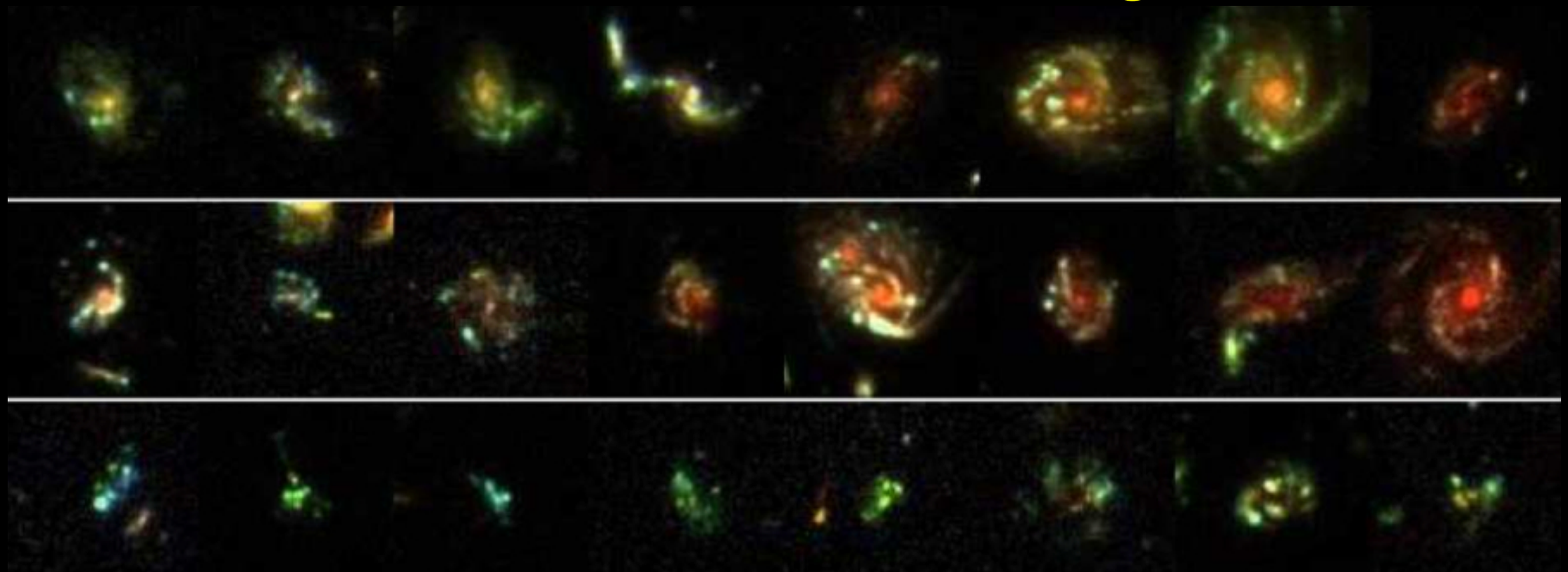

Clumps: Important Feature of High-redshift Star-formingGalaxies

- Seen in deep rest-frame UV (e.g., Elmegree+07, 09, Guo+12), rest-frame optical images (e.g., Forster Schreiber+11, Guo+12), and emission line maps (e.g, Genzel+08, 11)
- Span a wide redshift range: 0.5<z<5
- Typical stellar mass: 10^7~10^9 Msun, typical size: ~1 kpc
- Regions with blue UV—optical color and enhanced specific SFR (e.g., Guo+12, Wuyts+12)
- Many are in underlying disks, based on either morphological (e.g., Elmegreen+07,09) and kinematic (e.g., Genzel+11) analyses

About 60% of star-forming galaxies are clumpy at z ~ 2.5.

The evolution of the clump fraction is mass-dependent.

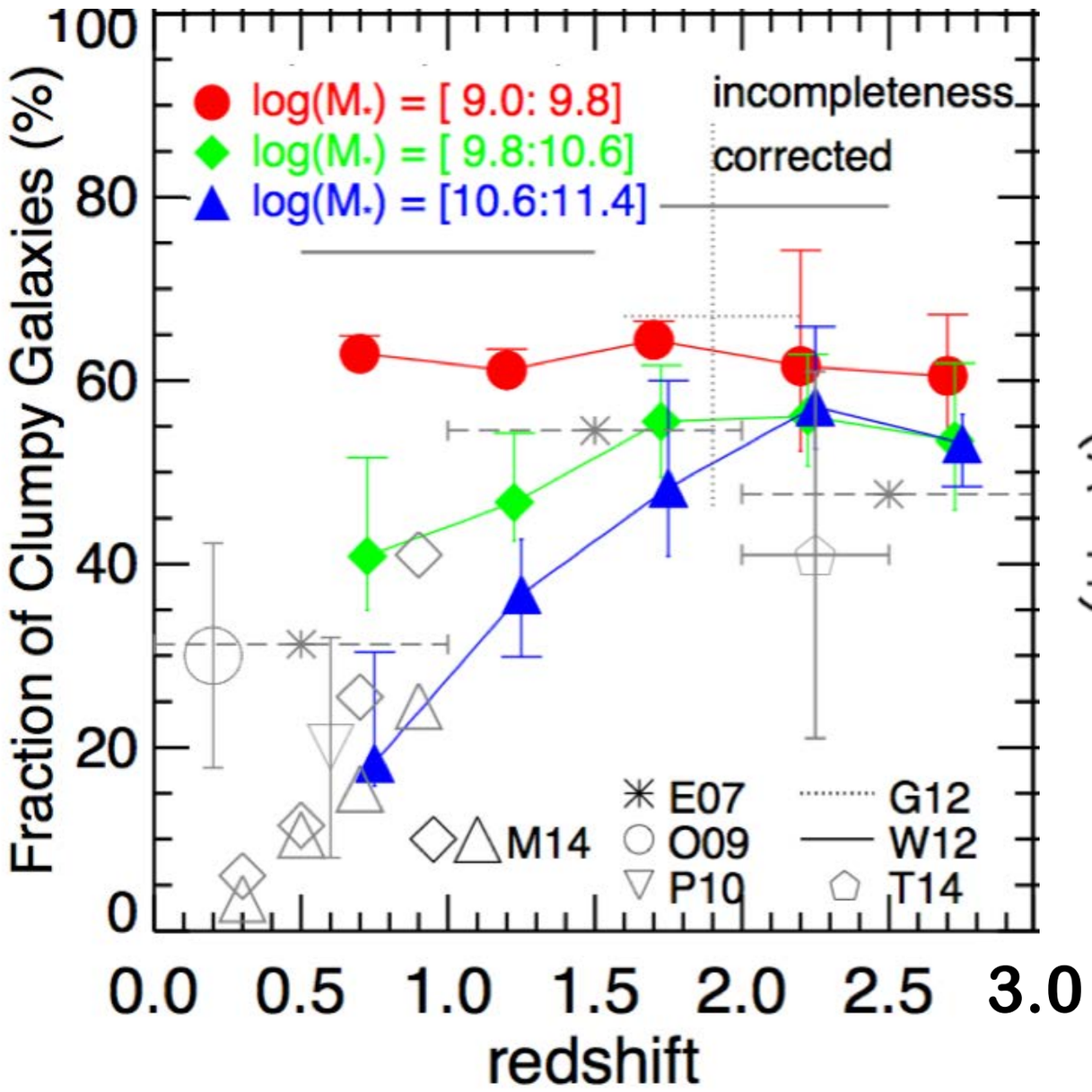

Yicheng Guo+2015

Clumps have radial variation of their UV-optical colors:

- outer clumps are bluer &

- central clumps are redder,

as clump radial migration predicts.

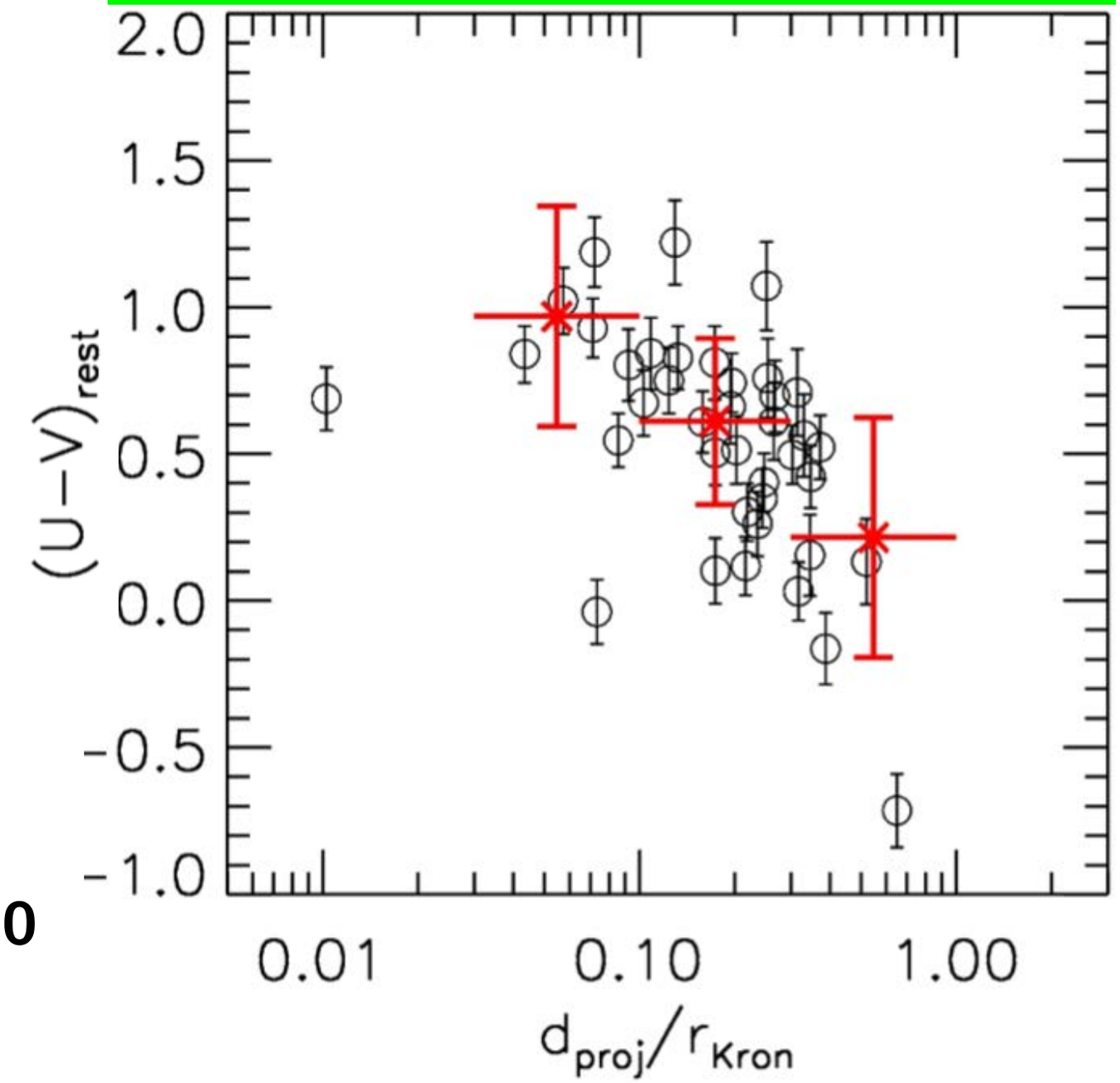

Yicheng Guo+2012

Clumpy Galaxies in CANDELS. II. Physical Properties of UV-bright Clumps at 0.5 < z <3

Yicheng Guo et al. ApJ 2018

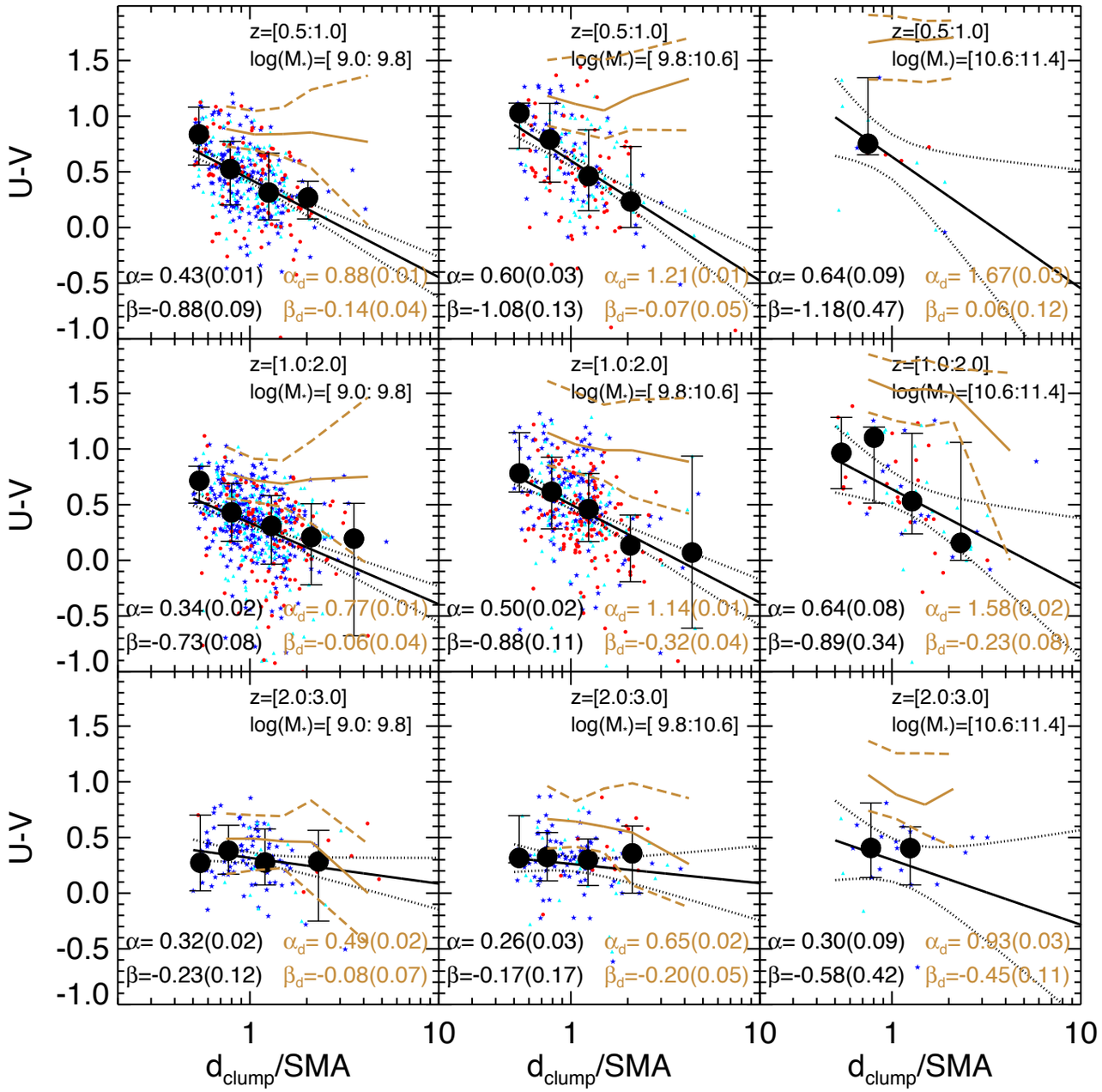

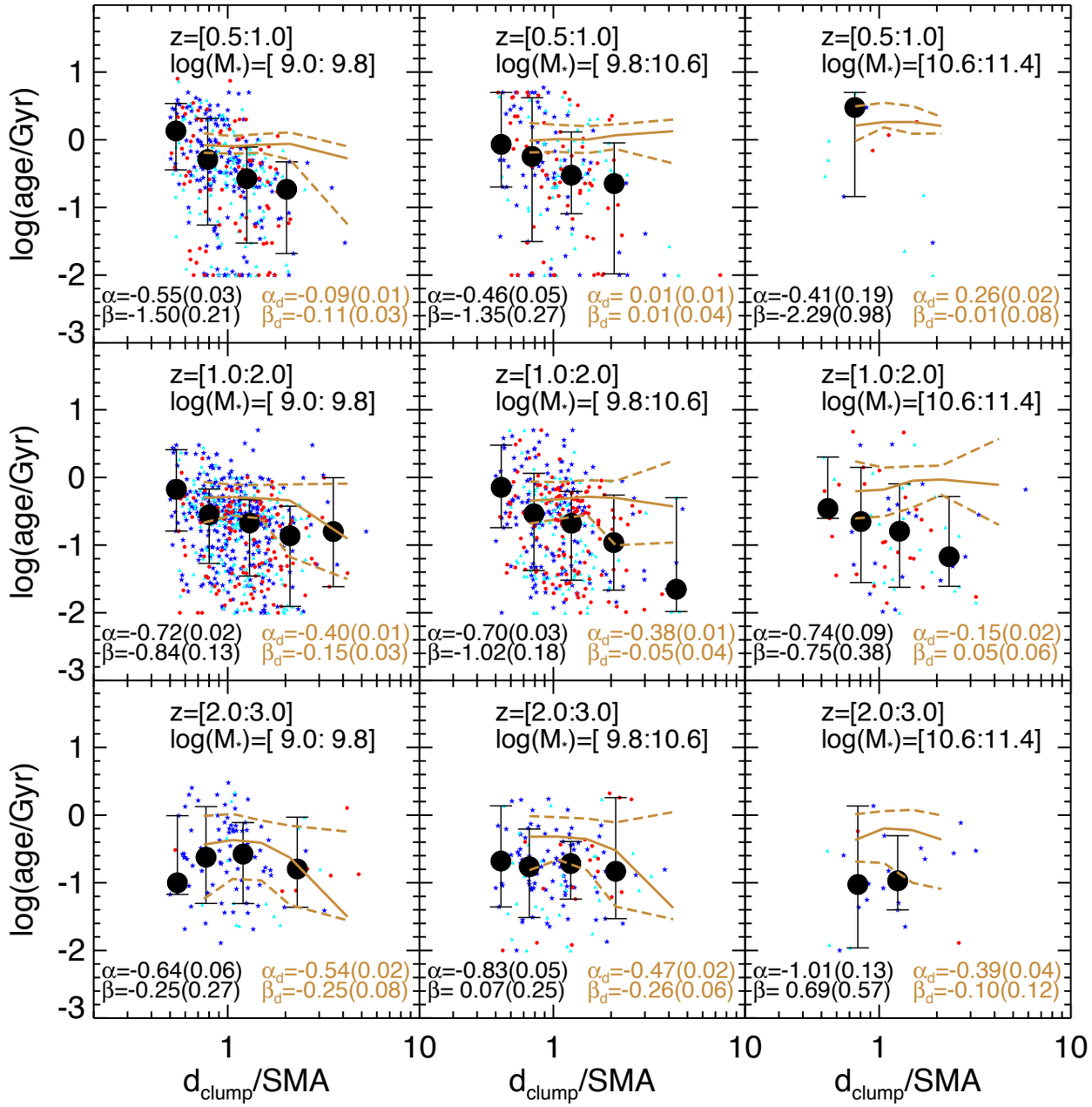

An important observation is that the clump gradients are steeper than those of the underlying "disk" at $z < 2$, so the clump gradients cannot be attributed to the "disk"

Yicheng's next clump paper will analyze the mock galaxy images from the VELA gen3 simulations. Christoph Lee and Marc Huertas-Company have a very fast deep learning code to do this that has been calibrated on Yicheng's clump catalog.

Giant clumps in simulated high-z Galaxies: properties, evolution and dependence on feedback

Nir Mandelker, Avishai Dekel, Daniel Ceverino, Colin DeGraf, Joel Primack, Yicheng Guo - **MNRAS 2017**

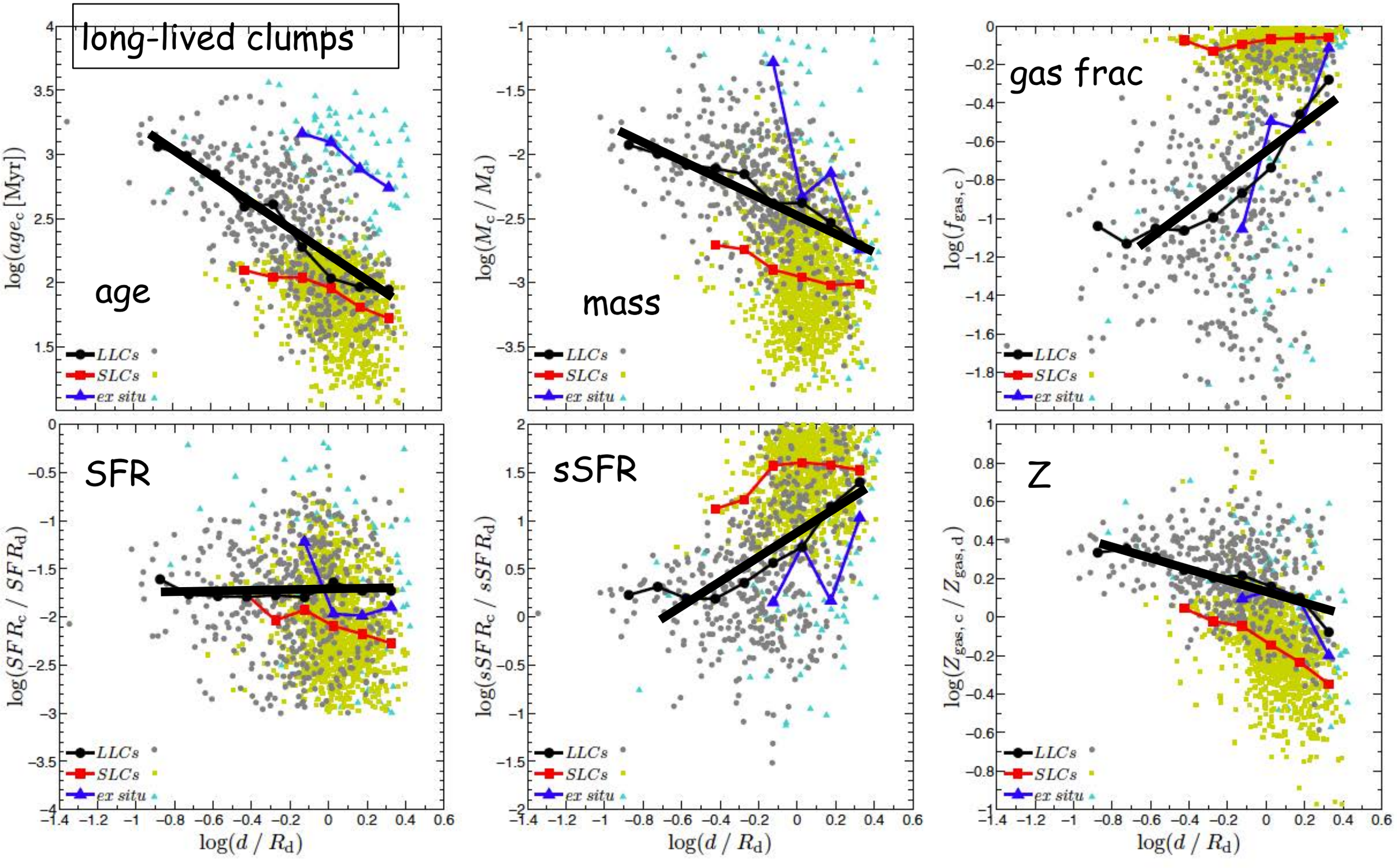

The Fast Track of Galaxy Evolution

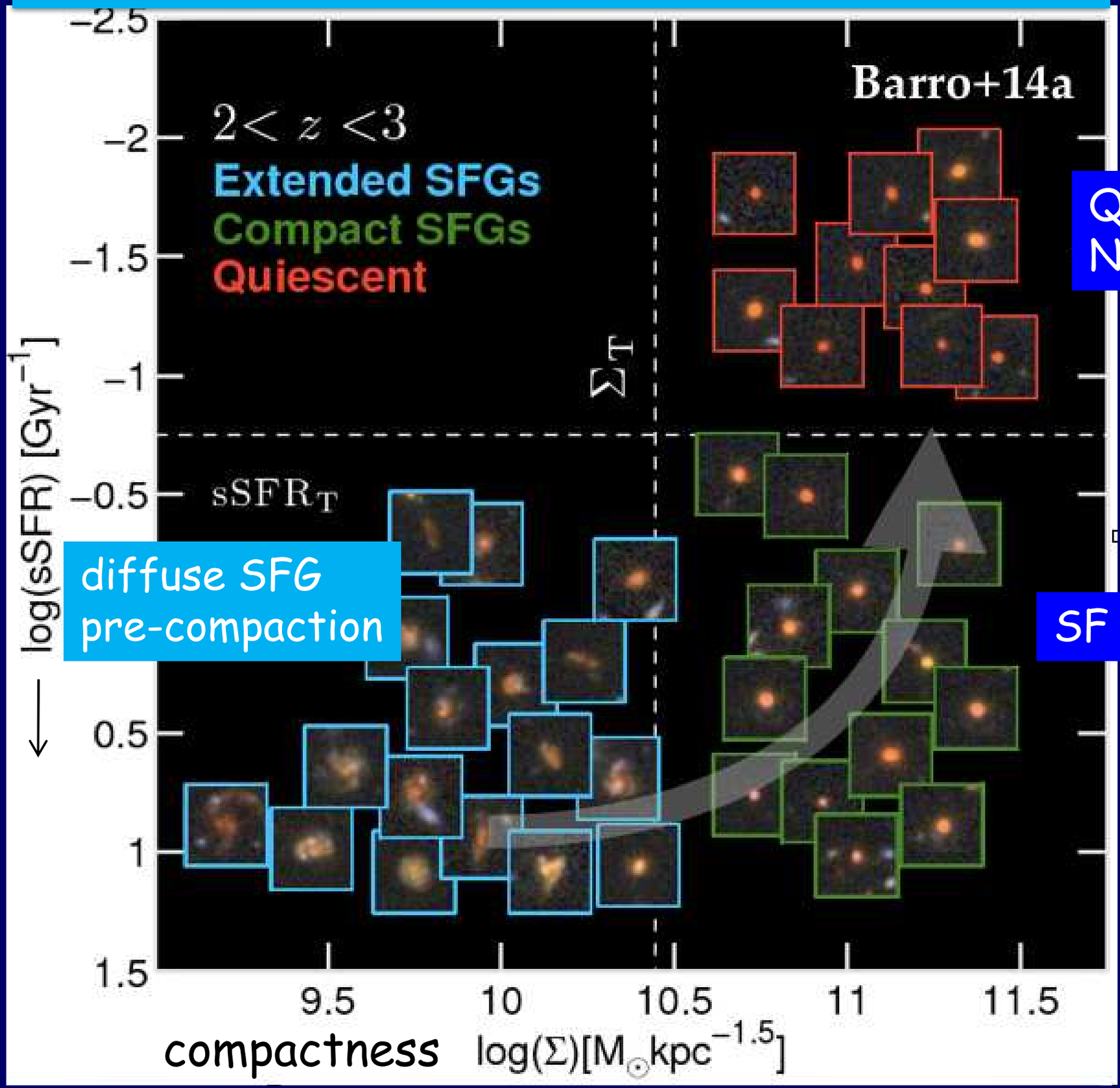

Quenched Nuggets

diffuse SFG pre-compaction

SF Nuggets

Ceverino+ RP simulations analyzed by Zolotov, Dekel, Tweed, Mandelker, Ceverino, & Primack MNRAS 2015

Barro+ (CANDELS) 2013

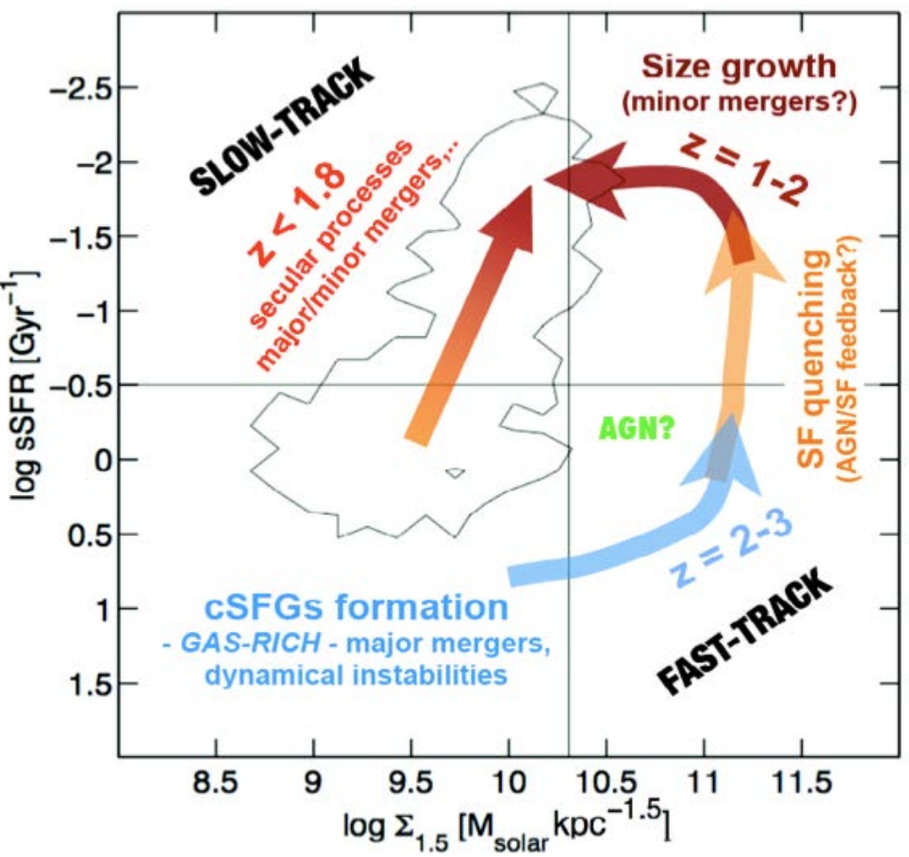

COMPACTION —>

major merger

minor merger

FAST-TRACK

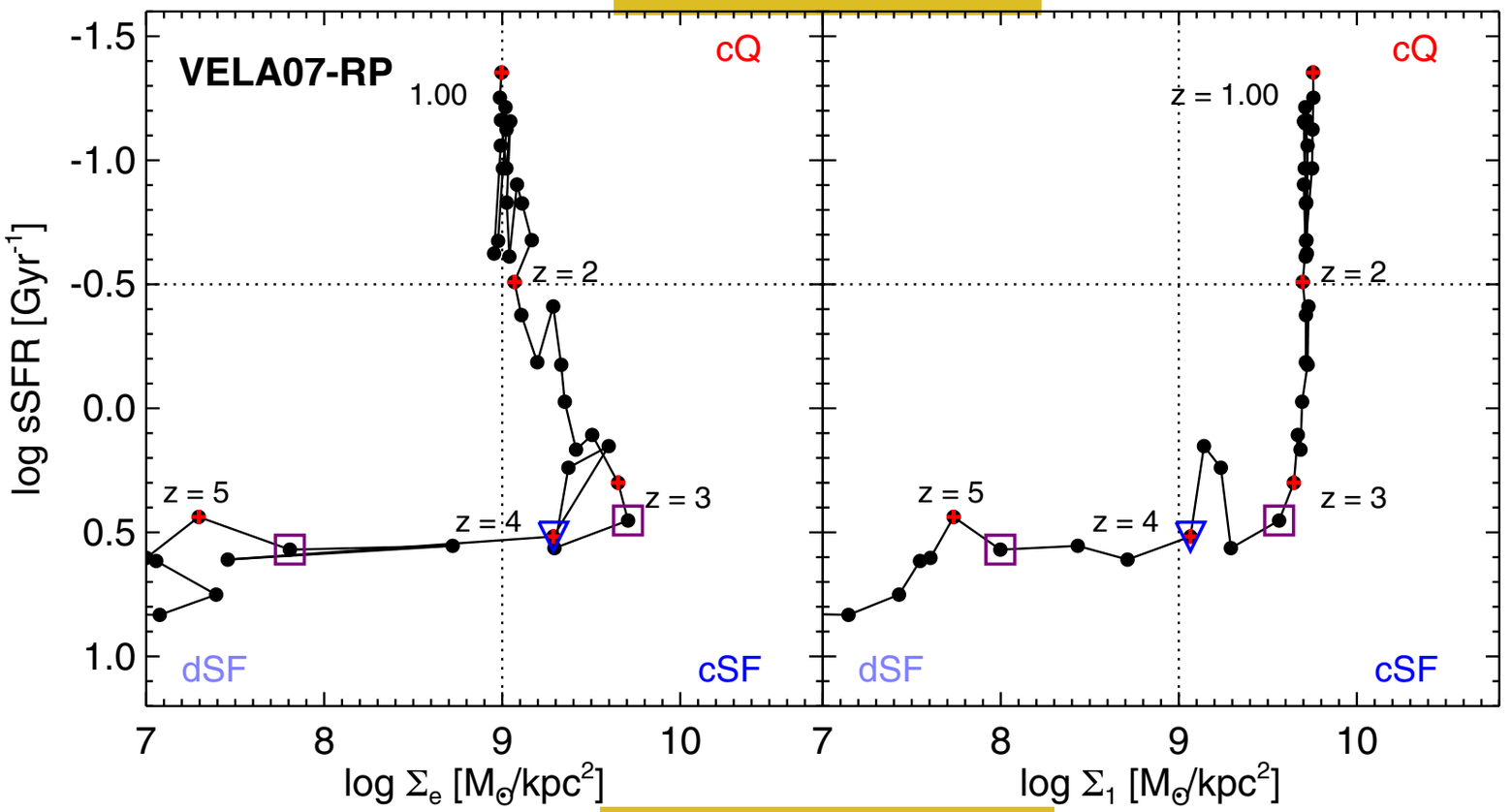

SLOW-TRACK

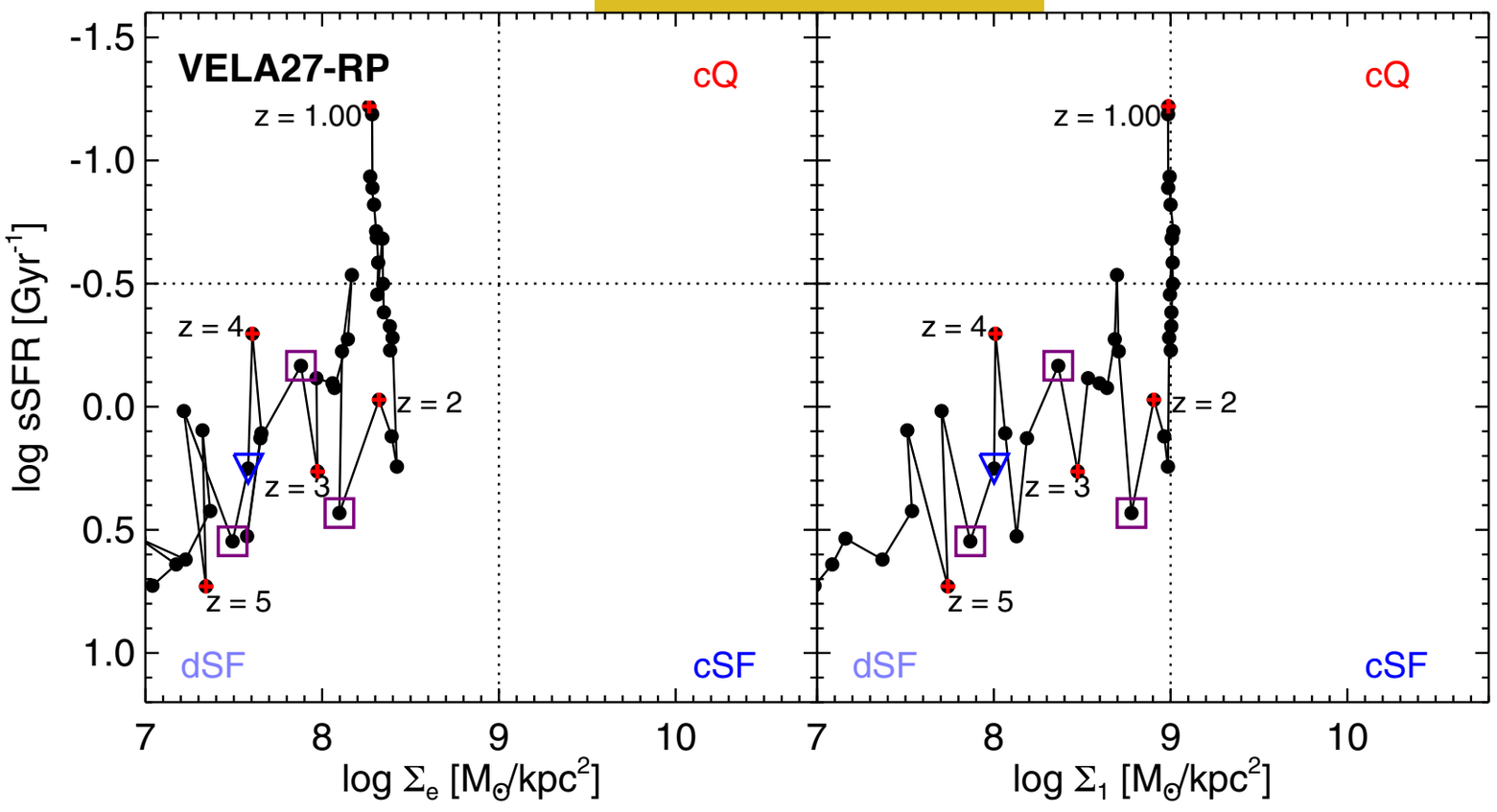

Zolotov+2015

Compaction and Quenching in the Inner 1 kpc

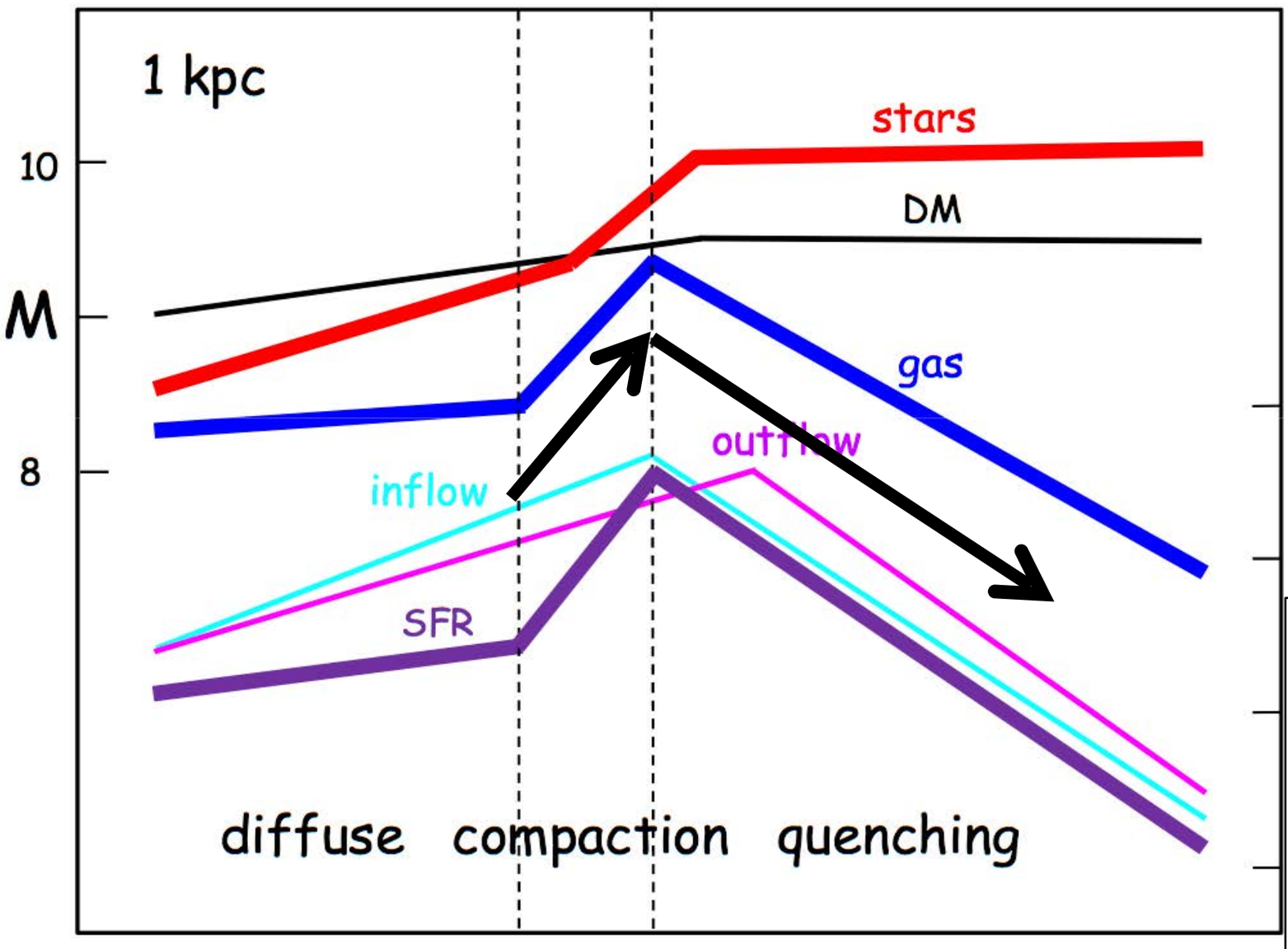

Inner 10 kpc

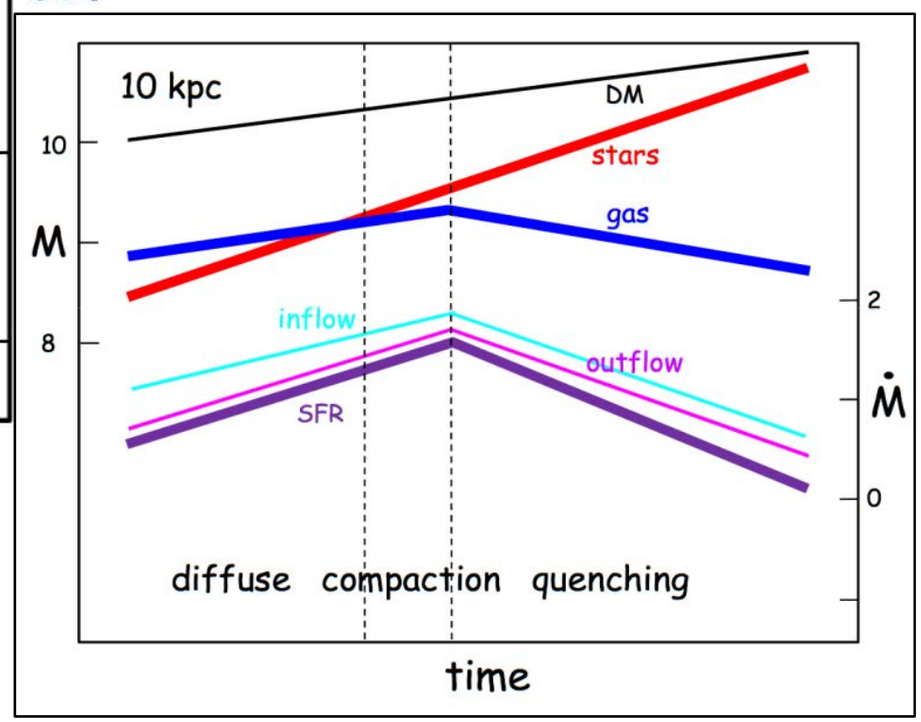

Avishai Dekel gen3 Zolotov+2015

VELA07-RP Animations z = 4.4 to 2.3

Daniel Ceverino, Nir Mandelker

DM
Gas
Stars

Compaction

Face-on

Edge-on

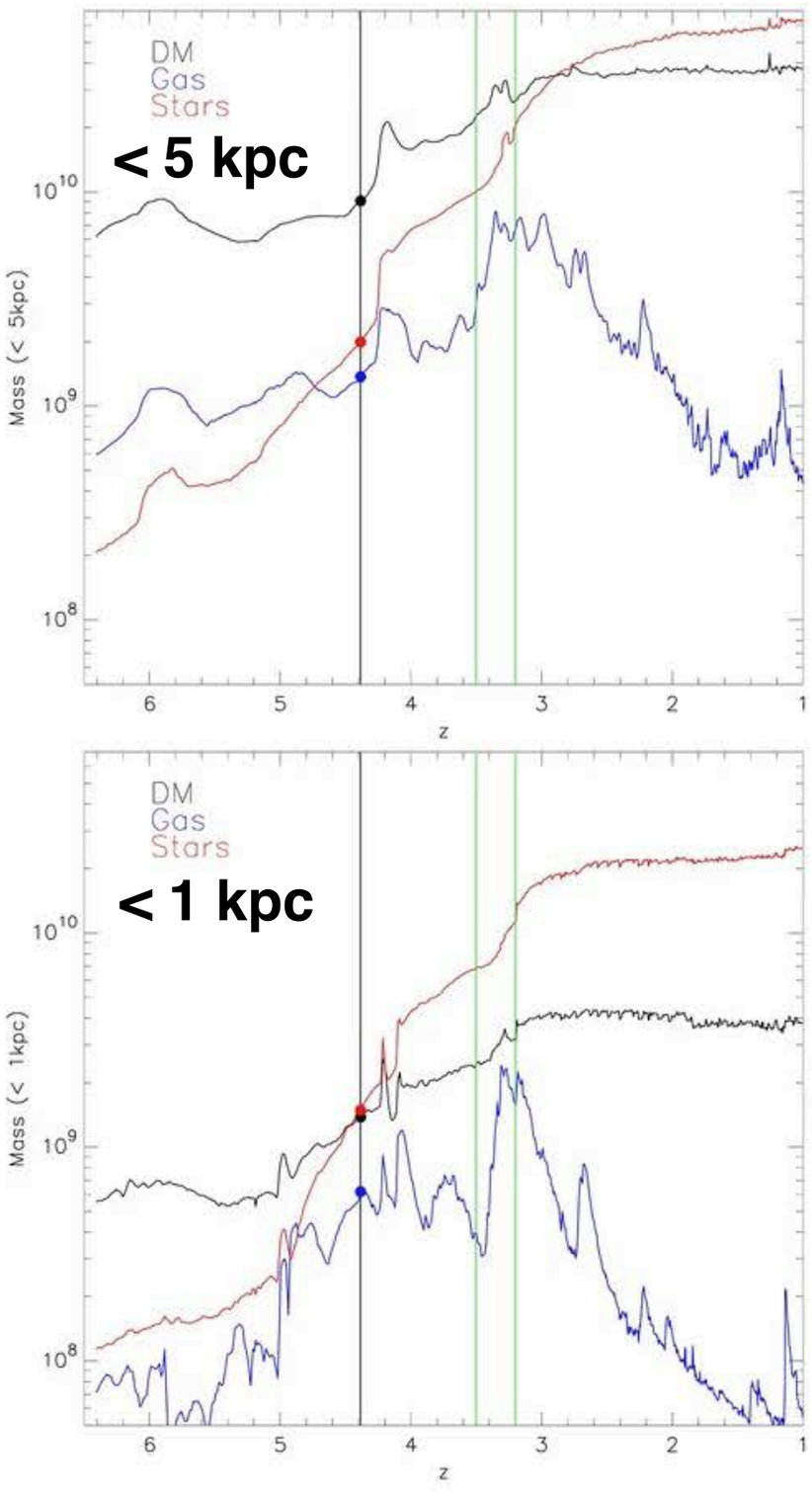

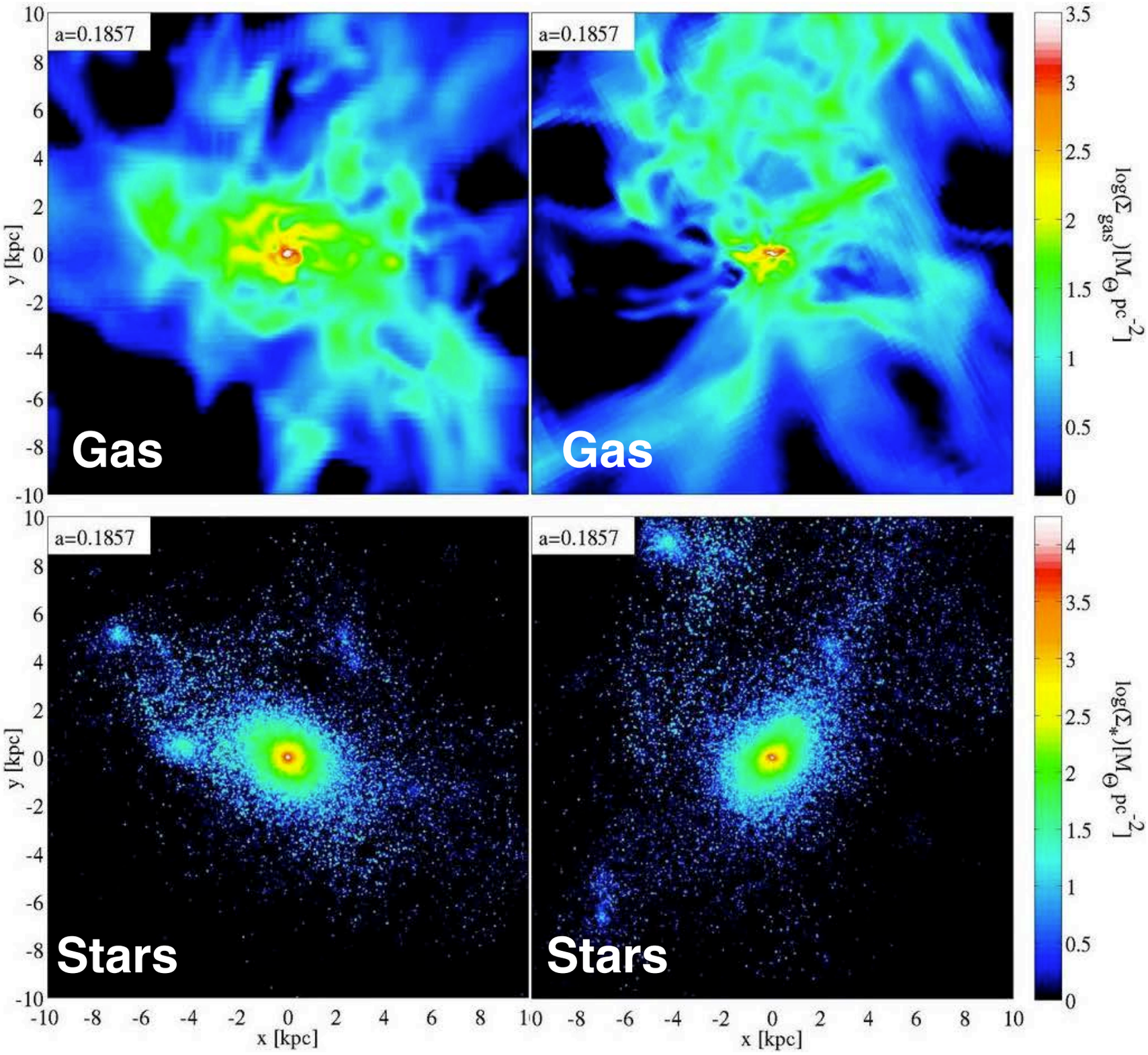

Phase of Compaction

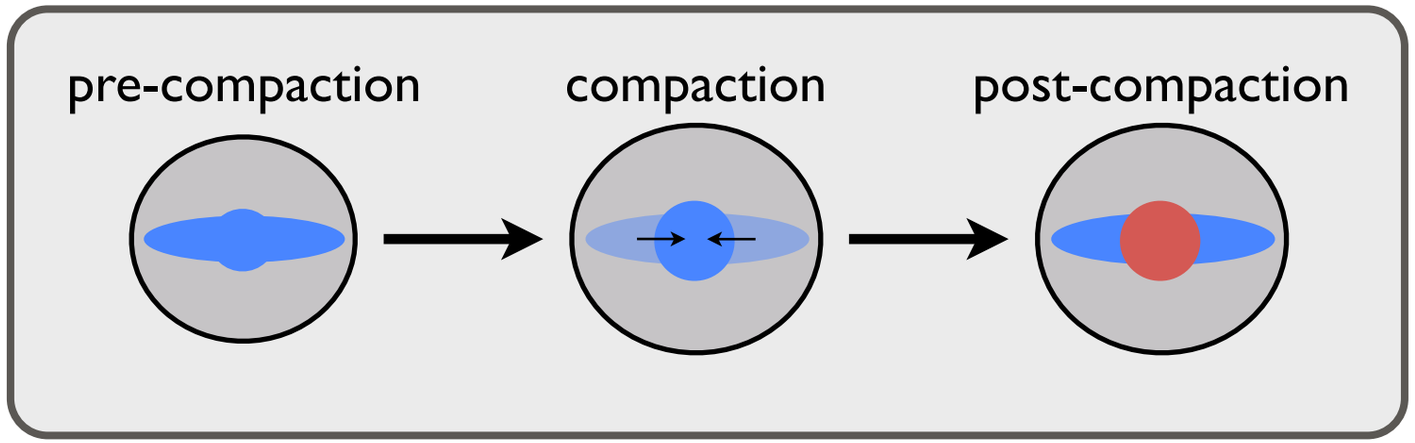

- stellar mass profiles:
  - growth self-similar
  - convergence in the center

- gas mass and SFR profiles:
  - cusp in the compaction phase
  - ring thereafter

- sSFR profiles:
  - inside-out quenching

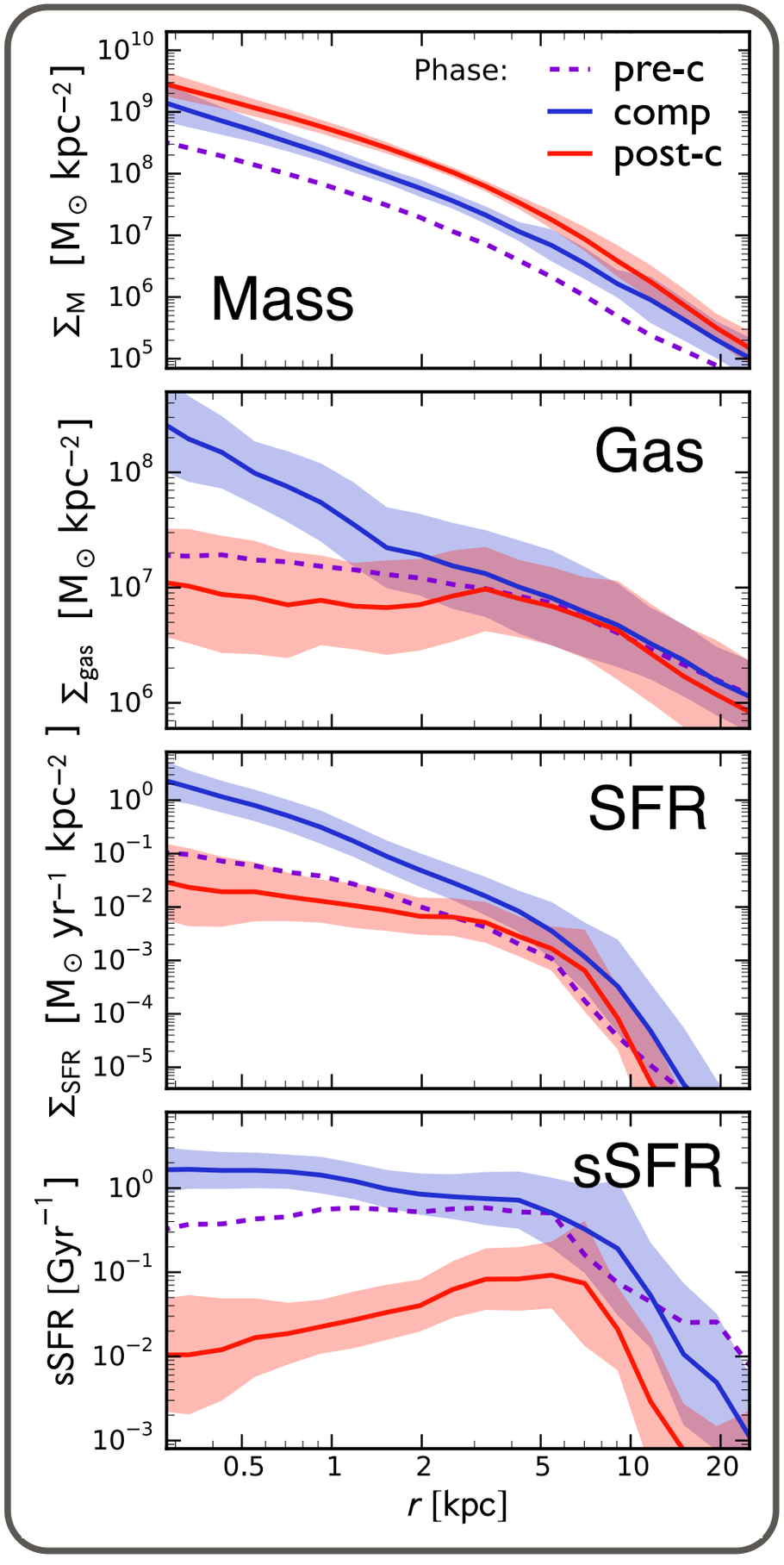

Tacchella+2016 Evolution of Density Profiles in High-z Galaxies: Compaction and Quenching Inside-Out

Comparison: Simulations — Observations

Stellar profiles agree over 4 orders of magnitude in surface density ➜

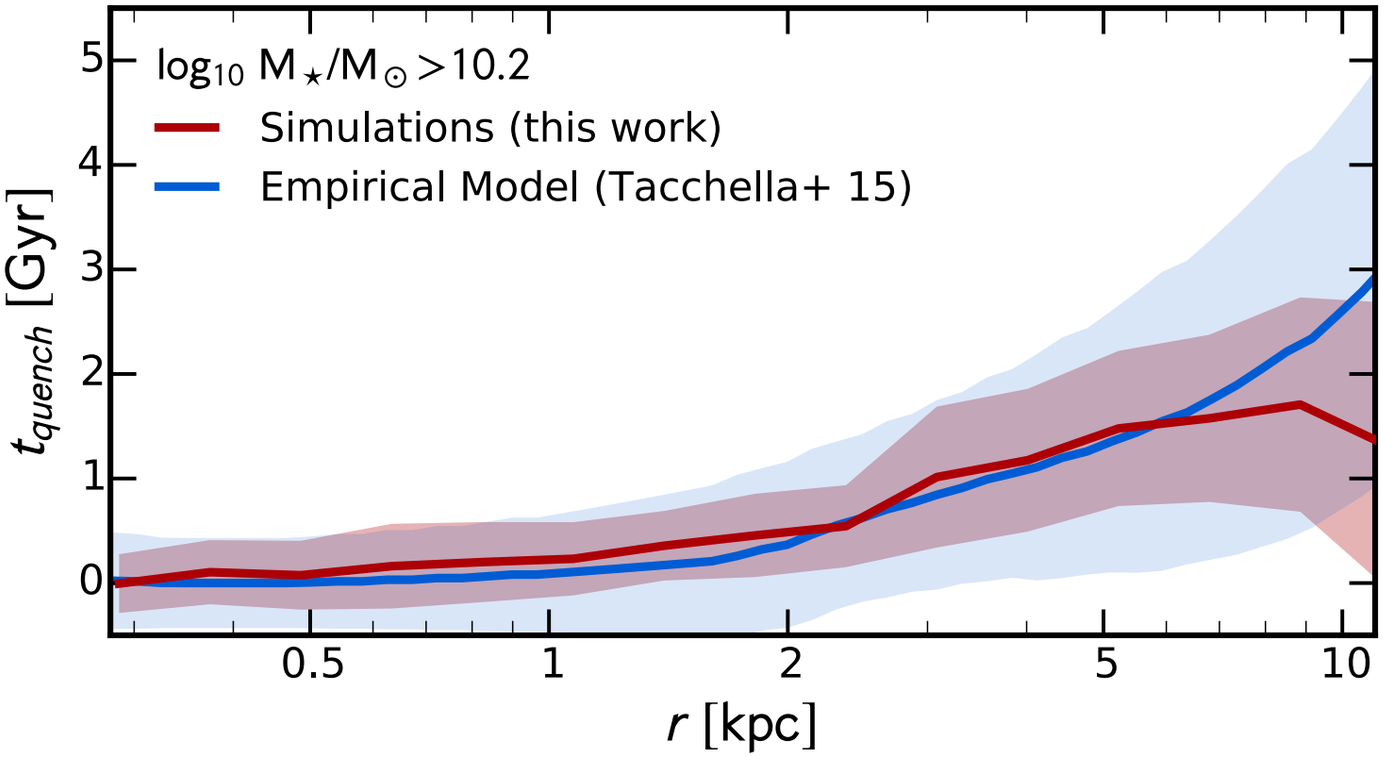

qualitative similar quenching progression in empirical model and simulations

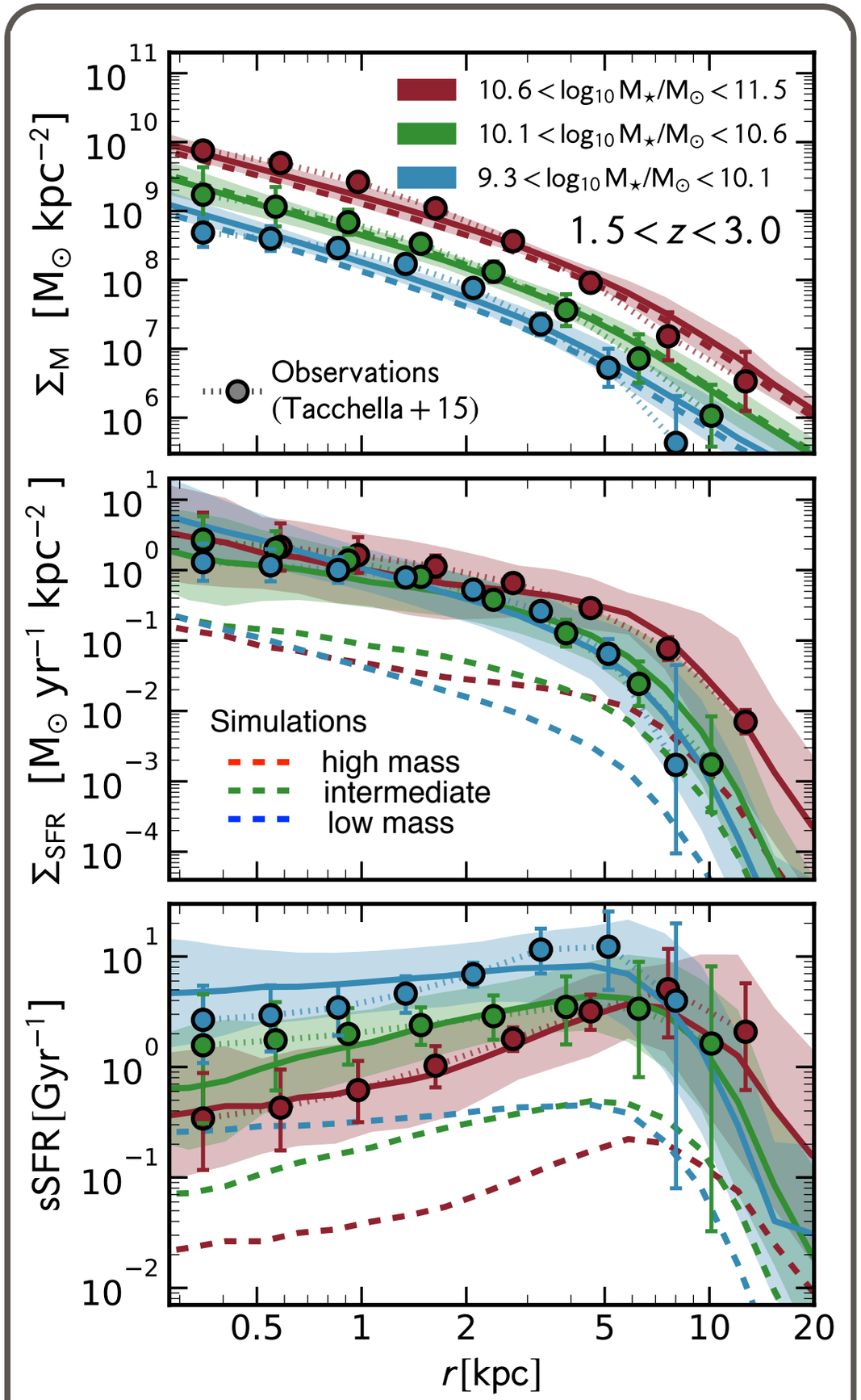

Tacchella+2016 Evolution of Density Profiles in High-z Galaxies: Compaction and Quenching Inside-Out

Evolution of the Average Size

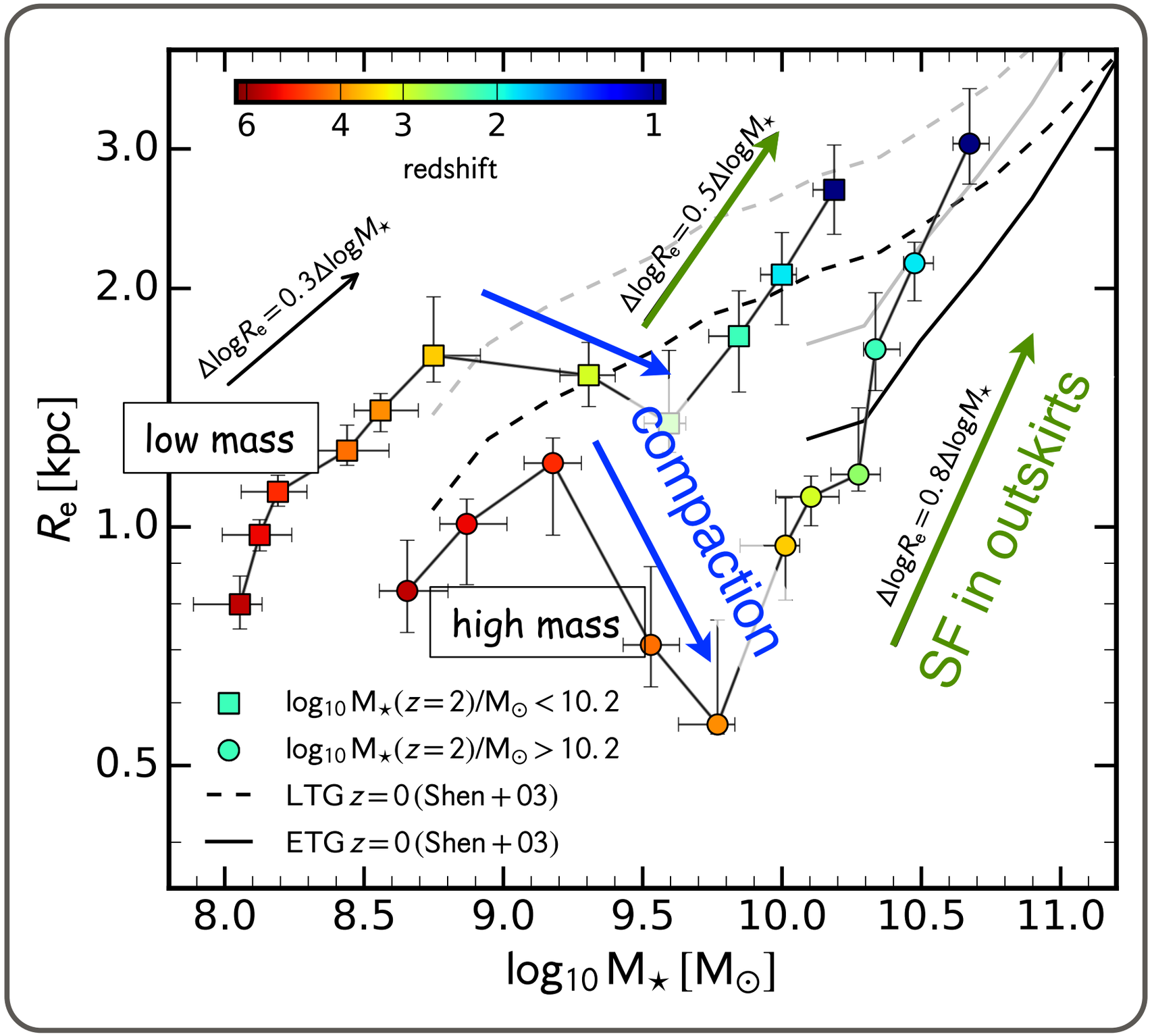

Tacchella+2016 Evolution of Density Profiles in High-z Galaxies: Compaction and Quenching Inside-Out

Star-Forming Main Sequence in the Simulations

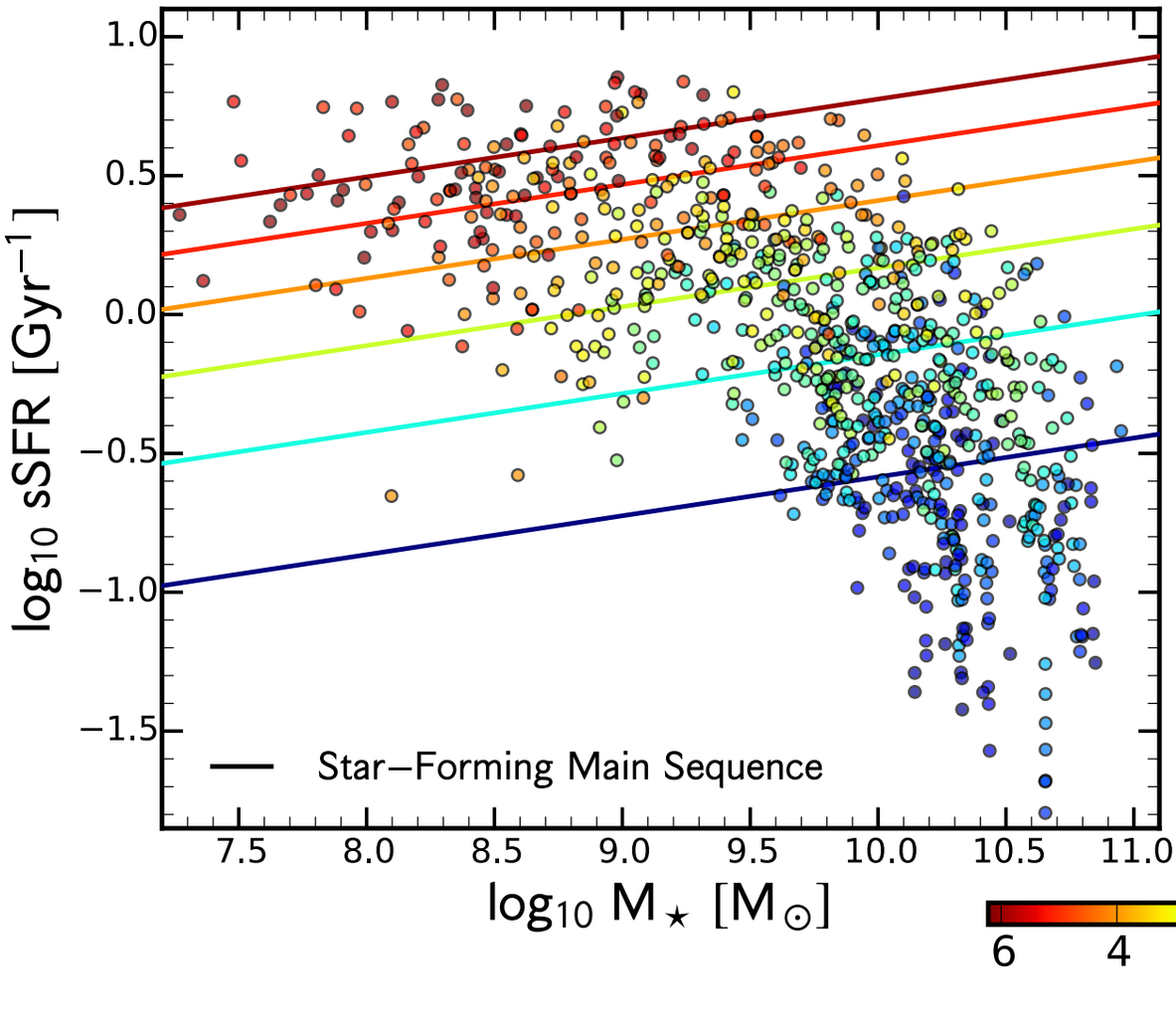

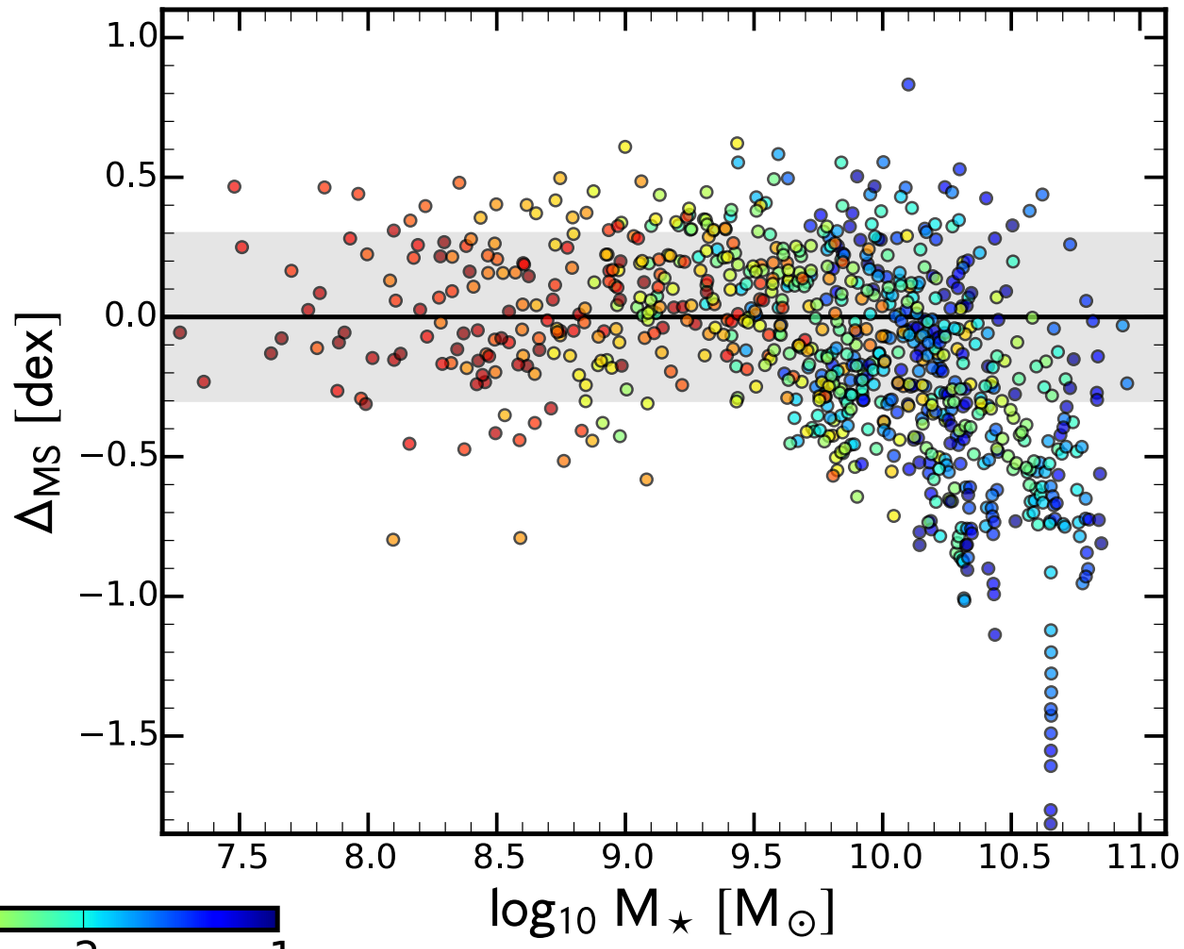

- distance from the MS:

$$\Delta_{\rm MS} = \log_{10}\left(\frac{\rm sSFR}{\rm sSFR_{MS}}\right)$$

$$\rm sSFR_{MS}(M_\star, z) = s \cdot \left(\frac{M_\star}{10^{10}\ M_\odot}\right)^{\beta} \cdot (1+z)^{\mu}\ \ Gyr^{-1}$$

- scatter in the simulations:

$$\sigma_{\rm MS} = 0.24\ \text{dex}\ (z=5) \rightarrow 0.31\ \text{dex}\ (z=3)$$

Tacchella+2016 The Confinement of Star-Forming Galaxies into a Main Sequence through Gas Compaction, Depletion and Quenching

Evolution of Galaxies about the Star-Forming Main Sequence

Tacchella+2016 The Confinement of Star-Forming Galaxies into a Main Sequence through Gas Compaction, Depletion and Quenching

Variety of triggers (mostly external)

High Gas Density

→ Dense Bulge Formation

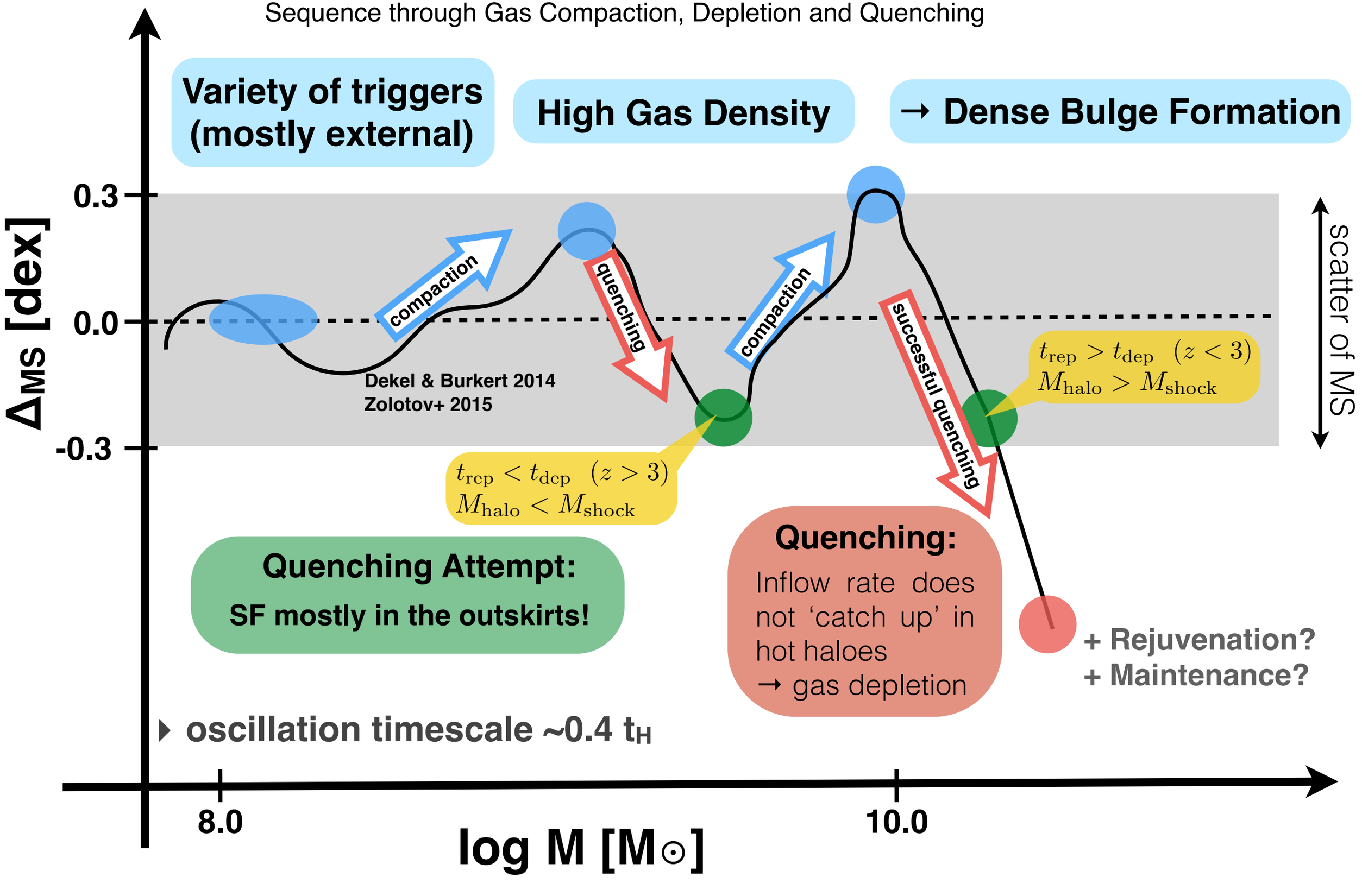

Quenching Attempt:

SF mostly in the outskirts!

Quenching:

Inflow rate does not 'catch up' in hot haloes
→ gas depletion

+ Rejuvenation?
+ Maintenance?

oscillation timescale ~0.4 t_H

Gradient across the Main Sequence

- galaxies at the upper envelope of the MS have …
  - … high central gas densities
  - … high total gas masses
  - … high gas to stellar mass ratios
  - … depletion time - MS correlation

  } **agree with Genzel+2015 observations**

- central gas mass density:

$$\log_{10} \rho_{\rm gas,1kpc} \propto 0.8 \times \Delta_{\rm MS}$$

- total gas mass:

$$\log_{10} M_{\rm gas} \propto 0.5 \times \Delta_{\rm MS}$$

- gas to stellar mass ratio:

$$\log_{10} M_{\rm gas}/M_\star \propto 0.5 \times \Delta_{\rm MS}$$

- depletion time:

$$\log_{10} t_{\rm dep} \propto 0.5 \times \Delta_{\rm MS}$$

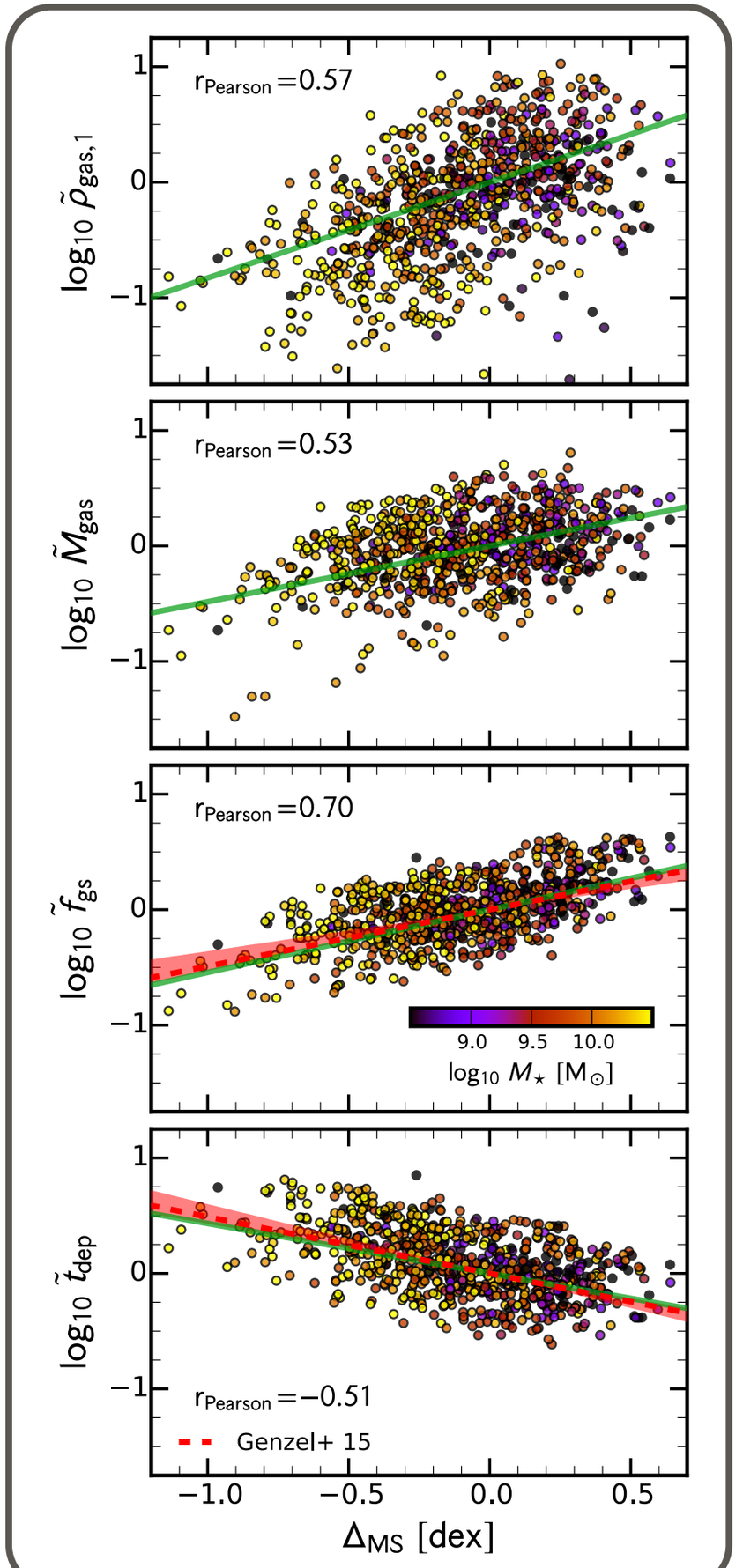

Tacchella+2016 The Confinement of Star-Forming Galaxies into a Main Sequence through Gas Compaction, Depletion and Quenching

“Face Recognition for Galaxies”

Deep Learning Identifies High-z Galaxies in a Central Blue Nugget Phase in a Characteristic Mass Range

Marc Huertas-Company, Joel Primack, Avishai Dekel, David Koo, Sharon Lapiner, Daniel Ceverino, Raymond Simons, Greg Snyder, et al. ApJ 2018

ABSTRACT

We use machine learning to identify in color images of high-redshift galaxies an astrophysical phenomenon predicted by cosmological simulations. This phenomenon, called the blue nugget (BN) phase, is the compact star-forming phase in the central regions of many growing galaxies that follows an earlier phase of gas compaction and is followed by a central quenching phase. We train a convolutional neural network (CNN) with mock “observed” images of simulated galaxies at three phases of evolution— pre-BN, BN, and post-BN—and demonstrate that the CNN successfully retrieves the three phases in other simulated galaxies. We show that BNs are identified by the CNN within a time window of ~0.15 Hubble times. When the trained CNN is applied to observed galaxies from the CANDELS survey at z =1–3, it successfully identifies galaxies at the three phases. We find that the observed BNs are preferentially found in galaxies at a characteristic stellar mass range, $10^{9.2–10.3}$ M_e at all redshifts. This is consistent with the characteristic galaxy mass for BNs as detected in the simulations and is meaningful because it is revealed in the observations when the direct information concerning the total galaxy luminosity has been eliminated from the training set. This technique can be applied to the classification of other astrophysical phenomena for improved comparison of theory and observations in the era of large imaging surveys and cosmological simulations.

Pre-Blue-Nugget-Stage **Blue-Nugget-Stage** **Post-Blue-Nugget-Stage**

High-resolution images from a computer simulation of a young galaxy going through the 3 phases of evolution

Same images from the computer simulation of a young galaxy going through the 3 phases of evolution, as it would be observed by Hubble Space Telescope

Hubble Space Telescope images of distant young galaxies classified into the 3 phases with a deep learning algorithm

Examples of simulated galaxy evolution through the 3 stages: Pre-Blue Nugget (often elongated, i.e. pickle shaped), Blue Nugget (compaction phenomenon: gas infall leads to central starburst), and Post-Blue Nugget (often with star-forming disk), with similar galaxies observed by Hubble Space Telescope. The width of each image is approximately 100,000 light years. Credits: simulations Daniel Ceverino and Joel Primack, simulated images Greg Snyder, HST observations CANDELS.

pre-BN

Age of the universe:

1.1 billion years

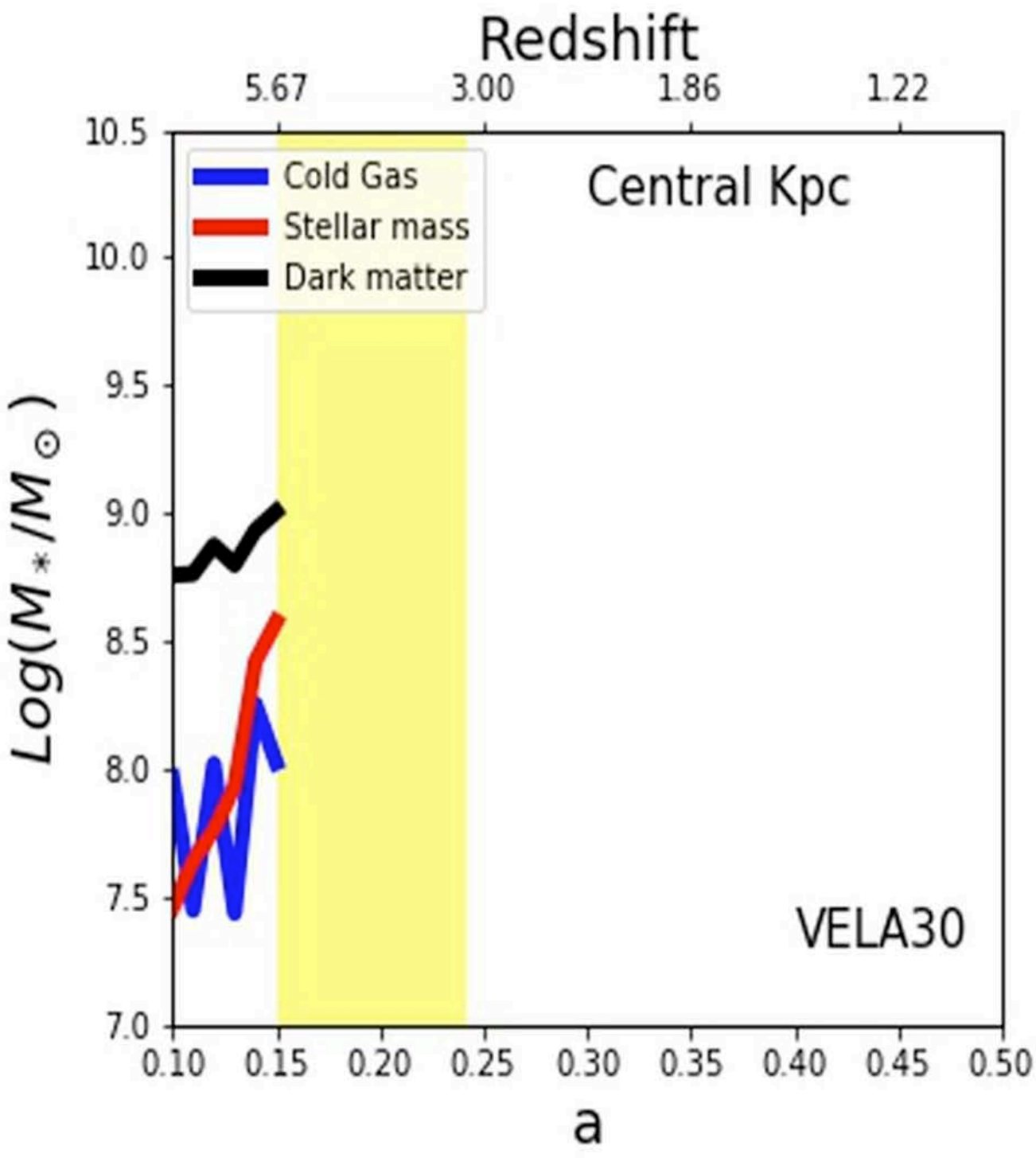

Simulated galaxy with single compaction event

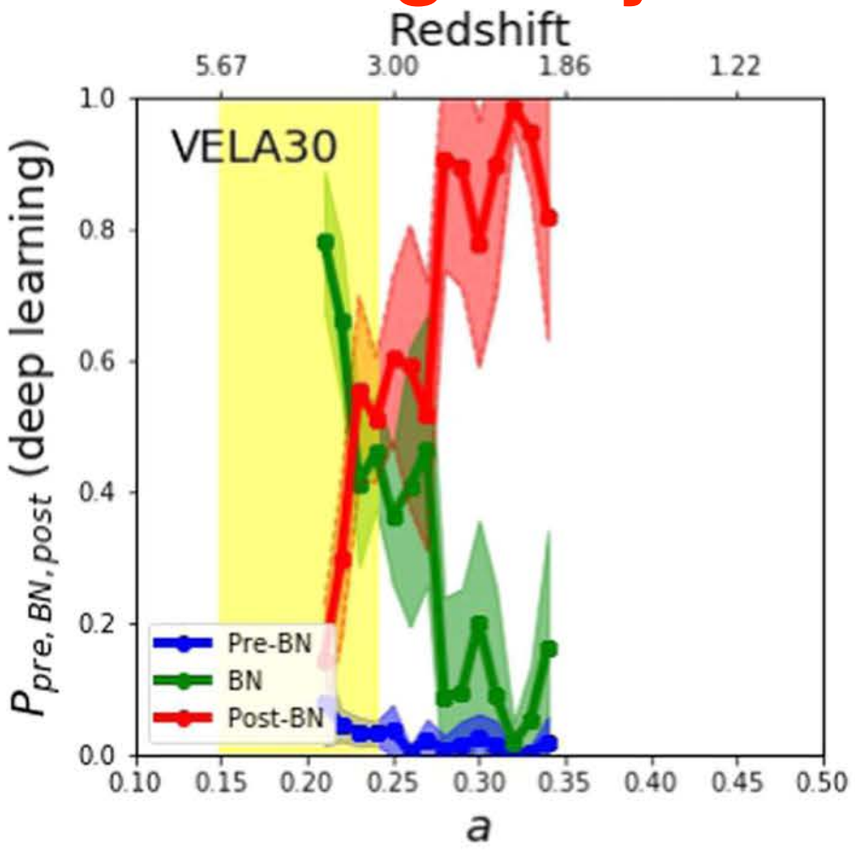

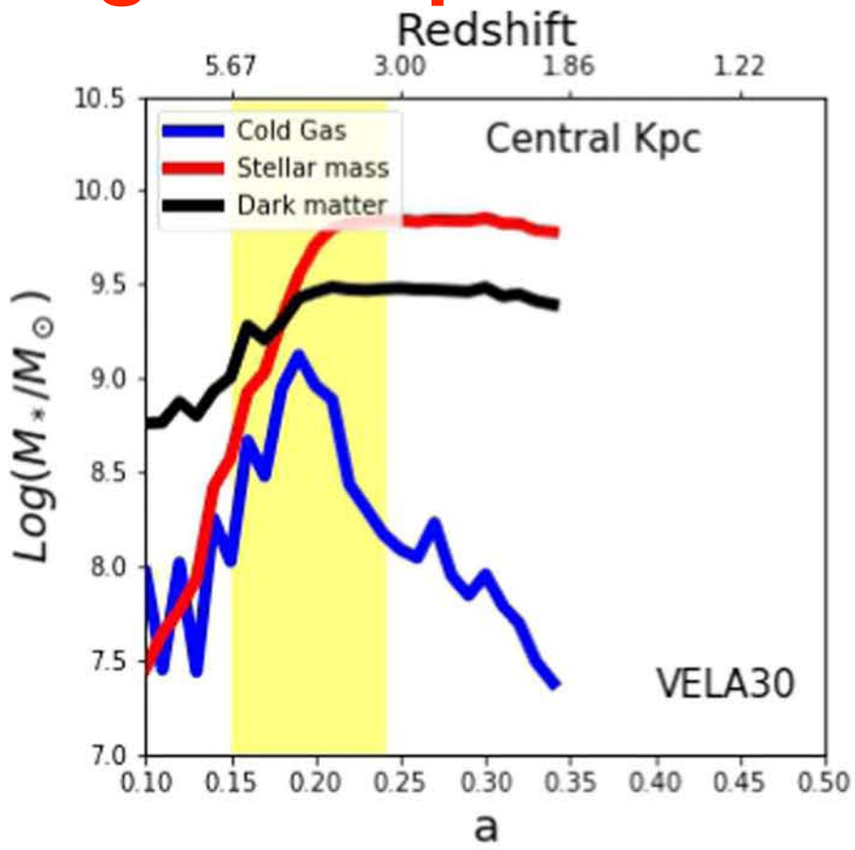

Simulated galaxy with two compaction events

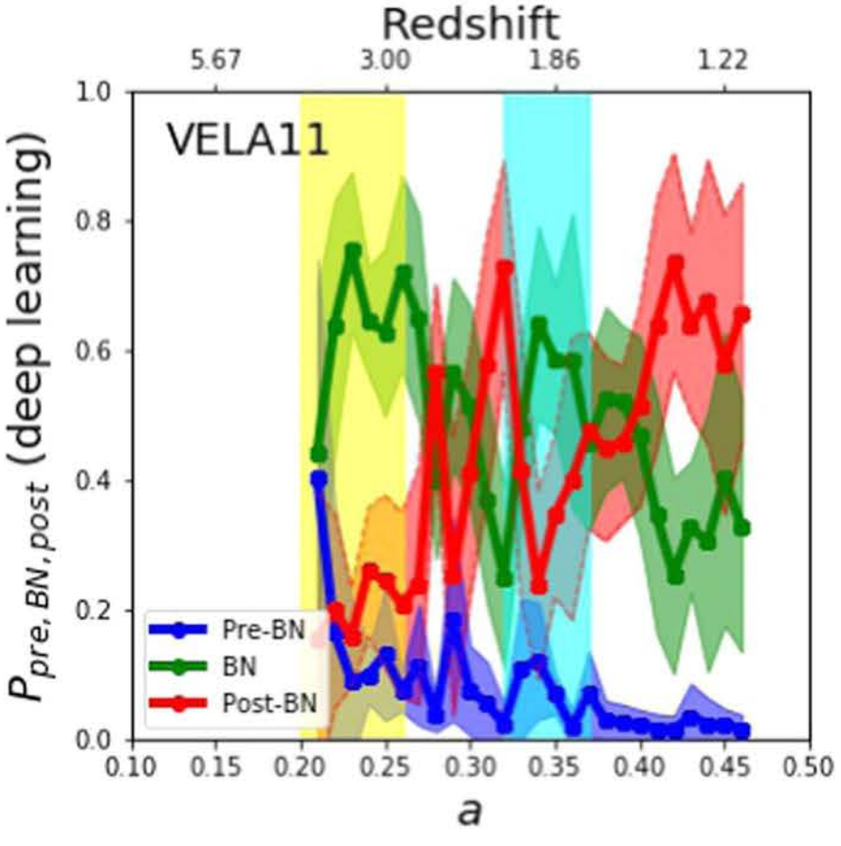

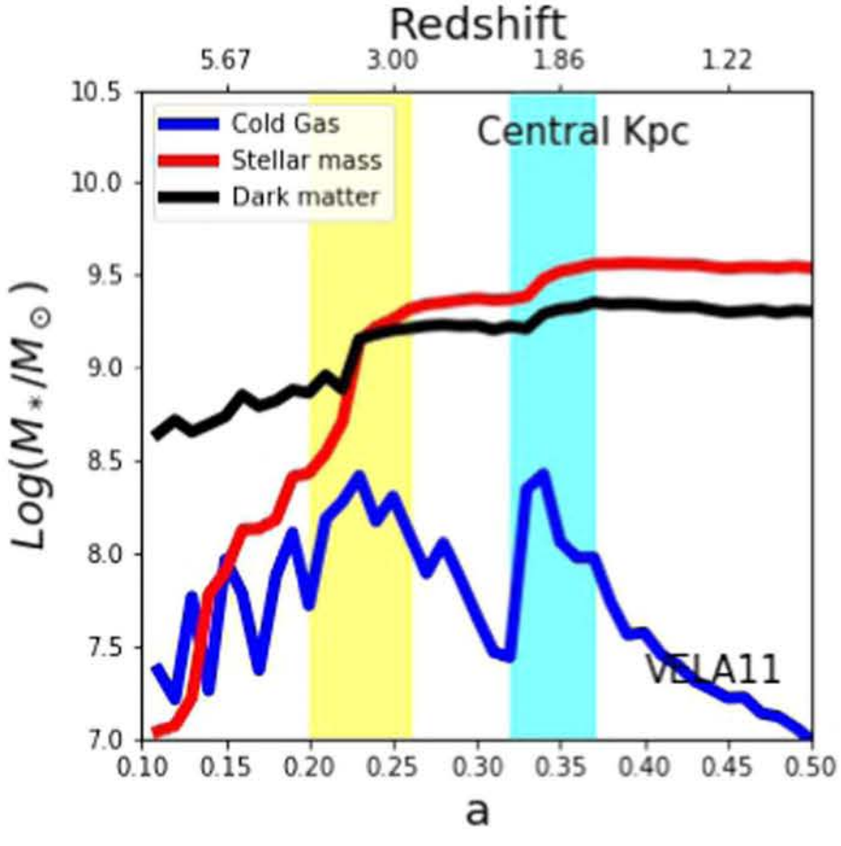

Examples of CANDELized simulated galaxy images

Pre-BN phase

BN phase

Post-BN phase

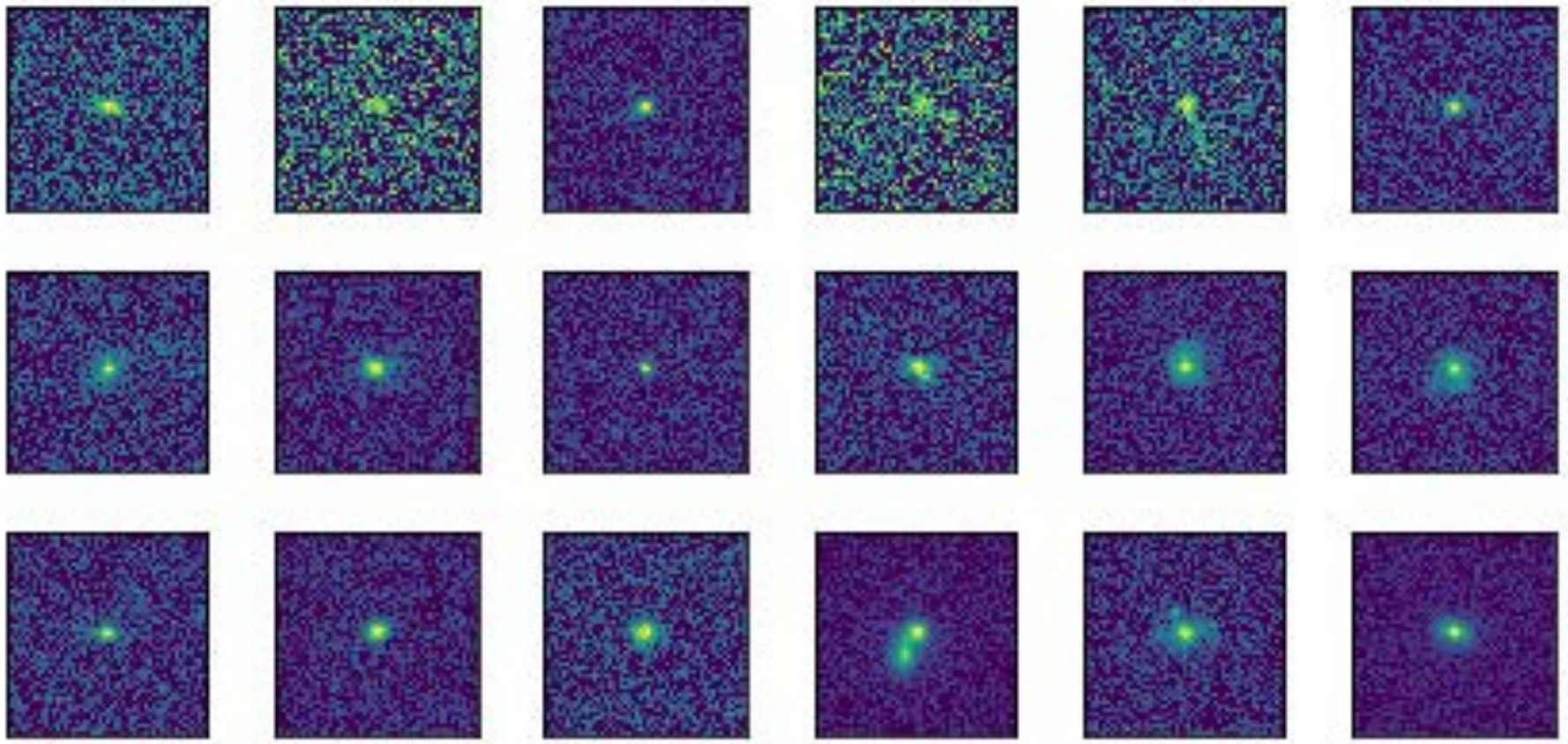

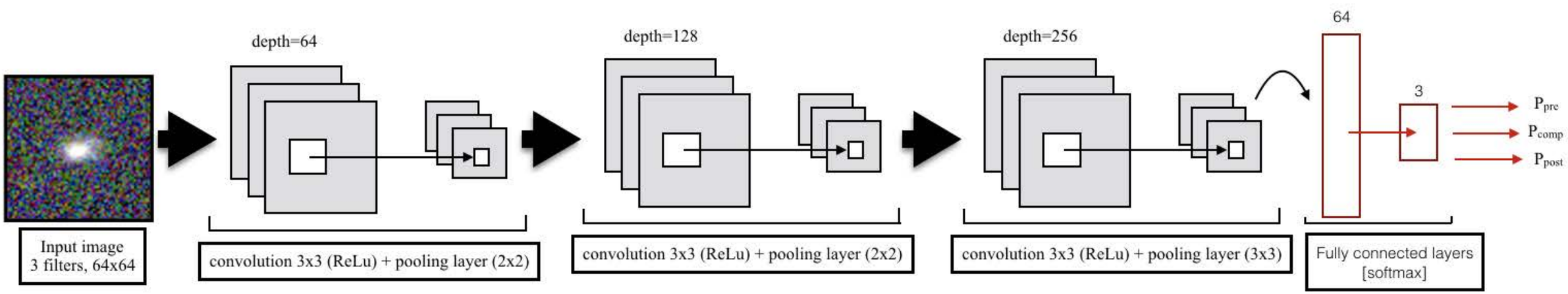

Architecture of the deep network used for classification in this work. The network is a standard and simple CNN configuration made of 3 convolutional layers followed by pooling and dropout.

Simulated CANDELized Images

Pre-BN phase

BN phase

Post-BN phase

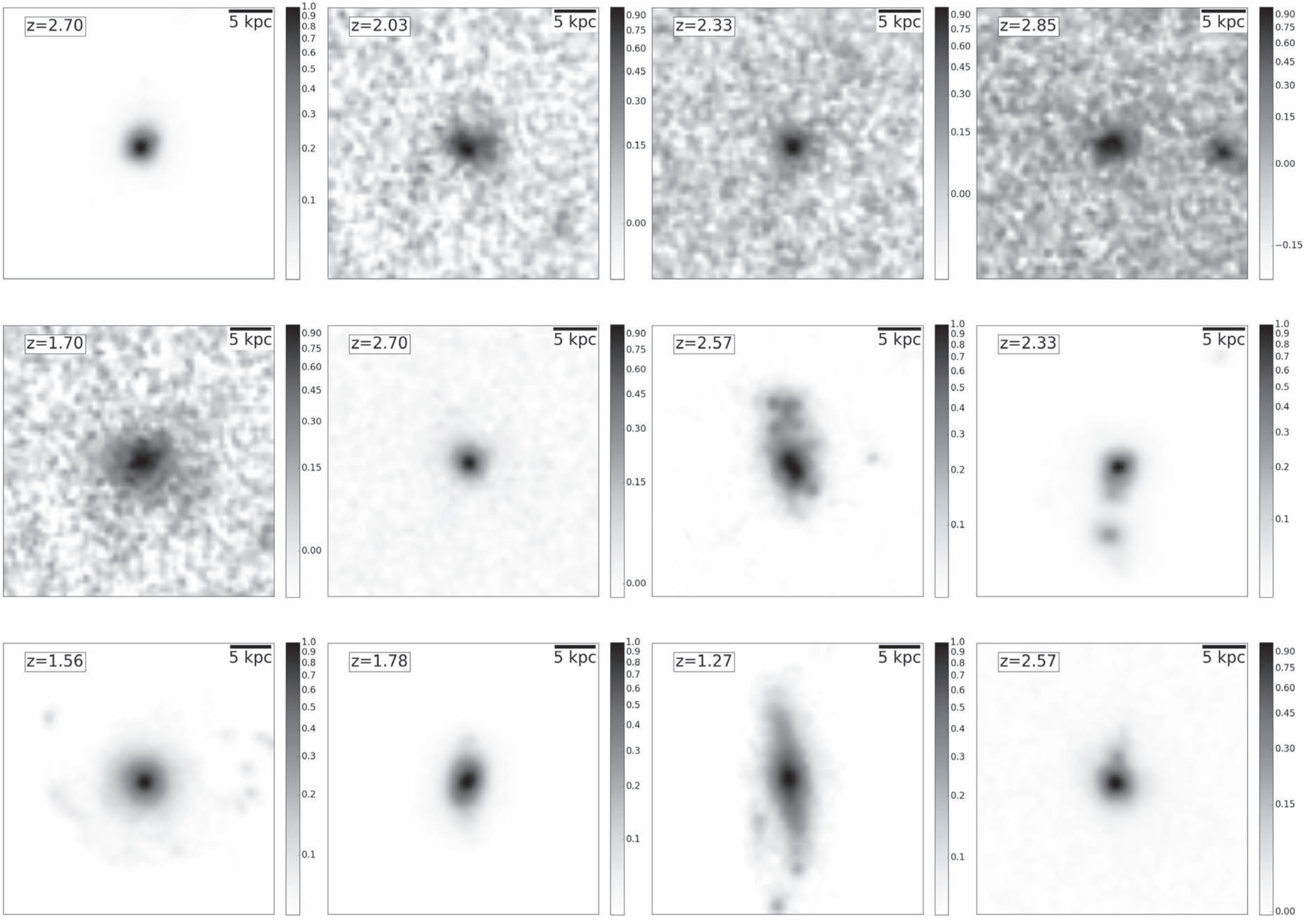

Figure 2. Random examples of simulated F160W CANDELized images in the three phases discussed in this work. The image size is $3\farcs8 \times 3\farcs8$. The top row shows pre-BN galaxies, the middle row shows galaxies in the BN phase, and the bottom row shows post-BN objects. The images have been rescaled so that they span the same range of luminosities in the three phases.

CANDELS Images

Pre-BN phase

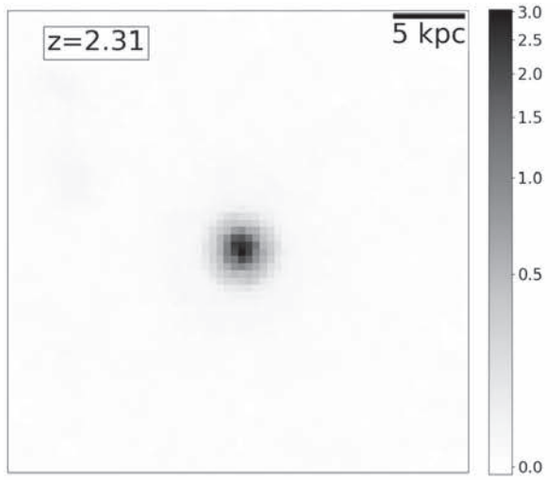

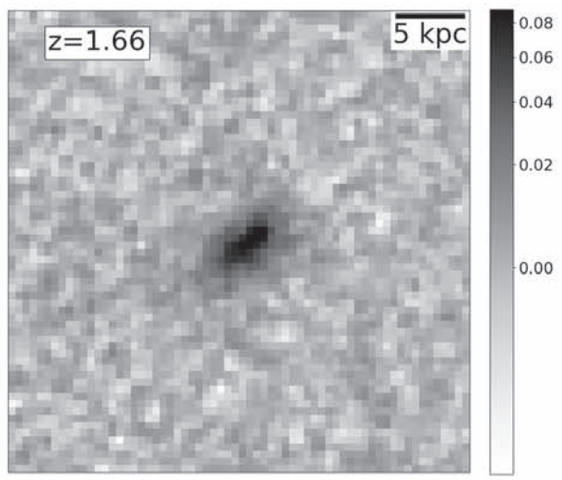

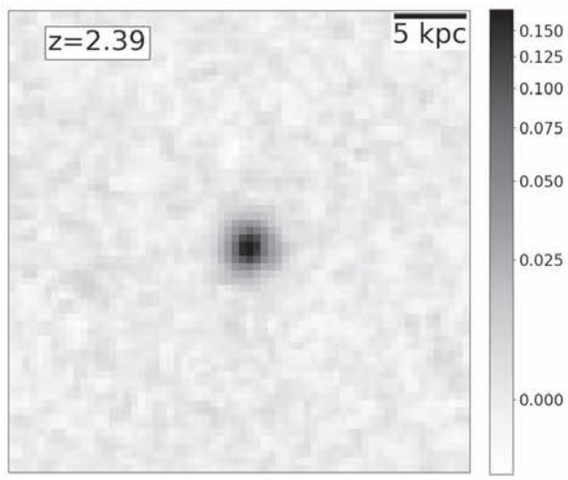

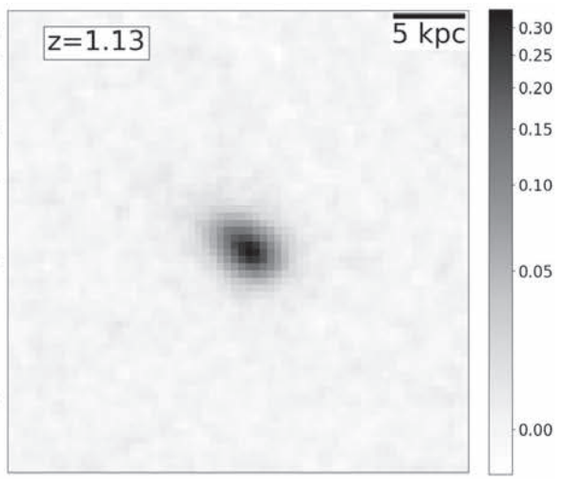

BN phase

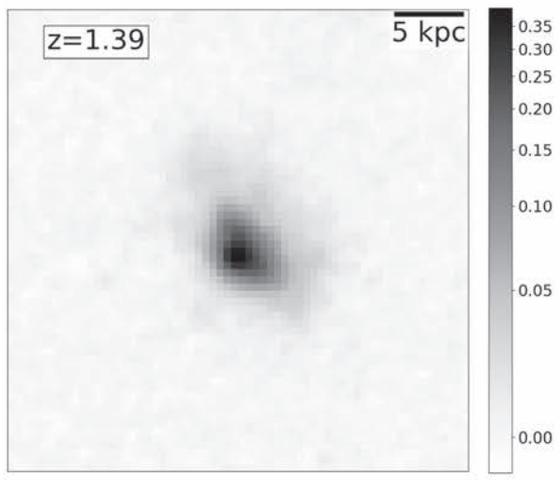

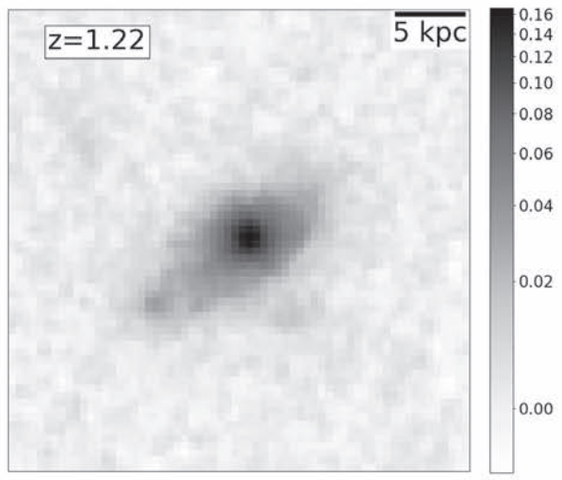

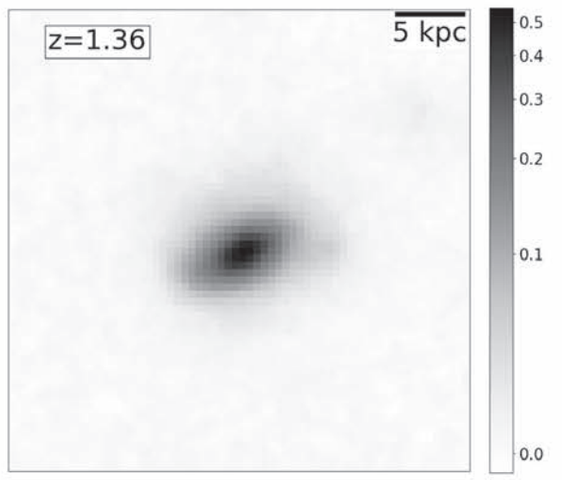

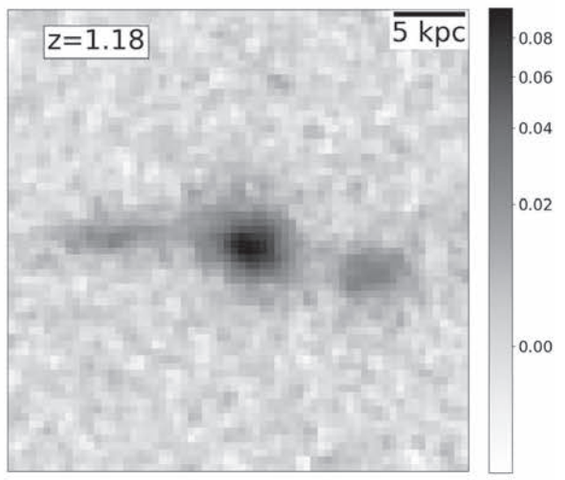

Post-BN phase

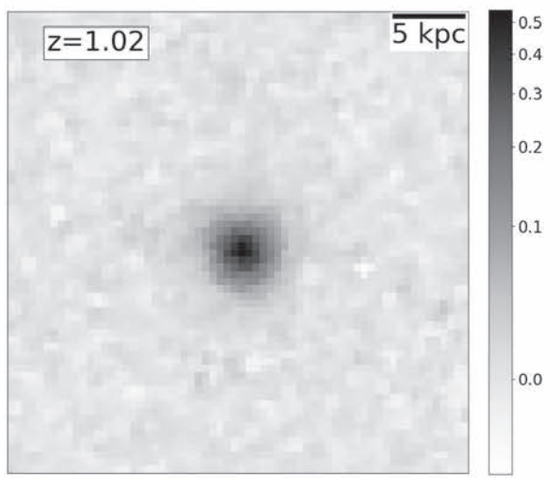

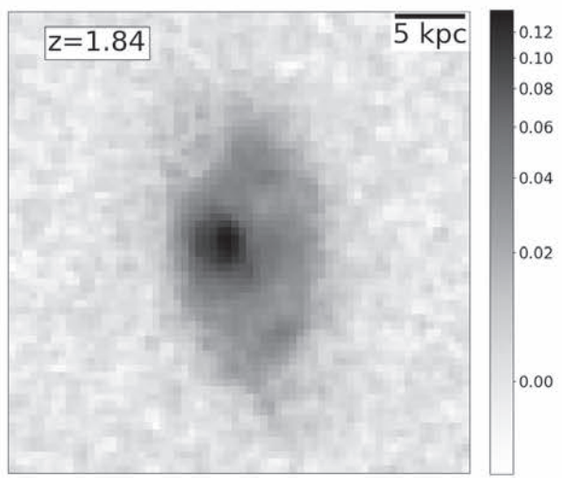

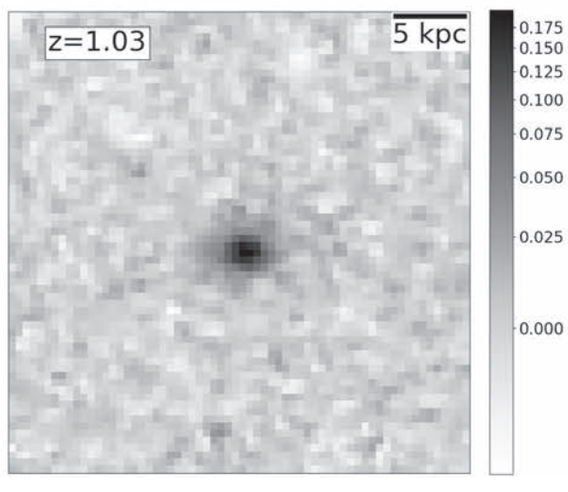

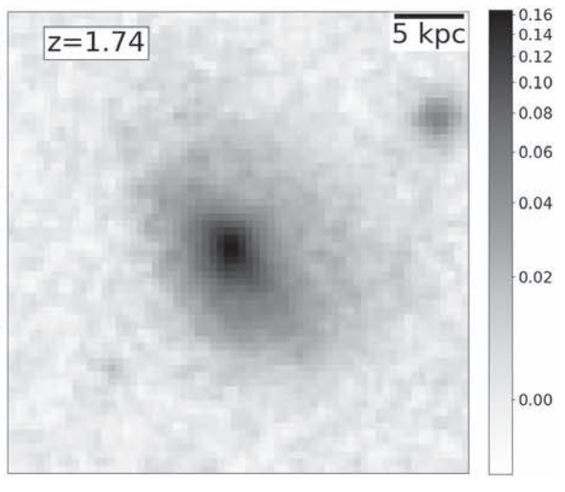

Testing the Trained Deep Learning Code

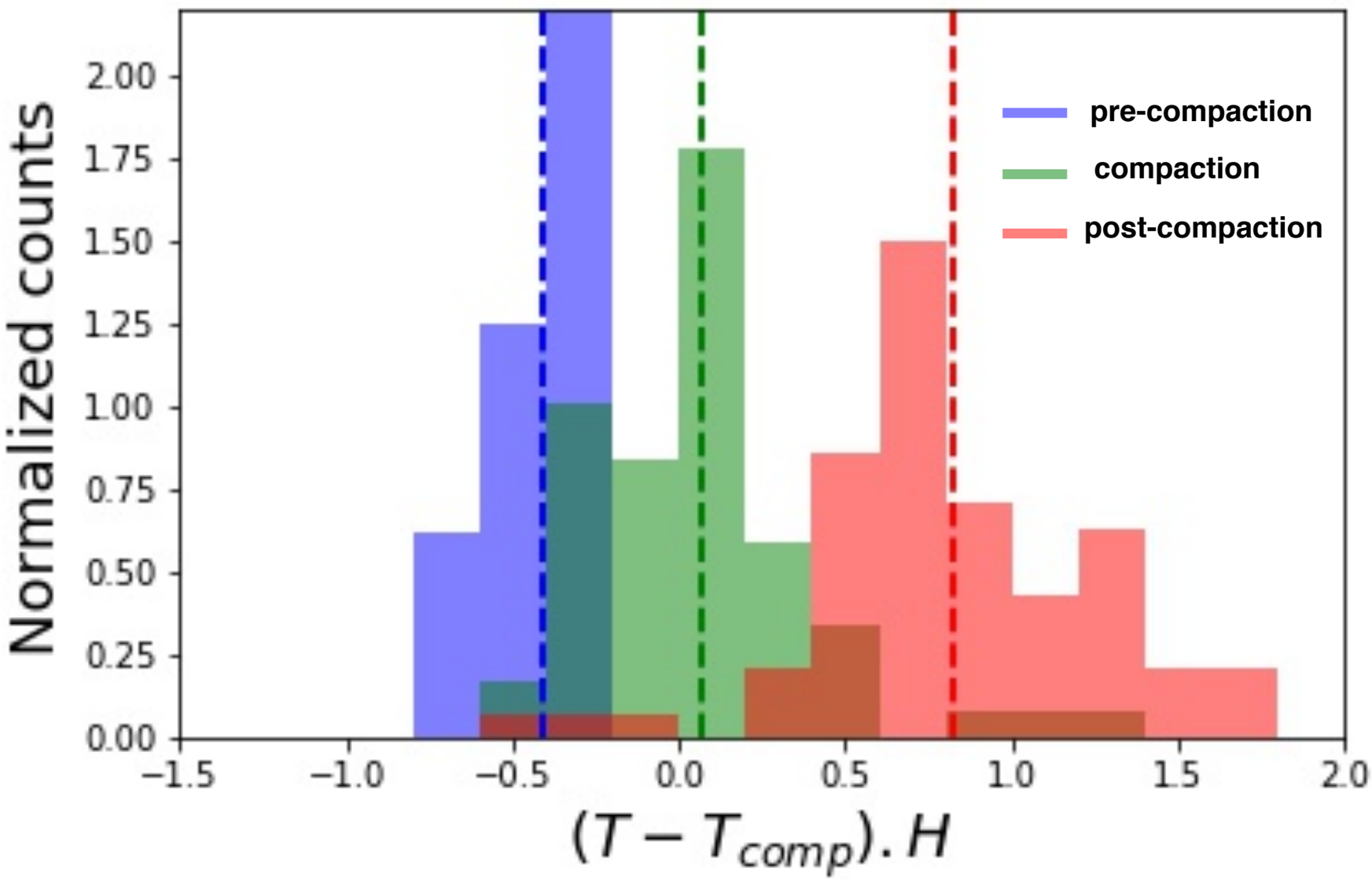

Observability of the compaction event with the calibrated classifier. The histograms show the distributions of time (relative to the Hubble time at the time of compaction). The dashed vertical lines show the average values for each class with the same color code. Despite some overlap, the classifier is able to establish temporal constraints on the different phases. Integrated gradient method shows that the classifier is using relevant pixels, not noise.

Integrated gradients output of the model. The left column is the original image and the other columns show the integrated gradients for the different wavelength filters. The network automatically detects the pixels belonging to the galaxy and used all of them to make the decisions.

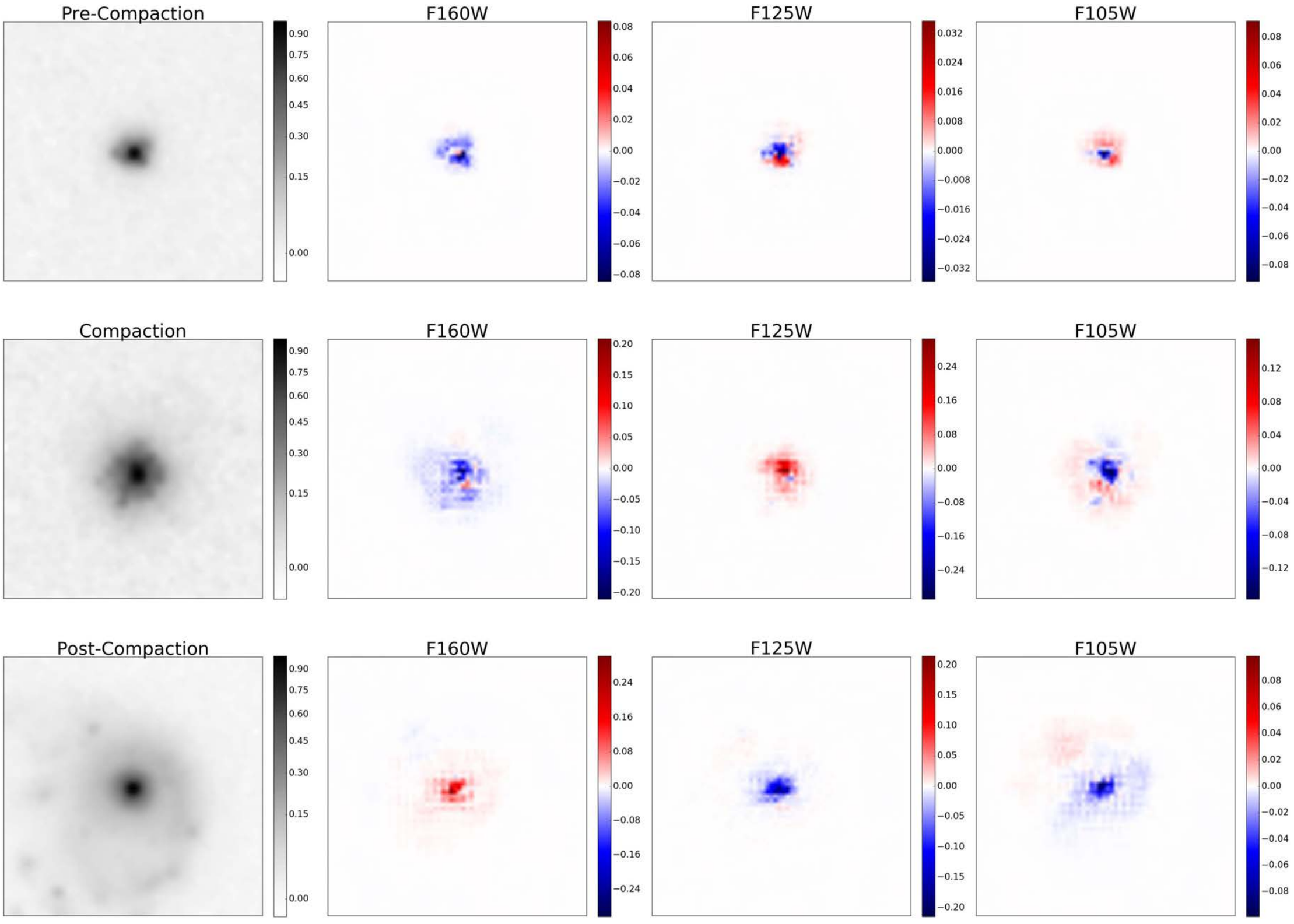

Applying the Trained Deep Learning Code to CANDELS Galaxies

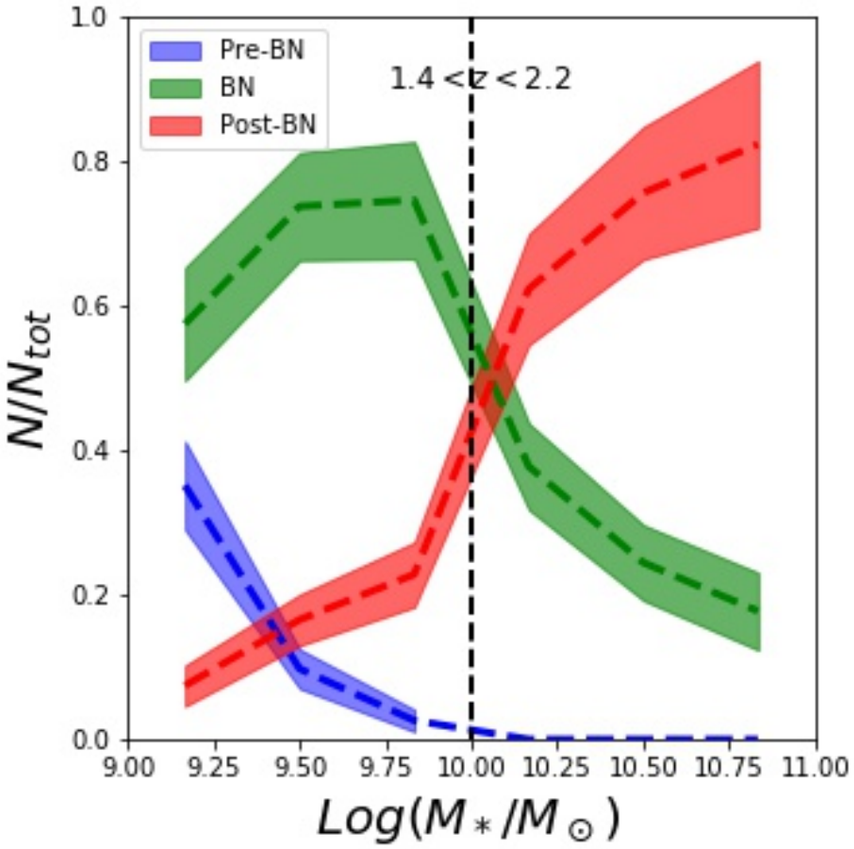

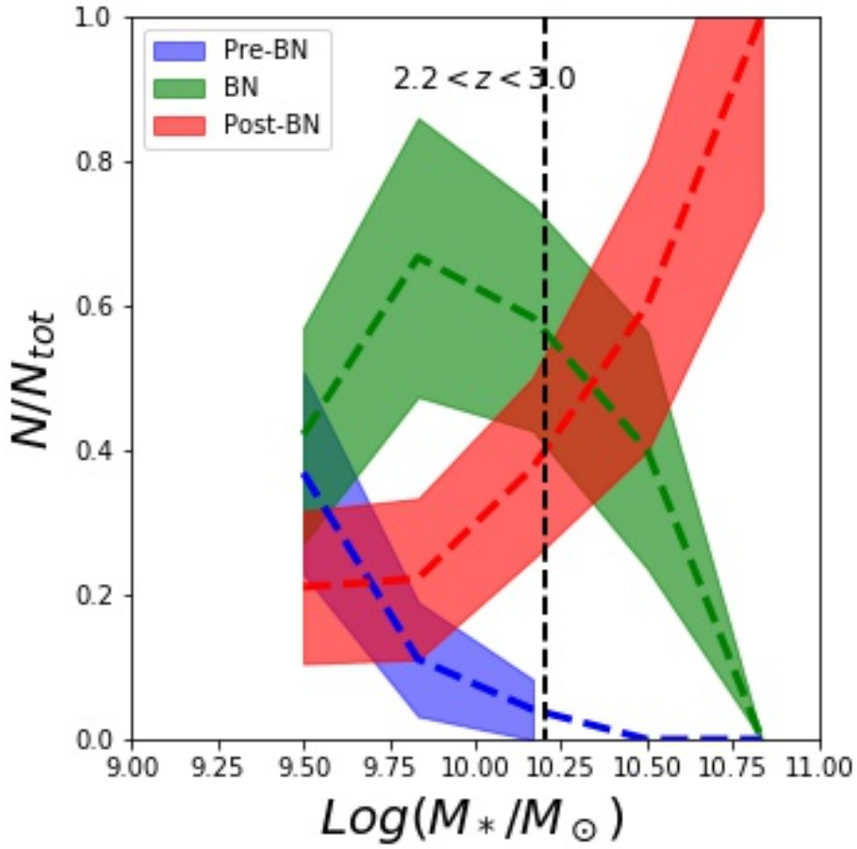

Stellar mass distributions of HST CANDELS galaxies in pre-compaction, compaction, and post-compaction phases in different redshift bins. The DL code correctly shows the temporal evolution. Galaxies in the compaction (BN) phase typically peak at stellar mass $10^{9.2–10.3}$ M_{sun}, as in the VELA simulations.

“Face Recognition for Galaxies”

Deep Learning Identifies High-z Galaxies in a Central Blue Nugget Phase in a Characteristic Mass Range

Cosmological zoom-in simulations model how individual galaxies evolve through the interaction of atomic matter, dark matter, and dark energy

Our VELA galaxy simulations agree with HST CANDELS observations that most galaxies start prolate, becoming spheroids or disks after compaction events

A deep learning code was trained with VELA galaxy images plus metadata describing whether they are pre-compaction, compaction, or post-compaction

The trained deep learning code was able to identify the compaction and post-compaction phases in CANDELized images

The trained deep learning code was also able to identify these phases in real HST CANDELS observations, finding that compaction occurred for stellar mass $10^{9.2\text{ -}10.3}$ M_{sun}, as in the simulations — and James Webb Space Telescope will allow us to do even better

Supported by grants from HST and Google

AGORA

A High-resolution Galaxy Simulations Comparison Initiative: www.AGORAsimulations.org

High-res Galaxy Simulations

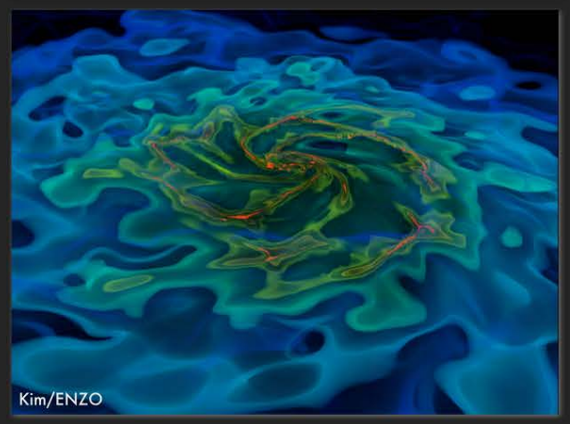

AGORA Comparison Infrastructure

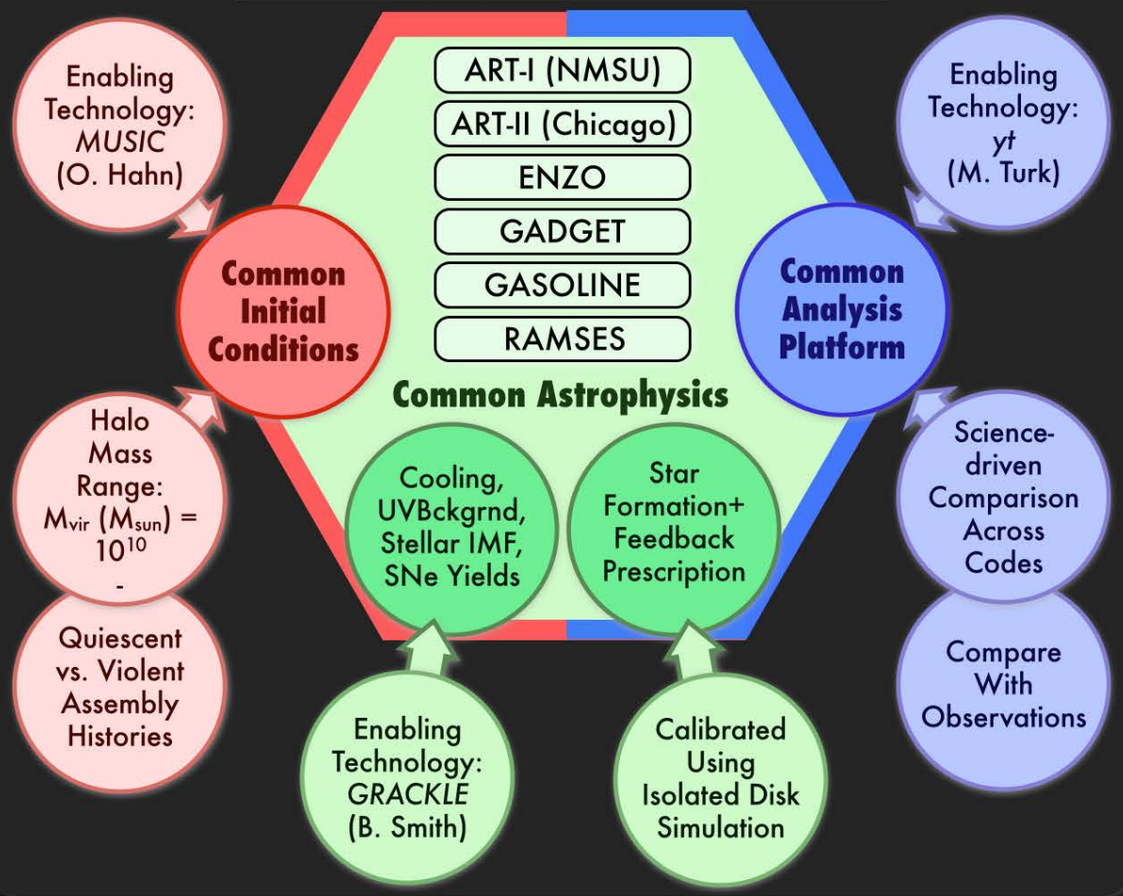

AGORA Goal & Team

- GOAL: A collaborative, multi-platform study to raise the realism and predictive power of galaxy formation simulations
- TEAM: 140+ participants from 60+ institutions worldwide, as of August 2016
- DATA SHARING: Simulations outputs and analysis softwares will be shared with the community

- Contact: santacruzgalaxy@gmail.com
- AGORA First Light: Flagship paper by Ji-hoon Kim et al. (ApJS 2014)
- Project funded in part by:

AGORA Isolated Disk Comparison

Milky Way-mass Disk Galaxy Formation with 80 pc Resolution

Summary:

- If carefully constrained, galaxy simulation codes agree well with one another despite having evolved largely independently for many years without cross-breedings
- Simulations are more sensitive to input physics than to intrinsic code differences.
- AGORA continues to promote collaborative and reproducible science in the community.

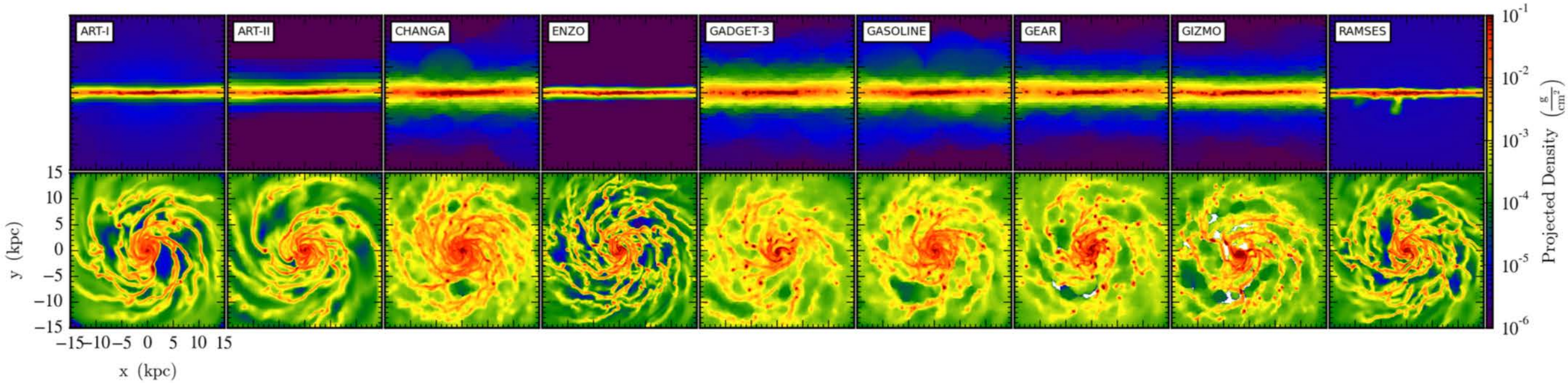

Figure 2. The 500 Myr composite snapshots of gas surface density from *Sim-1* with radiative gas cooling but without star formation or feedback. Each frame is centered on the location of maximum gas density within 1 kpc from the center of gas mass. Simulations performed by: Daniel Ceverino (ART-I), Robert Feldmann (ART-II), Spencer Wallace (CHANGA), Mike Butler (ENZO), Jun-Hwan Choi (GADGET-3), Ben Keller (GASOLINE), Yves Revaz (GEAR), Alessandro Lupi (GIZMO), and Romain Teyssier (RAMSES).

Website: AGORAsimulations.org

1. Joint Effort to Launch Papers "CGM" and "Clumps"

We decided to make a joint effort to launch both Papers "CGM" and "Clumps" (discussed in detail below) before the August Workshop 2018. After that, each Paper Group will write up its own paper using the same suite of simulations.

https://sites.google.com/site/projectagoraworkspace/collaborative-documents/progress-report-15

<table>
<tr><th></th><th>Task Force "CGM"+"Clumps"</th></tr>
<tr><td>GOALS</td><td>• Launch the simulations to be used in two Papers "CGM" and "Clumps" by Aug. 10, 2018.</td></tr>
<tr><td>TASK FORCE COORDINATOR</td><td>• Santi Roca-Fabrega (UCM)</td></tr>
<tr><td>CODE LEADERS</td><td>• Those who will actually carry out the calibrations #1, #2 and the production simulation:
<table>
<tr><th>Code</th><th>Contacts</th></tr>
<tr><td>ART-I</td><td>Ceverino</td></tr>
<tr><td>ENZO</td><td>Hummels</td></tr>
<tr><td>GADGET</td><td>Nakamura</td></tr>
<tr><td>GASOLINE</td><td>Shen</td></tr>
<tr><td>GIZMO</td><td>Lupi/Dong</td></tr>
<tr><td>RAMSES</td><td>Roca-Fabrega</td></tr>
</table></td></tr>
<tr><td>MILESTONES</td><td>• Step #1 (Jun. 12 – Jul. 7, 2018):
"Favorite" feedback calibration step #1 described in the Paper "CGM" Workspace (i.e., isolated disk IC, tweak each group's "favorite" feedback recipe to give a stellar mass of M* ~ 1e9 Ms produced in the first 1 Gyr, meanwhile check if your old run with the "common" feedback recipe produced a similar stellar mass). Do as many iterations as possible to finish this calibration. Please send your final entry to Santi as soon as possible, no later than June 30.

• Step #2 (Jul. 8 – Jul. 31, 2018):
"Favorite" feedback calibration step #2 described in the Paper "CGM" Workspace (i.e., cosmological IC, check each group's "common" and "favorite" feedback recipes to give a similar stellar mass at z=4). Do as many iterations as possible to finish this calibration. Please send your final entry to Santi as soon as possible so we can start comparing the data across the codes, no later than July 31.</td></tr>
</table>

Formation and Settling of a Disc Galaxy During the Last 8 Billion Years in a Cosmological Simulation

Daniel Ceverino, Joel Primack, Avishai Dekel, Susan A. Kassin MNRAS 2017

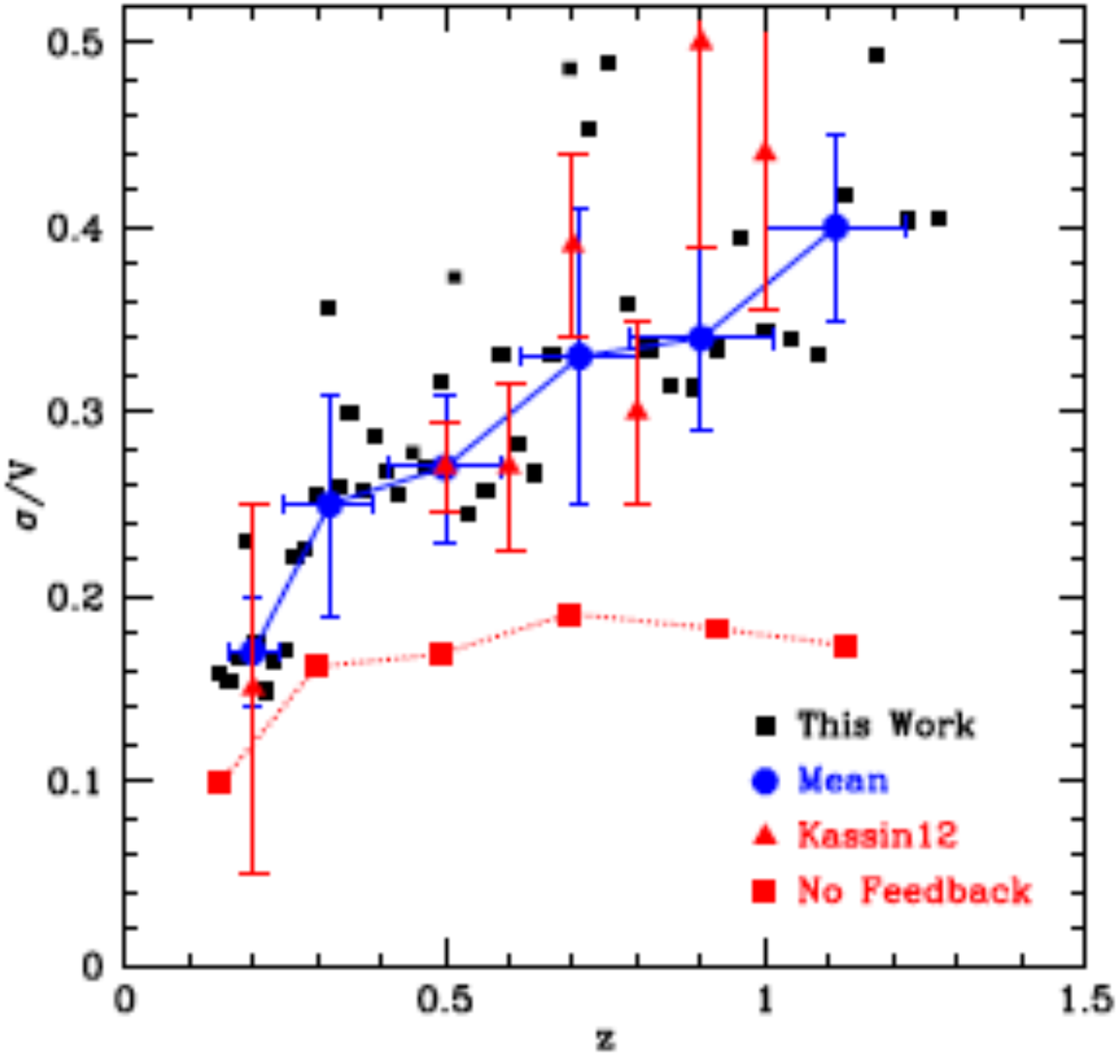

Disk Settling: σ/V declines as observed in similar-mass galaxies ($M_{halo} = 1.7x10^{11}$)
This is one of the AGORA initial conditions.

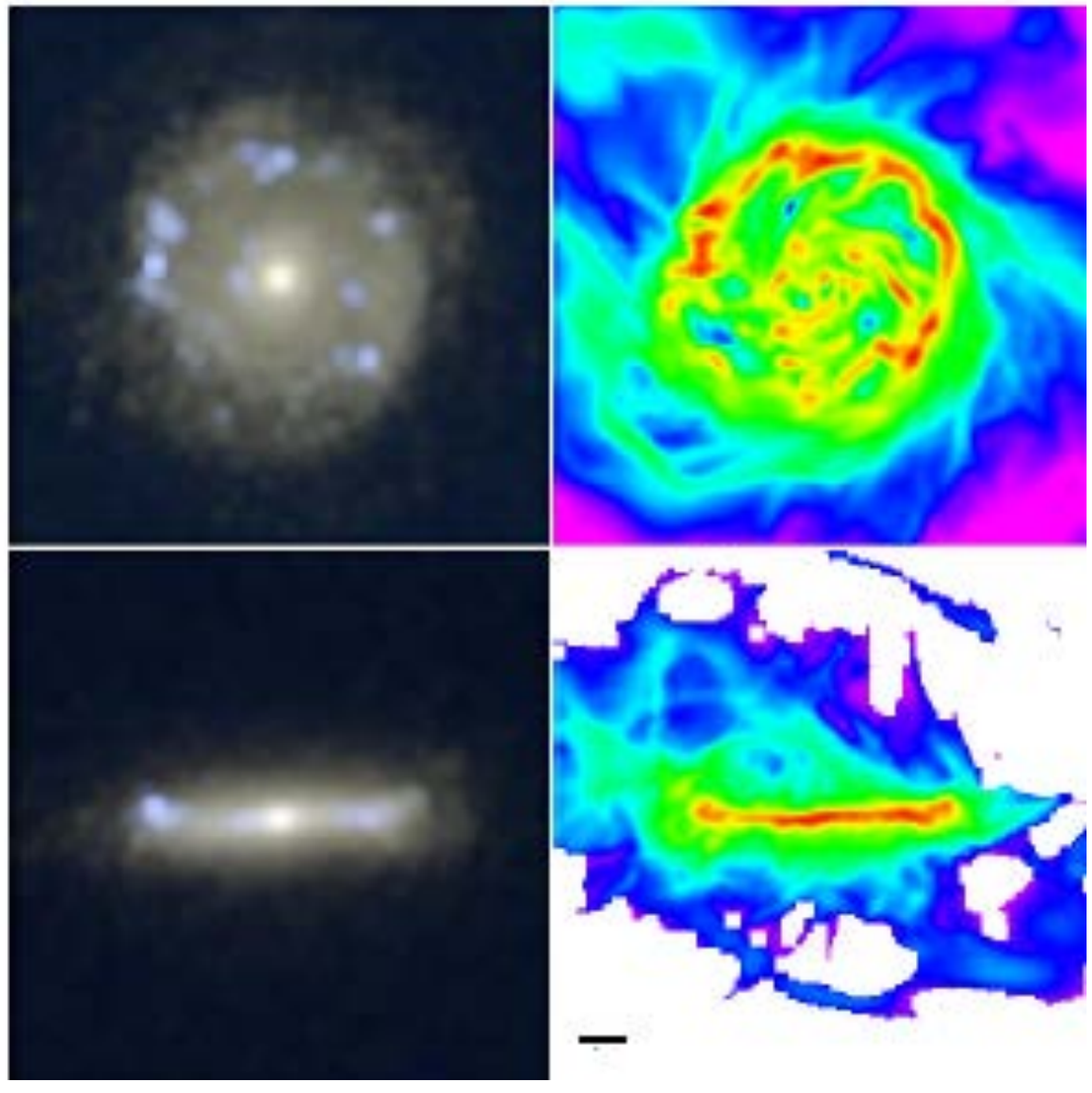

The simulation at $z = 0.1$ produces a thin disk, much like observed galaxies of this mass

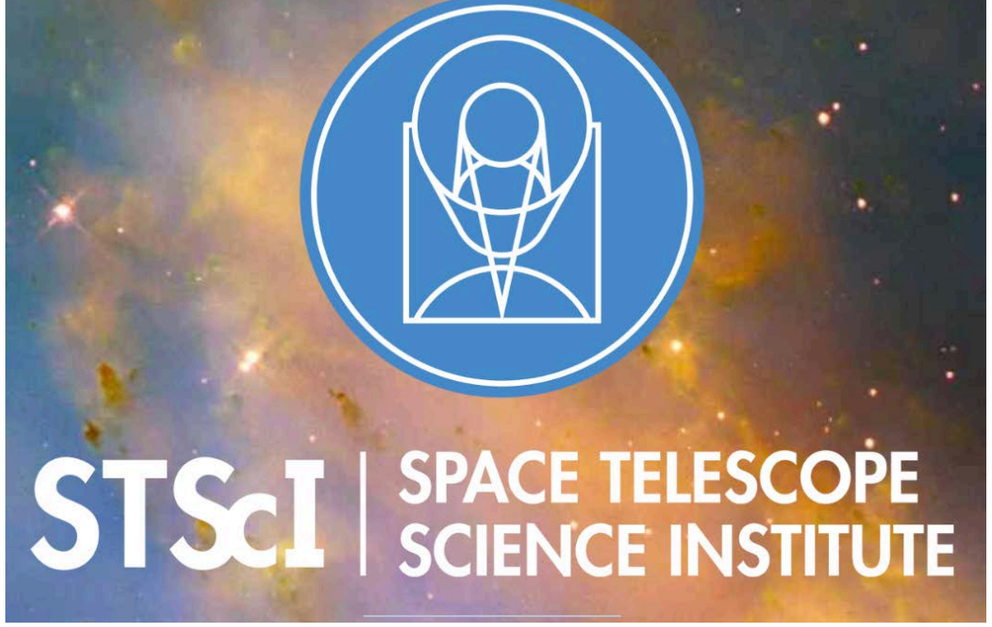

15 June 2018

New Insights on Galaxy Formation from Comparing Simulations and Observations

Joel Primack, UCSC

with collaborators including Aldo Rodriguez-Puebla, Christoph Lee, Peter Behroozi, Miguel Aragon Calvo, Avishai Dekel, Sandy Faber, Doug Hellinger, Kathryn Johnston, Anatoly Klypin, Viraj Pandya, Rachel Somerville, & undergraduate researchers Radu Dragomir, Elliot Eckholm, & Tze Ping Goh